Testing of chloride penetration and carbonation of concrete with superabsorbent polymers

Laurence De Meyst

Supervisor: Prof. dr. ir. Nele De Belie
Counsellors: ir. Bjorn Van Belleghem, dr. ir. Didier Snoeck

Master's dissertation submitted in order to obtain the academic degree of Master of Science in Civil Engineering

Department of Structural Engineering
Chair: Prof. dr. ir. Luc Taerwe
Faculty of Engineering and Architecture
Academic year 2015 - 2016

UNIVERSITEIT GENT

Testing of chloride penetration and carbonation of concrete with superabsorbent polymers

Laurence De Meyst

Supervisor: Prof. dr. ir. Nele De Belie
Counsellors: ir. Bjorn Van Belleghem, dr. ir. Didier Snoeck

Master's dissertation submitted in order to obtain the academic degree of Master of Science in Civil Engineering

Department of Structural Engineering
Chair: Prof. dr. ir. Luc Taerwe
Faculty of Engineering and Architecture
Academic year 2015 - 2016

UNIVERSITEIT GENT

Permission for consultation

"The author gives permission to make this master dissertation available for consultation and to copy parts of this master dissertation for personal use. In the case of any other use, the limitations of the copyright have to be respected, in particular with regard to the obligation to state expressly the source when quoting results from this master dissertation."

Laurence De Meyst
June 2016

Acknowledgement

This dissertation would not have been possible without the help of many people in many different ways.

First of all, I am sincerely grateful to my supervisor, Professor Nele De Belie for providing this interesting topic and for always showing interest in my research.

Special thanks to my two counselors Bjorn and Didier. Your comments, suggestions and supervision helped me to get through all the difficulties during my thesis.

I am grateful to Arn, Hugo, Kim, Philip and Yusuf for their advice, useful discussions and suggestions which helped me a lot.

I would like to thank the staff of Labo Magnel for their assistance and helping hand during my thesis: Bart, Dieter, Jan, Marc, Nathan, Nicolas, Peter L, Peter VdB, Sandra, Stefan, Tom and Tommy.

I also take this opportunity to thank my parents for their support and encouragement throughout my studies.

Thanks a lot to my two sisters, Valérie and Céline, for always being there for me, both in their own way. I am proud that you are my sisters!

And last but not least, Philippe. Your infinite belief in me kept me motivated through this whole journey. Thanks for reading many drafts of this thesis and for your critical advice. Thank you for always listening to me, even though it sometimes sounded like Chinese to you. The writing of this dissertation would not have been possible without your unconditional love and support.
Schat, ik zie je graag!

Laurence

Testing of chloride penetration and carbonation of concrete with superabsorbent polymers

Laurence De Meyst

Supervisor: Prof. dr. ir. Nele De Belie

Counsellors: ir. Bjorn Van Belleghem, dr. ir. Didier Snoeck

Master's dissertation submitted in order to obtain the academic degree of
Master of Science in Civil Engineering

Department of Structural Engineering
Chair: Prof. dr. ir. Luc Taerwe
Faculty of Engineering and Architecture
Academic year 2015-2016

Summary

Due to its low tensile strength, concrete is very susceptible to cracking. Cracks enable the penetration of harmful substances like chloride ions and CO_2 into the concrete, resulting in a more rapid corrosion of the reinforcement compared to uncracked concrete. Without proper treatment, costs for maintenance and repair can be very high. Fine cracks (< 30 µm) can close themselves by autogenous healing. This self-healing behavior of concrete can be stimulated by the use of superabsorbent polymers (SAPs) due to the further hydration of unhydrated cement particles and the stimulated precipitation of calcium carbonate. This research investigates the crack closure due to the stimulated autogenous healing in case SAPs are added to the concrete. Furthermore, chloride and CO_2 diffusion tests are performed in order to examine the efficiency of SAP addition in the prevention of chloride and CO_2 ingress. Due to the increased porosity upon shrinkage of the SAPs, both the chloride penetration and carbonation depths are found to be significantly larger than in the reference mixture. However, the results of the self-healing of the cracks show the beneficial effects of SAPs as in this case crack closing ratios up to 64% are found compared to the 24% in the reference mixture. The latter is very promising as this healing can have beneficial effects on the durability and service-life of concrete structures because of a lowered corrosion risk. Nevertheless, further research is needed on the topic of reduction of both chloride penetration and carbonation in cracked concrete due to the stimulated autogenous healing by SAPs.

Keywords

Superabsorbent polymers (SAPs), stimulated autogenous healing, chloride penetration, carbonation

Testing of chloride penetration and carbonation of concrete with superabsorbent polymers

Laurence De Meyst

Supervisors: prof. dr. ir. Nele De Belie, ir. Bjorn Van Belleghem, dr. ir. Didier Snoeck

Abstract **- Due to its low tensile strength, concrete is very susceptible to cracking. Cracks enable the penetration of harmful substances like chloride ions and CO_2 into the concrete, resulting in a more rapid corrosion of the reinforcement compared to uncracked concrete. Without proper treatment, costs for maintenance and repair can be very high. Fine cracks (< 30 µm) can close themselves by autogenous healing. This self-healing behavior of concrete can be stimulated by the use of superabsorbent polymers (SAPs) due to the further hydration of unhydrated cement particles and the stimulated precipitation of calcium carbonate. This research investigates the crack closure due to the stimulated autogenous healing in case SAPs are added to the concrete. Furthermore, chloride and CO_2 diffusion tests are performed in order to examine the efficiency of SAP addition in the prevention of chloride and CO_2 ingress.**

Due to the increased porosity upon shrinkage of the SAPs, both the chloride penetration and carbonation depths are found to be significantly larger than in the reference mixture. However, the results of the self-healing of the cracks show the beneficial effects of SAPs as in this case crack closing ratios up to 64% are found compared to 24% in reference mixtures. The latter is very promising as this healing can have beneficial effects on the durability and service-life of concrete structures because of a lowered corrosion risk. Nevertheless, further research is needed on the topic of reduction of both chloride penetration and carbonation in cracked concrete due to the stimulated autogenous healing by SAPs.

Keywords **- superabsorbent polymers (SAPs), stimulated autogenous healing, chloride penetration, carbonation**

I. Introduction

The formation of cracks in concrete structures is inevitable due to the low tensile strength of concrete. Cracks can create preferential pathways for the ingress of oxygen, chlorides, carbon dioxide and water into the interior of the concrete. These potentially harmful substances can facilitate the corrosion process of the steel reinforcement, resulting in a decreased durability and structural integrity of the concrete. In case no proper treatment is performed, costs for maintenance and repair can be very high.

Although concrete has the intrinsic property to heal cracks, the so called autogenous healing, this is only limited to very fine cracks (< 30 µm) and requires the presence of water ([1],[2]). As in reality larger crack widths occur frequently and water is not always available, a lot of research is done in order to find mechanisms that can heal these larger crack widths, even in case of dry periods [3]. A promising solution is the use of superabsorbent polymers (SAPs).

Superabsorbent polymers mixed in the concrete can absorb up to 500 times their own weight in aqueous solutions, resulting in a swollen hydrogel that can seal cracks. At a later stage in time, the SAPs can gradually release this absorbed water, leading to further hydration of unhydrated cement particles, and stimulate the precipitation of calcium carbonate. Due to these two mechanisms, the autogenous healing of the concrete is stimulated and makes it possible to close larger cracks.

The penetration of chlorides and the carbonation into the concrete can initiate respectively chloride-induced corrosion and carbonation-induced corrosion. Due to corrosion, expansive products are formed at the concrete-reinforcement interface, resulting in spalling and cracking of the concrete as well as a reduction of the cross section of the steel reinforcement and a loss of bond between steel and concrete. It is assumed that the use of SAPs can stimulate healing of cracks in concrete, leading to a decreased chloride penetration and carbonation. This has beneficial effects for the durability and service-life of concrete structures as the risk of corrosion is lowered.

II. Materials and Methods

A. Materials

For the determination of self-healing and chloride penetration, the studied concrete mixtures were composed of Ordinary Portland Cement (OPC) CEM I 52.5 N (HOLCIM), fly ash ASTM type F (OBBC), fine silica sand 0/4, gravel 2/8, gravel 8/16 and tap water. A polycarboxylate super plasticizer, Glenium 51, conc. 35% (BASF), was added to the concrete mixture to improve the workability (2 ml/kg binder). In the case of SAP-containing mixtures, commercially available synthetic SAPs, produced by SNF Floerger were added (0.5 m% and 1 m% of binder). The SAPs were cross-linked copolymers of acrylamide and acrylate obtained through bulk polymerization. The slump flow was kept constant for all mixtures (i.e. reference slump flow of 150 mm) by adding additional water to the SAP-containing mixtures. An overview of the used mixture compositions is given in Table 1.

For the determination of carbonation, similar mixtures were used, although in this case no fly ash was added as concrete with fly ash is more susceptible to carbonation [4]. Besides a concrete mixture without and with SAPs (1 m% of cement) also a cement mixture was studied. An overview of the used mixtures is given in Table 2.

Magnel Laboratory for Concrete Research, Faculty of Civil Engineering and Architecture, Ghent University (UGent), Ghent, Belgium.

Table 1: Mixture composition for self-healing and chloride penetration

		REF	SAP 0.5	SAP 1
Sand 0/4	[kg/m³]	696	667	640
Gravel 2/8	[kg/m³]	502	481	461
Gravel 8/16	[kg/m³]	654	626	601
CEM I 52.5N	[kg/m³]	318	304	292
Fly ash	[kg/m³]	56	54	51
SAP	[kg/m³]	-	1.5	2.9
Water	[kg/m³]	153	147	141
Extra water	[kg/m³]	-	41	78

Table 2: Mixture composition for carbonation

		CEM	CON	SAP
Sand 0/4	[kg/m³]	-	715	660
Gravel 2/8	[kg/m³]	-	516	476
Gravel 8/16	[kg/m³]	-	672	620
CEM I 52.5N	[kg/m³]	300	300	277
SAP	[kg/m³]	-	-	2.8
Water	[kg/m³]	143	165	152
Extra water	[kg/m³]	-	-	74

B. Methods

The swelling capacity of the SAPs in different solutions (demineralized water, cement filtrate, artificial seawater and a chloride solution) was determined with the filtration method, whereas the swelling time was obtained by the so-called vortex test.

Fresh concrete characteristics, like slump, flow, density and air content were determined according to the applied section of NBN EN 12350. In order to test the compressive strength of the concrete mixtures according to NBN EN 12390-3, three cubes with side 150 mm were cast per mixture and tested at the age of 28 days.

The open porosity of the samples was determined by means of a vacuum saturation test according to EN 1936.

Realistic cracks were induced in the cylindrical samples by means of a crack-width controlled splitting test at the age of 28 days. At both sides of the cylinder a Linear Variable Differential Transformer (LVDT) with a measuring range of 1 mm and an accuracy of 1 µm, was placed. The LVDT measures the crack width at both surfaces and the mean of these crack widths was used to control the splitting test. The intended crack widths were 100 µm and 300 µm. In between the cylinder and the loading plate, a thin piece of plywood was placed in order to create a uniform distributed line load instead of a high concentrated point load which could fracture the sample. A schematic representation of the test setup is shown in Figure 1 [5].

Artificial cracks with intended widths of 100, 300 and 500 µm are created by putting thin brass plates with a thickness corresponding to the desired crack width in the fresh concrete. After 24 hours, the brass plates were taken out of the concrete, leaving a straight artificial crack in the concrete. Figure 2 shows a schematic representation of the mould setup with the brass plate fixed at the desired crack depth.

Before exposing the specimens to wet-dry cycles, chlorides or carbon dioxide, crack widths were measured by means of an optical stereo microscope (Leica S8 Apo mounted with a DFC camera). A micrograph was taken every cm along the crack at the surface and these pictures were analyzed using the ImageJ software. Subsequently the average crack width and standard deviation could be calculated for each sample.

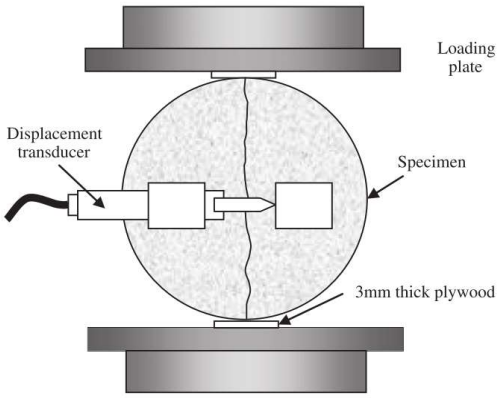

Figure 1: Schematic representation of the test setup of the crack-width controlled splitting test, by Jang et al. [5]

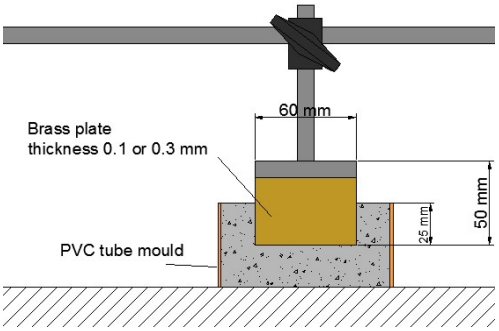

Figure 2: Schematic test setup for creating artificial cracks in cylinders

To investigate the self-healing efficiency of the SAPs, the samples were stored in wet-dry cycles for 28 days. One wet-dry cycle took 24 hours: 12 hours of immersion in demineralized water, followed by a drying period of 12 hours at 60 ± 5% relative humidity and 20 ± 2 °C. After 3, 7, 14 and 28 cycles, the crack widths were again measured by means of an optical microscope. The crack closing ratio (%) was expressed as the difference between the initial average crack width and the remaining average crack width compared to the initial average crack width:

$$\text{crack closing ratio [\%]} = \frac{w_{initial} - w_{remaining}}{w_{initial}} \times 100 \qquad (1)$$

The used chloride diffusion test is based on the NT Build 443 [6]. For this test, cylindrical samples with a height of 50 mm and a diameter of 100 mm were used. All sides of the cylinder, except the one to be exposed to chlorides, were coated with an epoxy resin. In this way, one-dimensional penetration of chlorides from one side of the sample was assured. Subsequently, the specimens were stored in a 165 g NaCl per ℓ solution for seven weeks. Afterwards, some samples were split perpendicularly to the crack and sprayed with silver nitrate in order to examine the chloride penetration depth from the exposed surface as well as perpendicular to the crack. The chloride-affected zone appeared to turn out white, whereas the chloride-free zone turned black/brown. Furthermore, the ratio of the area in which chlorides were penetrated to the total surface of the test piece was determined. The other samples were used to perform potentiometric titrations. Therefore concrete powders were collected from the samples by grinding layers of 2 mm

thickness parallel to the exposure surface in a zone around the crack. The determination of the total chloride concentration of each layer consisted of an acid-soluble extraction in a nitric acid (HNO_3) solution, followed by a potentiometric titration using silver nitrate as titration solution. In a next step, the values of the chloride surface concentration C_s and the non-steady-state diffusion coefficient D_{nssd} are obtained by fitting the second law of Fick to the measured chloride contents by means of a non-linear regression analysis in accordance with the method of least squares fit. The simplified second law of Fick is given by formula (2):

$$C(x,t) = C_s - 2\,(C_s - C_i)\left[\Phi\left(\frac{\sqrt{2}\,x}{\sqrt{4\,D_{nssd}t}}\right) - \frac{1}{2}\right] \qquad (2)$$

with C(x,t) the experimentally measured chloride concentration at depth x [mm] and time t [s], C_s the chloride concentration at the surface and C_i the initial chloride concentration.

For the CO_2 diffusion tests, cubes with sides 100x100x100 mm³ were used. All sides of the cubes, except the one to be exposed to CO_2, were coated with an epoxy resin in order to assure one-dimensional penetration of CO_2. At the age of 12 days, the specimens were placed in a carbonation chamber containing 1 vol% CO_2 with a temperature of 20 ± 2°C and a relative humidity of 60 ± 5%. Part of the cracked specimens were taken out of the carbonation chamber every four weeks and immersed for 24 hours in demineralized water in order to study the effect of different curing conditions. After 2, 4, 6 and 12 weeks, the carbonation depth from the exposed surface and perpendicular to the crack was determined by spraying phenolphthalein on the split surfaces of the samples. Non-carbonated zones turned out purple, whereas the carbonated zone stayed colorless.

III. Results and Discussion

A. Swelling behavior of SAPs

The SAPs have an absorption capacity of 240.0 ± 9.3 g fluid/g SAP in demineralized water, 21.2 ± 1.2 g fluid/g SAP in a chloride solution, 21.4 ± 1.3 g fluid/g SAP in sea water and 39.8 ± 1.1 g fluid/g SAP in cement filtrate. Cations like K^+, Na^+, Mg^{2+} or Ca^{2+} give rise to a so-called charge screening effect of the negatively charged polymer chains, resulting in a lowered absorption and less swelling of the SAP particles. As the amount of cations in demineralized water is limited, SAPs reach their highest absorption capacity in this fluid. The absorption of SAP particles in concrete is smaller than in cement slurry because of the weight exerted by the surrounding material and because the fluid inside concrete may differ from the artificial cement slurry [7]. Brüdern and Mechtcherine [8] state that the swelling capacity in a concrete mixture is about half the one in filtered cement slurry. Based on the results of the filtration method, the statement of Brüdern and in order to obtain a similar workability as mixtures without SAPs, the amount of additional water to compensate for the loss in workability amounts 27 g/g SAP.

The swelling time for the SAPs is 38 ± 2 s in demineralized water, 36 s in chloride solution and 28 s in sea water. All obtained swelling times are lower than the mixing time with water (150 s) when making concrete, so it can be assumed that the SAPs will already swell to their maximum dimensions during mixing and settlement of the concrete.

B. Concrete properties

The measured concrete properties for the different mixtures are summarized in Table 3 and Table 4.

Table 3: Concrete properties (1)

		REF	SAP_0.5	SAP_1
Slump	[mm]	150	150	155
Flow	[mm]	440	430	430
Strength	[MPa]	65.5 ± 1.3	49.2 ± 0.8	38.2 ± 1.2

Table 4: Concrete properties (2) (- not applicable)

		CON	SAP	CEM
Slump	[mm]	165	150	-
Flow	[mm]	500	430	-
Air content	[%]	2.6	4.2	-
Density	[kg/m³]	2345	2220	-
Open porosity	[%]	11.9 ± 0.4	17.4 ± 0.4	41.9 ± 0.3

From the almost identical obtained values for the slump and flow of the different mixtures, it can be concluded that the amount of additional water, namely 27 g/g SAP, indeed results in the intended similar workability

When the amount of added SAPs is increased, a significant lower compressive strength at 28 days is found due to the formation of macro pores upon shrinkage of the SAPs.

The mean open porosities of the three test series are significantly different from each other. An increase in open porosity will have an influence on both chloride penetration and carbonation.

C. Crack formation

The measurements of the targeted 100 µm artificial crack widths show that the observed crack widths at the surface are somewhat larger than the thickness of the brass plates. In case of the targeted 300 µm crack widths however, the observed crack widths are almost the same as the thickness of the plates. A reason for this can be found in the more difficult intact removal of 100 µm plates from the hardened concrete. A lot of wiggling was needed to pull out the very thin plates, whereas the thicker 300 µm plates could easily be removed. In case of artificially made cracks of 100 µm, the cracks were almost fully blocked with impurities, probably originating from the polishing of the surface.

It is quite difficult to obtain realistic cracks with the intended crack width by a crack-width controlled splitting test. Several reasons contribute to this phenomenon: crack recovery during unloading, the heterogeneity of the samples as well as personal influences of the executor, for example the eccentric placing of the sample in the apparatus. As the obtained crack width varies a lot along the crack, this results in large standard deviations. Due to the realistic crack formation method, secondary micro-cracks were sometimes created in the sample. The influence of these micro cracks on the chloride penetration is not further investigated as it is assumed that their influence is rather limited, as they will probably heal autogenously due to their small crack width.

In case of artificial cracks, the type of mixture plays a role in the obtained crack width. A possible explanation can be a difference in bonding between the plates and the mixture and/or the presence of fines at the interface that creates a lubricating layer around the plates. Also in the case of realistic cracks, a significant difference in mean crack width was obtained for the different mixtures. As the formation of

realistic cracks is done with a splitting test, the difference in compressive strength between series REF, SAP_0.5 and SAP_1 is probably the governing factor. Further research is needed to verify these hypotheses.

D. *Self-healing of the cracks*

A first test series did not show any visible crack healing at the surface. This is probably due to the sample preparation: after demoulding the samples, their surfaces were wet polished in order to obtain a smooth surface. This operation might result in a very low amount of unhydrated cement particles and SAPs at the surface, which are both needed in order to stimulate self-healing. A second test series was therefore made, without saw cutting of the surface. The average crack closing ratios after 3, 7, 14 and 28 cycles of the three different mixtures are depicted in Figure 3.

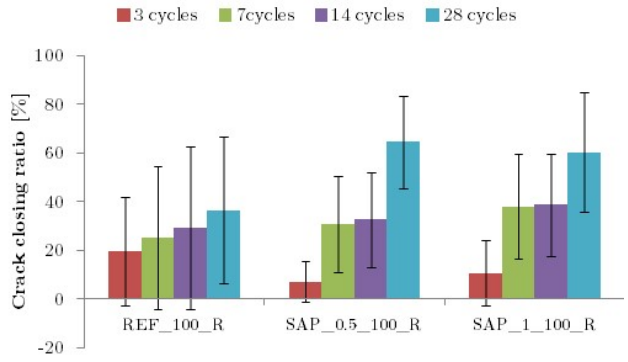

Figure 3: Average crack closing ratio [%] after 3,7, 14 and 28 cycles

Small cracks (< 30) µm closed completely after 28 days, even in the absence of SAPs, due to autogenous healing. This is in accordance with the findings of Snoeck and De Belie [1] and Li and Yang [2]. Larger crack widths are only (partially) healed in case SAPs were present in the mixture. From this, the beneficial effect of SAPs on the stimulated autogenous healing can be seen: the SAPs are working as water reservoirs that gradually release their absorbed water. This will lead to a further hydration of unhydrated cement particles on the one hand but will also stimulate the precipitation of calcium carbonate on the other hand as the CO_2 will dissolve in water and will react with Ca^{2+} present in the concrete. The final crack closing ratios after 28 cycles are significantly higher than the one of the reference mixture REF of 37% (or 24% in case an outlier is omitted). The values are 64% and 60% in the case 0.5 m% and 1 m% SAPs are added respectively. An example of complete crack healing in a mixture containing 0.5 m% SAP is shown in Figure 4. The crack steadily closes in time as it is filled with whitish carbonate crystals. Also the smaller micro-crack has completely disappeared.

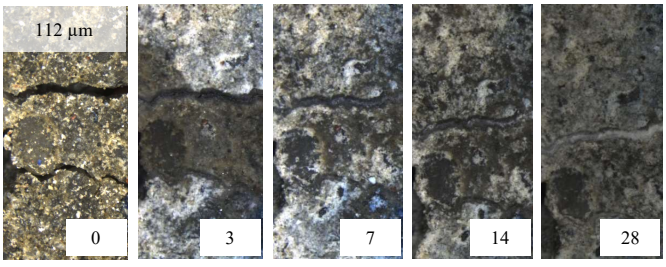

Figure 4: Crack healing after 3,7, 14 and 28 cycles

The difference between the ratios for SAP_0.5 and SAP_1 is found not to be significant, after neither amount of cycles. This result seems counterintuitive at first sight and is in contrast to findings in literature [9] as it could be expected that the more SAPs are added, the more water is available for further hydration and the better the self-healing will be. From this result however, it can be concluded that increasing the amount of SAPs from 0.5 to 1 m% has no significant influence on the self-healing. The amount of water available seemed to suffice.

E. *Chloride diffusion tests*

The test series that did not show visible healing of the crack at the surface were further investigated to examine the influence of SAPs on chloride penetration. After the samples were split perpendicularly to the crack and sprayed with $AgNO_3$, the ratio of the area in which chlorides were penetrated to the total area was calculated, see Figure 5. In case of uncracked, artificial 100 and artificial 300, the area ratio increases when the amount of SAPs is increased, leading to a higher porosity and thus a larger area penetrated by chlorides. This phenomenon is not observed for realistic cracks, due to the larger variation of created crack widths and thus larger variation in the area affected by chlorides. The latter makes it impossible to draw similar conclusions in case of realistic cracks. However, for realistic cracks the affected area was significantly larger than in case of artificial cracks with the same intended crack width. A reason for this is that the realistic cracks are through-going whereas the artificial cracks are only limited in depth. As stated earlier, in case of realistic cracks secondary micro cracks can be formed, which might increase the chloride penetration as well.

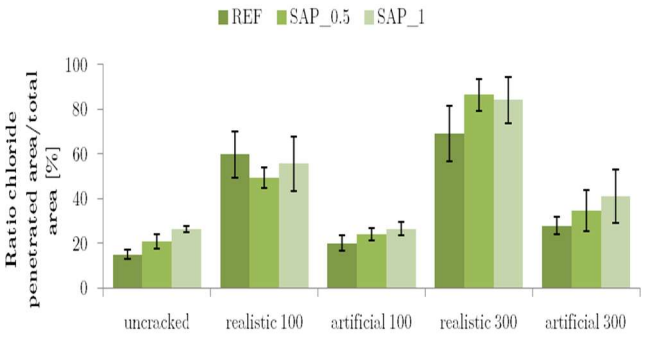

Figure 5: Ratio of chloride penetrated area to the total area

In the case of 300 µm cracks, the area ratio is found to be significantly larger than the ones obtained for 100 µm cracks, for both artificial and realistic cracks. This result could be expected as in case of wider cracks, a larger amount of chlorides can more easily penetrate into the crack and further into the concrete.

Next, the chloride penetration depth from the exposed surface was measured, see Figure 6. Increasing the amount of SAPs from 0 m% to 0.5 m% and finally to 1 m% leads in each step to an additional ±2 mm penetration from the surface due to the more porous structure due to the presence of SAPs.

With respect to the chloride penetration perpendicular to the crack, no significant difference in penetration depth was found when SAPs were added at the mixture, see Figure 7. When looking at the crack formation method, the chloride penetration perpendicular to realistic cracks was significantly

higher compared to the penetration perpendicular to artificial cracks. In case of realistic cracks, micro-cracks along the crack face can occur, creating preferential pathways for the chlorides to penetrate into the concrete. When looking at artificial cracks, the presence of a higher amount of fines at the crack face can impede chloride ingress perpendicular to the crack. In case of 300 µm cracks, the mean penetration depth perpendicular to the crack is found to be significantly larger than the ones obtained for 100 µm cracks.

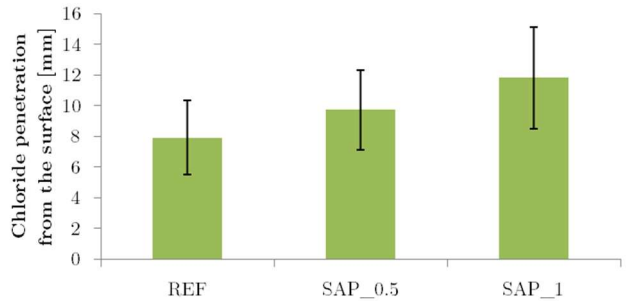

Figure 6: Chloride penetration from the exposed surface

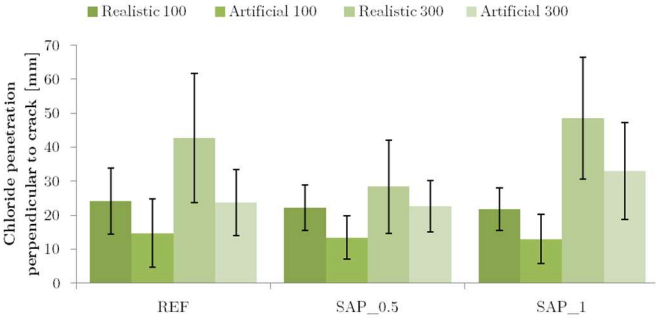

Figure 7: Chloride penetration perpendicular to crack

The penetration depth to both sides of the crack is in most cases approximately twice the penetration from the exposed surface. When assuming a symmetrical penetration perpendicular to the crack, this means that the penetration perpendicular to only one side of the crack is similar in nature with the one from the exposed surface. These results are in accordance with the findings of Win et al. [10] and Audenaert et al. [11].

Three samples of each series were used for potentiometric titrations. When plotting the measured total chloride concentration (expressed as m% binder) versus the depth below the exposed surface, the total chloride profile is obtained. Subsequently, a mathematical profile based on the second law of Fick is fitted to the measured profiles of the three samples and the chloride surface concentrations (Table 5) and non-steady-state diffusion coefficients (Table 6) were deducted for each test series.

Table 5: Chloride surface concentrations [m% binder]

[m% binder]	**REF**	**SAP_0.5**	**SAP_1**
Uncracked	4.17 ± 0.85	4.33 ± 1.12	7.34 ± 1.90
Realistic 100	4.23 ± 0.64	5.08 ± 1.31	6.13 ± 1.71
Artificial 100	4.03 ± 0.81	4.82 ± 0.67	6.82 ± 0.45

Table 6: Non-steady-state diffusion coefficients [10^-12 m²/s]

[10^{-12} m²/s]	**REF**	**SAP_0.5**	**SAP_1**
Uncracked	3.61 ± 2.10	4.80 ± 1.66	5.65 ± 1.55
Realistic 100	4.70 ± 3.11	7.56 ± 3.35	6.15 ± 2.80
Artificial 100	5.55 ± 2.09	9.43 ± 1.67	12.95± 2.96

The chloride surface concentration as well as the diffusion coefficient increase with the amount of SAPs added to the concrete. The more SAPs present in the concrete, the more macro pores are formed, resulting in a more porous matrix where chlorides can more easily penetrate. However, this increase was found not to be significant at a 5% level of significance

When looking at the effect of cracks on the diffusion coefficient, it can be seen that cracked samples show higher values, especially in the case of artificial cracks. However, this observation was found not to be significant for none of the studied mixtures.

F. CO_2 diffusion tests

Even after 12 weeks of exposure to 1 vol% CO_2, the penetration perpendicular to the artificial crack of 500 µm was not visible by spraying phenolphthalein or was very limited in case of cement paste (< 1 mm). This is not in correspondence with literature as Alahmad et al. [12] found that for crack widths > 60 µm, the perpendicular-to-crack carbonation depths are similar to the surface carbonation depth, for both artificial and realistic cracks. The lack of carbonation around the artificial cracks made by brass plates, suggests again that a reaction took place at the plate-mixture interface, resulting in an impermeable layer for CO_2. Further research should verify this hypothesis.

The average carbonation depth from the exposed surface for uncracked specimens is depicted in Figure 8.

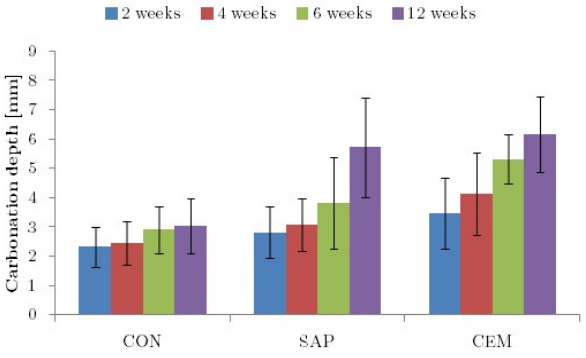

Figure 8: Carbonation depth, uncracked samples

The test series uncracked and cracked that were not periodically immersed in water, show two similar trends: 1) the penetration depth slowly increases in time, due to the low CO_2% in the carbonation chamber and 2) the cement paste has the largest penetration depth, followed by the concrete containing SAPs and the concrete mixture CON. The latter is explained by investigating the determined open porosity: the more open the structure of the concrete, the easier it is for the CO_2 molecules to penetrate into the concrete and thus the larger the penetration depth at a certain point in time. This trend is not valid for the cracked test series that was periodically immersed in water every four weeks. In this case, the SAP mixture showed larger penetration depths than the CEM mixture, see infra. Another reason can be found when looking at the amount of $Ca(OH)_2$ present in the mixture. The more $Ca(OH)_2$ is present, the more CO_2 can react and the more carbonation will occur. As the CEM mixture contains initially the largest amount of $Ca(OH)_2$, these mixtures show larger penetration depths. However, the carbonation rate will

slow down in time, resulting in smaller penetration depths compared to the concrete mixtures. Prolonged tests are needed to verify this explanation.

When the samples are periodically immersed in water, the obtained penetration depths are significantly lower than in case the samples are not immersed in water. In case of CON and SAP, the penetration depth is on average 36% and 32% respectively lower. For CEM, the penetration depth is even lower, namely 69%. This is due to the large open porosity and the further hydration of the high amount of unhydrated cement particles resulting in a more dense structure. When immersed in water, the open pores are filled with water instead of air. The carbonation diffusion is much slower in water than in air [13], resulting in smaller penetration depths. The water first needs to dry out before the CO_2 molecules can steadily penetrate into the concrete again.

In case of periodical immersion in water, the SAP mixture shows the largest penetration depths. This seems contradictory as due to the absorbed water by the SAPs, these samples will take longer to dry out, what should result in smaller penetration depths as the carbonation rate is slowed down. Also the further hydration of unhydrated cement particles will result in a less porous structure, which is beneficial for the resistance against carbonation. A possible explanation for the larger carbonation depths can be that carbonation requires a certain amount of water since CO_2 must dissolve first before reacting with Ca^{2+} present in the concrete and calcium carbonate can be formed. The small amounts of water provided by the SAPs seem to be ideal for this purpose, resulting in larger concentrations of dissolved CO_2 and as a consequence a higher production of calcium carbonate. This second mechanism is apparently more dominant than the first, resulting in higher carbonation depths at the end. It seems like the addition of SAPs at the concrete has no beneficial effect on the resistance against carbonation. This is contradictory to the findings of Mönnig [14], who found that the addition of SAPs caused a significant retardation of the carbonation rate.

IV. CONCLUSIONS

The addition of SAPs has a beneficial influence on the self-healing of 100 µm cracks subjected to wet-dry cycles, due to the combined effect of further hydration and the stimulated precipitation of calcium carbonate. Although none of the samples showed 100% healing at the surface, the mixtures containing SAPs show higher crack closing ratios (up to 64% compared to 24% in the reference mixture), even in the case of cracks that are too wide to close autogenously (> 30 µm).

The more porous structure due to the presence of SAPs leads to a significant increase in chloride penetration from the surface, as increasing the amount of SAPs from 0 m% to 0.5 m% and finally to 1 m% leads in each step to an additional ±2 mm penetration from the surface. The potentiometric titrations showed that both the chloride surface concentration and the chloride diffusion coefficient increase with the higher porosity as a result of the embedded SAPs. However, these results are found not to be significant at a 5% level of significance.

Several authors state that for crack widths smaller than a critical value, the chloride transport in the crack is very slow and the crack has almost no influence on the chloride transportation process and could thus assumed similar to uncracked concrete. Although there is no agreement on this critical value, it is clear that a reduction of the crack width due to stimulated self-healing upon the addition of SAPs, could have beneficial effects on the resistance against chloride penetration.

The addition of SAPs to the concrete has no beneficial effect on the resistance against carbonation. The combination of the higher open porosity together with the seemingly more easy dissolution of CO_2 in the small amounts of water stored by the SAPs, leads to higher penetration depths compared to the reference concrete. Furthermore, in case the swelling of the SAPs leads to partially blocking the open porosity, the pores will not be filled with water but remain filled with air. This results in even higher carbonation rates and hence larger carbonation depths. However, as these results are not in accordance with findings in literature and some even seem to be contradictory, further research on this topic is needed.

The second batch made in this thesis showed autogenous healing and it could be expected that this has beneficial effects on the resistance against both chloride penetration and carbonation. As chlorides and CO_2 can no longer penetrate in fully healed cracks, both the chloride penetration and carbonation of the cracked specimens would decrease to values similar to uncracked concrete. Even in the case the cracks are not completely filled by healing products, the reduced crack widths can impede chloride and CO_2 ingress, especially in case they are below a critical crack width.

A lot of research is still needed on the influence of SAPs on carbonation and chloride penetration, especially in cracked concrete. However, it is expected by the author that the stimulated self-healing of cracks due to the addition of SAPs can reduce and/or slow down the ingress of harmful substances through cracks significantly and thus increase the service life and durability of concrete structures.

REFERENCES

[1] Snoeck, D. and De Belie, N., "From straw in bricks to modern use of microfibers in cementitious composites for improved autogenous healing – A review," *Construction and Building Materials*, vol. 95, 2015, pp. 774–787.

[2] Li, V. and Yang, E.-H., *Self Healing in Concrete Materials*, vol. 100. 2008.

[3] Van Tittelboom, K. and De Belie, N., "Self-healing in cementitious materials- A review," *Materials*, vol. 6, no. 6, 2013, pp. 2182–2217.

[4] Van Den Heede, P., "Durability and Sustainability of Concrete with High Volumes of Fly Ash," 2014.

[5] Jang, S. Y., Kim, B. S., and Oh, B. H., "Effect of crack width on chloride diffusion coefficients of concrete by steady-state migration tests," *Cement and Concrete Research*, vol. 41, no. 1, 2011, pp. 9–19.

[6] NT Build 443, "Concrete, Hardened: Accelerated Chloride Penetration." 1995.

[7] Snoeck, D., Steuperaert, S., Van Tittelboom, K., Dubruel, P., and De Belie, N., "Visualization of water penetration in cementitious materials with superabsorbent polymers by means of neutron radiography," *Cement and Concrete Research*, vol. 42, no. 8, Aug. 2012, pp. 1113–1121.

[8] Brüdern, a.-E. and Mechtcherine, V., "Multifunctional use of SAP in strain-hardening cement-based composites," *International RILEM Conference on Use of Superabsorbent Polymers and Other New Additives in Concrete 15-18 August*, no. August, 2010, pp. 11–22.

[9] Mignon, A., Snoeck, D., Schaubroeck, D., Luickx, N., Dubruel, P., Van Vlierberghe, S., and De Belie, N., "pH-responsive superabsorbent polymers: A pathway to self-healing of mortar," *Reactive and Functional Polymers*, vol. 93, no. JUNE, 2015, pp. 68–76.

[10] Win, P. P., Watanabe, M., and Machida, A., "Penetration profile of chloride ion in cracked reinforced concrete," *Cement and Concrete Research*, vol. 34, no. 7, Jul. 2004, pp. 1073–1079.

[11] Audenaert, K., De Schutter, G., and Marsavina, L., "Influence of cracks and crack width on penetration depth of chlorides in concrete," *European Journal of Environmental and Civil Engineering*, vol. 13, no. 5, 2009, pp. 561–572.

[12] Alahmad, S., Toumi, a., Verdier, J., and François, R., "Effect of crack opening on carbon dioxide penetration in cracked mortar samples," *Materials and Structures*, vol. 42, no. 5, 2009, pp. 559–566.

[13] Thiery, M., Villain, G., Dangla, P., and Platret, G., "Investigation of the carbonation front shape on cementitious materials: Effects of the chemical kinetics," *Cement and Concrete Research*, vol. 37, no. 7, 2007, pp. 1047–1058.

[14] Mönnig, S., "Superabsorbing additions in concrete : applications, modelling and comparison of different internal water sources," 2009.

Contents

List of Acronyms & Symbols

A_c	Loaded area of a specimen's cross-section [mm^2]
$A_{accelerated}$	Accelerated carbonation coefficient [$mm/\sqrt{week}$]
A_{field}	Field carbonation coefficient [$mm/\sqrt{week}$]
AE	Acoustic emission
Ag^+	Silver ion
AgCl	Silver chloride
$AgNO_3$	Silver nitrate
C(x,t)	Chloride concentration at depth x and time t [m% binder]
$c_{accelerated}$	CO_2 concentration in accelerated carbonation test [%]
c_{field}	CO_2 concentration in field conditions [%]
C_i	Initial chloride concentration [m% binder]
C_s	Chloride concentration at the surface [m% binder]
$CaCl_2$	Calcium chloride
$CaCO_3$	Calcium carbonate
CaO	Calcium oxide
Ca^{2+}	Calcium ion
$Ca(OH)_2$	Calcium hydroxide
CCB	Color change boundary
CMOD	Crack mouth opening displacement
Cl	Chloride
Cl^-	Chloride ion
CO_2	Carbon dioxide
C-S-H	Calcium-silicate-hydrate
DIC	Digital image correlation
D_{nssd}	Non-steady-state diffusion coefficient [m^2/s]
EDX	Energy Dispersive X-ray
EPMA	Electron probe micro-analyzer
erf	Error function
F	Maximum load at failure [N]
f_c	Compressive strength [N/mm^2]
H_2CO_3	Carbonic acid
HNO_3	Nitric acid
H_2O	Water
ICP-MS	Inductively coupled plasma mass spectrometry
K^+	Potassium ion
LIBS	Laser Induced Breakdown Spectroscopy
LVDT	Linear Variable Differential Transformer
m%	Mass percentage of cement weight or binder weight
m_a	Mass of the saturated sample [g]
m_d	Mass of the oven-dried sample [g]
m_w	Mass of the saturated sample measured under water [g]

Mg^{2+}	Magnesium ion
$MgCl_2$	Magnesium chloride
MIP	Mercury intrusion porosimetry
Na^+	Sodium ion
NaCl	Sodium chloride
Na_2SO_4	Sodium sulphate
OH^-	Hydroxide
OPC	Ordinary Portland cement
p_o	Open porosity [%]
PDF	Probability density function
PVC	Polyvinylchloride
ρ	Density [kg/m³]
r_0	Initial maximum dimension dry SAP [µm]
r_{max}	Final maximum dimension swollen SAP [µm]
RCT	Rapid Chloride Test
RH	Relative Humidity
SAP	Superabsorbent polymer
SEM	Scanning electron microscope
SP	Super plasticizer
t	Exposure time to NaCl solution [s]
t	Exposure time to CO_2 [weeks]
TGA	Thermogravimetric Analysis
V_c	Volume of the container [m³]
vol%	Volume percent [%]
W_{all}	Weight of the container filled with fresh concrete [kg]
W_c	Weight of the container [kg]
(w/b)	Water-to-binder ratio [-]
$(w/b)_{add}$	Additional water-to-binder ratio [-]
$(w/b)_{eff}$	Effective water-to-binder ratio [-]
$(w/b)_{tot}$	Total water-to-binder ratio [-]
(w/c)	Water-to-cement ratio [-]
$(w/c)_{add}$	Additional water-to-cement ratio [-]
$(w/c)_{eff}$	Effective water-to-cement ratio [-]
$(w/c)_{tot}$	Total water-to-cement ratio [-]
$w_{dry\ SAP}$	Mass of dry SAPs [g]
$w_{fluid\ added}$	Mass of fluid before filtration [g]
$w_{fluid\ not\ absorbed}$	Mass of fluid that was not absorbed by the SAPs [g]
$w_{initial}$	Initial crack width [µm]
$w_{remaining}$	Remaining crack width [µm]
x	Distance from the exposed surface to the middle of the layer [mm]
x	Carbonation depth from the surface [mm]
XRD	X-ray diffraction
XRF	X-ray fluorescence spectrometry

1 Introduction

The formation of cracks in concrete structures is inevitable due to the low tensile strength of concrete. Cracks can create preferential pathways for the ingress of oxygen, chlorides, carbon dioxide and water into the interior of the concrete. These potentially harmful substances can facilitate the corrosion process of the steel reinforcement, resulting in a decreased durability and structural integrity of the concrete. In case no proper treatment is performed, costs for maintenance and repair can be very high.

Although concrete has the intrinsic property to heal cracks, the so called autogenous healing, this is only limited to very fine cracks (< 30 µm) and requires the presence of water. As in reality larger crack widths occur frequently and water is not always available, a lot of research is done in order to find mechanisms that can heal these larger crack widths, even in case of dry periods. A promising solution is the use of superabsorbent polymers (SAPs).

Superabsorbent polymers mixed in the concrete can absorb up to 500 times their own weight in aqueous solutions, resulting in a swollen hydrogel that can seal cracks. At a later stage in time, the SAPs can gradually release this absorbed water, leading to further hydration of unhydrated cement particles, and stimulate the precipitation of calcium carbonate. Due to these two mechanisms, the autogenous healing of the concrete is promoted and makes it even possible to close larger cracks (up to 100 µm).

Chloride-induced corrosion and carbonation-induced corrosion can be initiated by the penetration of chlorides and the carbonation into the concrete respectively. Due to corrosion, expansive products are formed at the concrete-reinforcement interface, resulting in spalling and cracking of the concrete as well as a reduction of the cross section of the steel reinforcement and a loss of bond between steel and concrete. It is assumed that the use of SAPs can stimulate healing of cracks in concrete, leading to a decreased chloride penetration and carbonation. This has beneficial effects for the durability and service-life of concrete structures as the risk of corrosion is lowered.

In this thesis, the stimulated self-healing of concrete due to the addition of SAPs is investigated. In a next step, chloride diffusion tests and CO_2 tests were performed in order to examine the efficiency of SAPs mixed into the concrete in the prevention of chloride and CO_2 ingress.

2 Literature review

In order to find out what is already known about the topic of this thesis, a systematic literature review is conducted. By doing this, possible gaps and/or contradictions as well as interesting results and comments on the topic can be found.

2.1 Methodology Literature Review

A systematic literature review is conducted using the principles and guidelines mentioned in the paper of Kitchenham and Charters [1].
As this paper mainly focuses on software engineering, some small adjustments were carried out in order to make it more suitable for the purpose of this master thesis. By doing such an extensive literature review, all existing research relevant to the specific subject of this thesis, can be accumulated in a systematic way, reducing the risk of not-including relevant papers or including non-relevant papers. In the next step, all this information can be used to classify and compare current research, trace contradictions, draw conclusions, identify gaps in the current research and, based on the latter, propose future research questions. In the following part of this paragraph, the different steps of the used search strategy are documented, as well as the assessed inclusion and exclusion criteria.

A systematic literature review involves several steps:

1. Specifying the research question(s);
2. Selection of primary studies, using inclusion and exclusion criteria;
3. Data synthesis based on primary studies.

It is important to remark that during the whole process of this literature review, all of these steps can be updated and refined based on the found information and increased understanding of the topic. In that way it is sometimes necessary to go one or more steps back in the process.

2.1.1 Specifying the research question(s)

The first and most important part of a systematic review is specifying the research question(s) in order to determine what should be examined. In this case the given title of the thesis “Testing of chloride penetration and carbonation of concrete with superabsorbent polymers” is used as a starting point, resulting in the following questions:

- Question 1: What is already known about testing of chloride penetration and carbonation of concrete healed by superabsorbent polymers?
- Question 2: Where does this research fit in the current research and knowledge?

As question 1 is still quite wide (and not much information will be found on this very specific topic), it can be further split in some sub-questions:

- Question 1a: What is already known about concrete healed by superabsorbent polymers?
- Question 1b: What is already known about testing of chloride penetration in concrete?
- Question 1c: What is already known about testing of carbonation in concrete?

In the end, the answers to these 3 sub-questions can be combined to provide a general answer to research question 1.

2.1.2 Selection of primary studies

The selection of primary studies is started from a paper set of 14 papers, provided by the counselors of this thesis ([2]–[15]). In a first step, these 14 papers were read thoroughly to have a first understanding of the topics of this master thesis. In the next step, a further search of primary studies is performed based on back- and forward snowballing of this basic set of 14 papers. In the case of forward snowballing, the papers that have cited at least one of the basic 14 papers were checked, resulting in 415 papers. In the case of backward snowballing, all the references of the basic paper set were checked, resulting in 337 papers. The digital sources searched to identify these primary studies were Google Scholar, ScienceDirect, Research Gate and the digital database of the library of the University of Ghent. After this step a total of 766 papers is obtained. However, a first practical restriction arises as the full text of some of these papers is not accessible through a UGent VPN connection (LIMITATION 1). This limitation leads to a paper set of 426 papers. This paper set however still includes duplicates which have to be eliminated, resulting in a paper set of 379 papers. In the next step only papers that are written in English or Dutch are retained (LIMITATION 2), leading to a paper set of 368 papers. The further selection of primary studies is based on inclusion and exclusion criteria that determine which studies are included in or excluded from the systematic literature review. These criteria are based on the research questions. At first, these inclusion and exclusion criteria are only applied on the title, abstract and keywords of the papers. In a second phase, these criteria are applied on the full text.

The following inclusion criteria are used:

- Any study that describes concrete healed by superabsorbent polymers
- Any study that describes the testing of chloride penetration in concrete
- Any study that describes the testing of carbonation in concrete

The following exclusion criteria are used:

- Any paper that mainly focuses on corrosion of reinforcement
- Any paper that focuses on numerical simulations and modeling in software of chloride ingress or carbonation of concrete
- Any paper that mainly focuses on mechanical properties of concrete healed by SAPs (for example compression strength, tensile strength, creep, fatigue, Young's modulus, ductility)

After applying the inclusion and exclusion criteria on the title, abstract and keywords a total of 130 papers is obtained. As this is still a large amount of papers to be studied, a further selection is done by applying the criteria on the full text, keeping in mind the assessed research questions. After this second selection, a paper set of 82 primary studies is obtained.
Figure 1 summarizes the different steps involved in the used selection procedure for the primary studies, together with the amount of papers in each step.

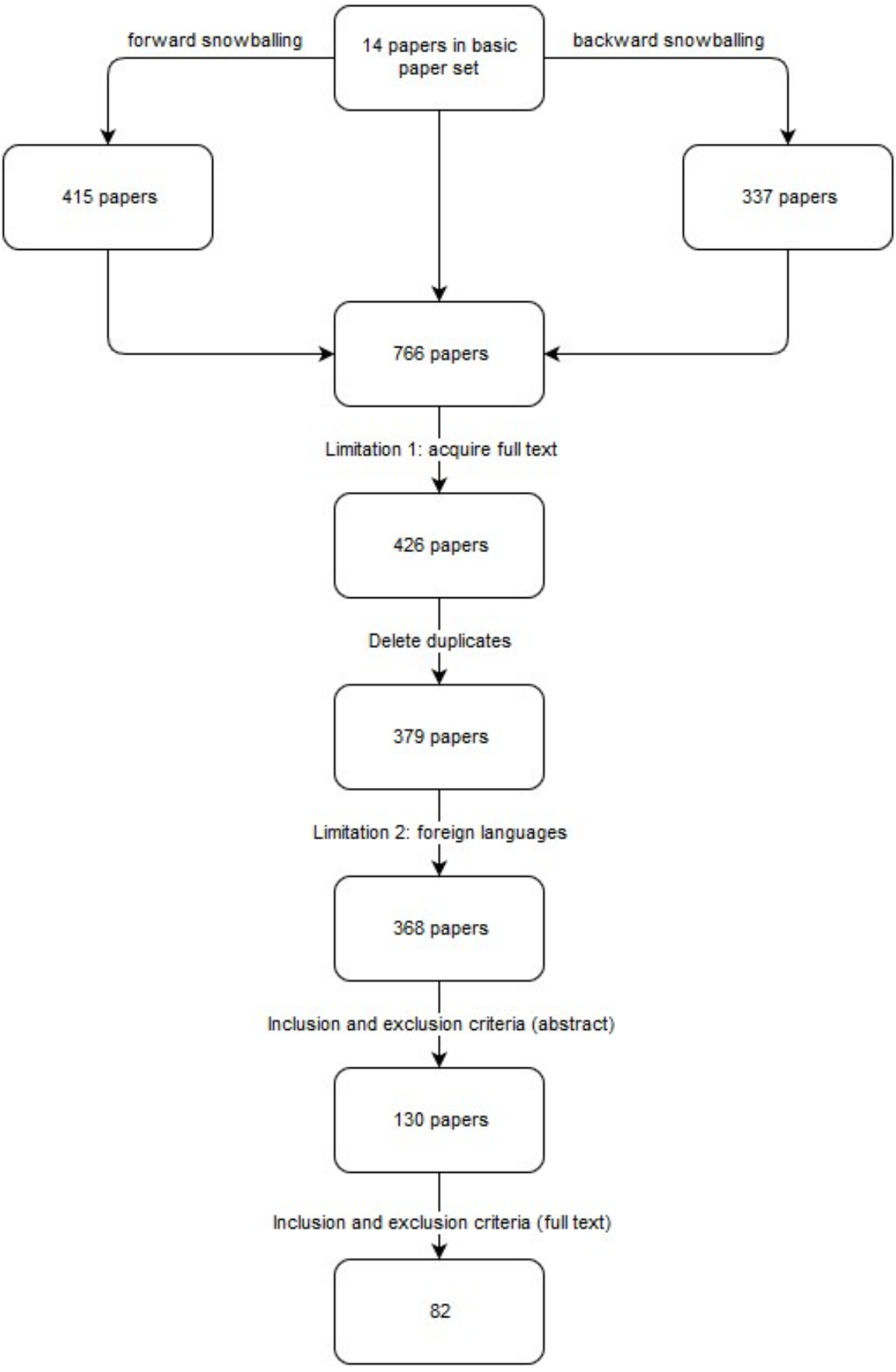

Figure 1: Selection procedure primary studies

2.1.3 Data synthesis based on primary studies

The third and last step in a systematic literature review is the extraction of data from the obtained primary studies in order to collect all the information needed to answer the review questions. In this case, it was examined whether each primary paper provides (part of) the answer to one or more research questions. In order to do this, these questions are further split up in smaller topics that deal with a specific part of the question, as illustrated in Table 1. In the end, all the obtained information is aggregated to provide an answer to the specific research question, based on the found literature.

Table 1: Classification of papers with respect to research questions

	Research Question 1a					**Research Question 1b**			**Research Question 1c**		
	SAPs	Cracks	Self-healing of concrete	Testing of self-healing	Concrete healed by SAPs	Chloride penetration	Influence of cracks	Testing of chloride penetration	Carbonation	Influence of cracks	Testing of Carbonation
Paper											

In Figure 2 an overview is given of the number of primary studies categorized according to the research questions. It is clear that only few papers are dealing with all three sub-questions at once. This confirms the earlier made choice to split up research question 1 in three sub-questions. Another observation is the fact that the amount of studies on carbonation is also limited in comparison to the studies on chloride penetration. This can be due to the fact that the consequence of chloride penetration, i.e. chloride-induced corrosion is more often noticed in real structures compared to carbonation-induced corrosion, as the latter takes much more time to manifest itself.

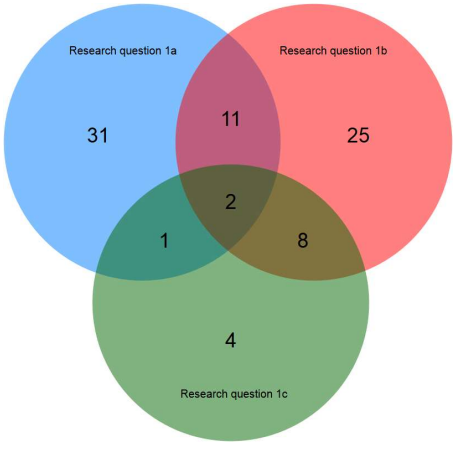

Figure 2: Classification of primary studies based on the research questions
Question 1a: What is already known about concrete healed by superabsorbent polymers?
Question 1b: What is already known about testing of chloride penetration in concrete
Question 1c: What is already known about testing of carbonation in concrete?

In the following parts, the found literature is categorized and presented in order to answer the previously identified research questions.

2.2 Concrete healed by superabsorbent polymers

Research question 1a "What is already known about concrete healed by superabsorbent polymers?", is further split in following topics:

- Superabsorbent polymers (SAPs);
- Cracks;
- Self-healing of concrete;
- Testing of self-healing and self-sealing;
- Concrete healed by SAPs.

2.2.1 Superabsorbent polymers (SAPs)

Superabsorbent polymers (SAPs) are cross-linked polymers that have the ability to absorb a large amount of liquid from their surroundings and retain it within their structure without dissolving [16]. SAPs can absorb 500 – 1500 times their own weight in aqueous solutions due to osmotic pressure, resulting in the formation of a swollen hydrogel ([11],[17]). The amount of water that is absorbed by the SAPs is depending on the properties of the SAPs on the one hand and parameters of the exposure environment like temperature, relative humidity, pressure and ionic composition of the exposure liquid on the other hand ([17],[18]). Reversely, when subjected to drying, the SAPs will shrink back to their initial dry size. The absorption capacity of SAPs can be measured in different ways, as described by Jensen et al. [17]: gravimetric methods, optical microscopy or the tea bag method. Gravimetric methods are usually performed on a single SAP particle. The particle is submerged into the liquid of interest (e.g. tap water, demineralized water). At certain points in time the particle is removed from the liquid, the particle surface is dried with absorbent paper, the particle is weighed and put back in the liquid. This method is very simple but requires relatively large particles, at least mm-size in the dry state, to enable handling of the particle and to ensure a proper removal of the water from the particle surface. However, as the particle size of SAPs used in cementitious systems is typically much smaller than millimeters, optical microscopy is often used to measure the absorption capacity of a single SAP particle, provided that the particle has a regular geometry. In this method, the diameter of the particle is measured by an optical microscope in both the dry state and the swollen state. From this change in diameter, the absorption capacity can be measured, although in an uncertain way since measurement uncertainties are scaled to the third power as volume ~(diameter)^3. The abovementioned

methods focus on the measurement of the absorption capacity of a single SAP particle. However, in practice, multiple SAP particles will be present and exposed to the liquid. The teabag method is frequently used to measure the absorption capacity of SAP particles, as it is easy and quick. In this method, dry SAP particles are placed in a permeable bag which is submerged into a fluid. The difference in mass before and after submersion equals the absorption capacity. However, this technique leads to a small overestimation of the absorption capacity as it is impossible to remove all the water from dry SAPs.

Different types of SAPs are available. On a chemical base, two extreme types can be distinguished: ionic and non-ionic polymers [17]. Commercial SAPs are mostly ionic polymers due to their higher absorption capacity. Another distinction can be made on the type of cross links between the polymers: covalent, ionic or hydrogen. These cross links are essential parts of the SAPs as they prevent the SAPs from dissolving [17]. Another classification is based on the type of production method of the SAPs: mass polymerization, emulsion polymerization, solution polymerization or suspension polymerization. The production process has large influence on the appearance and physical properties of the SAPs ([17],[19]).

Nowadays, SAPs are used in a variety of industries: from the hygiene, medical and agricultural industry to firefighting, food packaging, and the building industry ([11],[19]).

2.2.2 Cracks

Due to the low tensile strength of concrete, cracks are inevitable in concrete structures. Cracks also can be induced by thermal effects, shrinkage, creep, fatigue, freeze-thaw cycles, corrosion of reinforcement, impact, alkali-aggregate reaction, overloading etc. ([20],[21],[22]). These cracks provide preferential pathways for the ingress of harmful substances like for example water, oxygen, carbon dioxide, salts, sulfates and chlorides. When these substances reach the steel reinforcement of the concrete, it will lead to corrosion, with all its negative consequences for the durability, integrity and service-life of the structure. In order to simulate real behavior of (cracked) concrete in test set ups or to investigate the efficiency of self-healing and self-sealing of cracks, cracks have to be introduced in the samples, preferably in a controlled and reproducible way. In this paragraph, a distinction is made between artificial and realistic crack formation.

Artificial cracks, also called notches, are created by saw-cutting [22] or by putting thin metal plates in the mould before casting the concrete ([23],[24],[25]). These plates are later on removed before the concrete totally hardens, resulting in a straight crack with parallel crack walls and a crack width that does not differ that much from the thickness of the metal plates. Artificial cracks have as advantages

the high reproducibility of cracks as well as the good control of the crack width, depth and length. A disadvantage however is the formation of parallel walled cracks, which is not in accordance with realistic, mostly tapered cracks. Furthermore, by using this technique one single crack is obtained in the sample, whereas in reality multiple, connected cracks are formed, resulting in different crack densities [26]. Notwithstanding the fact that these cracks are not realistic, they are often used in case the results will be implemented in numerical models and simulations due to their modeling simplicity ([20],[21],[25]).

Realistic cracks are induced by means of a Brazilian splitting test [27], a wedge splitting test [28], three-point bending test or four-point bending test [29], the use of ring shaped discs with an expansive core [5] or rapid freeze-thaw exposure [6]. In order to control crack formation in these cases, different techniques can be used: linear variable differential transformers (LVDT) and crack mouth opening displacement (CMOD) ([30],[31]), acoustic emission (AE) [32], digital image correlation (DIC) ([28],[33]), electrical resistance measurements [28] or ultrasonic wave propagation [29]. Despite these controlling techniques, realistic crack formation results in less controllable crack widths and depths in comparison to artificial crack formation. Especially in the case of mechanical loading some closure of the crack during unloading, the so-called crack recovery, has to be taken into account [31]. The properties of cracks induced with one of the abovementioned techniques however, for example the crack tortuosity, connectivity and crack wall roughness, will resemble real cracks in concrete structures in a better way, but are as a disadvantage very hard to model. Another difficulty concerning the formation of realistic cracks, is the heterogeneity of concrete (especially due to the presence of aggregates) which will result in different crack geometries as cracks are mostly formed at the interface paste-aggregate [28]. This is in contrast to the artificial cracks where straight cracks are created at the predefined position of the metal plates.

Both crack formation techniques thus have their advantages and disadvantages and the choice is depending on the purpose of the test setup. Crack width measurements are mostly done at several locations along the crack length, by means of an optical microscope ([20],[22],[23]), fluorescence microscopy [29] or a scanning electron microscope (SEM) [23] amongst others.

2.2.3 Self-healing of concrete

Self-healing in cementitious materials, e.g. concrete, can be classified into two main groups: (improved) autogenous healing and autonomous healing [34]. As concrete itself has the intrinsic property due to the composition of the cementitious matrix to heal cracks, this phenomenon is called autogenous healing. This healing mechanism can be improved by the restriction of crack widths, increasing the

amount of reactive binder agents and the implementation of additional water [34]. In the case of autonomous healing, the healing is obtained by incorporating self-healing mechanisms inside the concrete material. The material to close the crack does not originate from the concrete itself, but originates from another, external source [35]. A lot of advantages are coupled with self-healing concrete: damage is repaired without any external intervention, a reduction of maintenance and repair costs, healing of cracks that are not accessible or not visible, decreased risk of corrosion etc. In the following paragraphs these two mechanisms, together with some examples, are discussed.

Different mechanisms and their combined effect contribute to the autogenous healing of cracks ([34],[35]): the continued hydration of unhydrated cement particles, the carbonation of calcium hydroxide $Ca(OH)_2$ resulting in the precipitation of calcium carbonate crystals $CaCO_3$, the swelling of calcium silicate hydrates (C–S–H) and the blocking of cracks by loose particles or impurities. No agreement is found in literature on which of these mechanisms is the most dominant one [36]. However, from environmental conditions a first indication of the dominant mechanism can be obtained as further hydration only requires the presence of water inside the crack whereas for $CaCO_3$ precipitation both water and CO_2 need to be present. Snoeck and De Belie [35] and Li and Yang [37] stated that there are three needed conditions for autogenous crack healing to occur. These are the presence of specific chemical ions (e.g. Ca^{2+}, CO_2, unhydrated particles); the exposure to humid environmental conditions (e.g. wet/dry cycles, submersion in water) and small crack widths (<30 µm). This last requirement follows from the observation that cracks smaller than 30 µm show complete healing, whereas cracks smaller than 150 µm only show partial healing. However, when examining literature, different maximum crack widths that can be healed by autogenous healing are reported: 30 µm [35], 20 -100 µm [33], 50 µm [38], 150 µm [39] and 200 µm [40]. A reason for this can be found in the fact that a lot of other factors influence the maximum width that can be healed by autogenous healing: shape of the crack, exposure conditions (temperature, relative humidity), cause of cracking, composition of the concrete, age, curing conditions… However, it is confirmed by every author that larger cracks are more difficult to heal. The mechanisms to improve autogenous healing follow directly from these conditions. A first improvement can be obtained by increasing the amount of reactive binder agents, e.g. partial cement replacement by fly ash or blast-furnace slag [40]. This is not only beneficial for the environment, but will also result in more unhydrated cement particles that can hydrate later on and in concrete with higher amounts of Ca^{2+} that can react with CO_2 to form $CaCO_3$. In order to provide additional water into the concrete, SAPs can be used. Once in contact with water, the SAPs at the crack face will absorb water entering through the crack and swell, resulting in sealing of the cracks. The absorbed water can be released afterwards towards the

cementitious matrix to stimulate the autogenous healing. In order to obtain small crack widths, microfibers can be mixed into the concrete ([35],[41]).

In the case of autonomous healing, the healing is obtained by incorporating self-healing mechanisms inside the concrete material. Crack initiation will trigger the self-healing activity, the repair components are transported towards the damage and the crack is healed [33]. The material to close the crack does not originate from the concrete itself, but originates from another, external source [35]. Autonomous healing of cracks in concrete can be obtained by different means: incorporation of bacteria ([34],[42]), addition of SAPs ([33],[38],[43],[44]), release of encapsulated healing agents (one or two components agents) in spherical, cylindrical or tubular capsules ([33],[45],[46]) or granulated expansive agents [47]. More information on the different types of autonomous healing in concrete can be found in an extensive review by Van Tittelboom and De Belie [48] or by Li et al. [41].

Besides the difference between autogenous and autonomous self-healing, another subdivision is made between self-healing and self-sealing [35]. Self-sealing focuses on the closure of the crack, possibly without strength regain, whereas self-healing includes additionally the regain in mechanical properties. Mechanical properties, like for example stiffness and strength, will mostly be inferior after healing compared to the virgin specimens ([32],[48]). Çopuroglu et al. [29] uses other definitions for self-healing and self-sealing: crack sealing is the recovery against environmental actions, whereas crack healing is the recovery against mechanical actions.

2.2.4 Testing of self-healing and self-sealing

The healing efficiency is usually evaluated by reloading the healed specimen and comparing the obtained mechanical properties to the original ones without healing [35]. For this purpose, the classical tests to obtain the mechanical properties of a concrete specimen are used: compression test, tensile test, 3-point bending test, 4-point bending test, impact loading… As these tests are often used and well-known, they are not further discussed in this review.

The self-sealing efficiency of cracked concrete is generally evaluated by measuring the decrease in water permeability and air flow through a crack. The last few years more sophisticated methods like neutron radiography and tomography are more frequently used in the view of determining the self-sealing efficiency.

An overview of frequently used techniques to evaluate the healing and sealing efficiency is summed up by Van Tittelboom and De Belie [48] and Çopuroglu et al.

[29]. In the next paragraphs, the techniques used in the selected primary studies are discussed.

Due to the ongoing hydration of unhydrated cement particles, heat is produced. This heat flow can be measured using isothermal calorimetry. The produced heat flow give rise to a temperature gradient across the sensor, generating a voltage. As this voltage is proportional to the heat flow, this is an indication of the amount of further hydration of the sample [40].

Optical microscopy in combination with image analysis is often used to see healing of the cracks at the surface. In this case especially the precipitation of white crystalline material of the $CaCO_3$ crystals can be observed as well as its evolution in time. With this technique, only healing at the surface can be examined. Other techniques like thin section analysis ([14],[49]) and computed micro tomography [45] are better suited to examine the inner parts of the crack. Another frequently used technique to visualize the crystal deposition is Scanning Electron Microscopy (SEM) [43].

Neutron radiography can be used to visualize the capillary water uptake in cement based samples. The principle of neutron radiography consists of recording the intensity of the radiation that passes through an object. As the attenuation of the radiation in the object depends on the isotopic number density and the geometry of the sample, the image contains qualitative and quantitative information on the composition of the sample. When the sample is rotated during this test, three-dimensional neutron tomographs are obtained ([2],[45],[50]).

X-ray radiography and X-ray tomography are based on the same principles as neutron radiography and tomography, the only difference is that in this case X-rays are used instead of neutrons. With X-ray diffraction analysis (XRD), the spacing between layers or rows of atoms can be determined and in this way, the crystal structure of the material can be found [29].

Raman spectroscopy is a technique based on the inelastic scattering of monochromatic light from a laser. From the shift in frequency of photons in monochromatic laser light due to the interaction with a sample, information about the chemical composition of the sample can be obtained [29].

A simple way to examine the effect of self-healing of a crack is a water permeability test. Different alternatives of this test exist and are widely used: low-pressure water permeability test and high-pressure water permeability test ([2],[15]). The principle of these test is the following: water pressure is generated at the top of a sample by means of a water column. The amount of water that leaks through the sample is measured in time. From this, the water permeability of the

sample can be calculated using Darcy's Law [29]. A modified version on this test created by Van Tittelboom et al. ([2],[45]) evaluates the crack healing efficiency by measuring capillary water absorption. With this absorption test, results can be obtained within a few hours. Since concrete in practice will almost never be fully saturated, absorption will be the dominant mechanism for the water uptake in most cases, resulting in more realistic results compared to the water permeability tests.

Besides the water permeability, the air permeability can also be an indication of self-sealing efficiency of concrete. Mostly liquid methanol or oxygen as a gas source is used. From this test, the air permeability coefficient can be calculated [14].

Another way of evaluating the self-healing of concrete according to Çopuroglu et al. [29], makes use of the difference in osmotic pressure between samples with healed and non-healed cracks. However, none of the selected primary studies used this technique.

Resonance frequency analysis can also be used as the presence of cracks makes it more difficult for elastic waves to propagate through cementitious materials. When applying this test before and after healing, the extent of healing can be determined [39].

Ultrasonic measurements are based on the fact that ultrasonic waves travel at different speeds in different mediums. A speed up to 5000 m/s can be reached in hardened concrete, where the speed in water (1480 m/s) or in air (350 m/s) is much lower. As a result, the presence of cracks (filled with air or water) will lead to an increase in transmission time. However, when the cracks are healed, the waves will be able to travel at a higher speed through the crack and by this the transmission time will be reduced again ([6], [51]).

Acoustic emission was used by Granger et al. [32] and De Belie et al. [33] to qualify autogenous crack healing. The principle of this technique is based on detecting elastic waves by means of transducers on the surface of the specimen. As these waves are generated due to dislocations and cracks, the received signal can be used to identify possible self-healing of cracks.

Infrared spectroscopy is based on the vibrations of the atoms of a molecule. It can be used to determine the chemical composition of formed precipitates during self-healing, for example $CaCO_3$ crystals [43].

It is stated by several authors that the most accurate results are obtained when different techniques are combined.

2.2.5 Concrete healed by SAPs

The disadvantage of autogenous healing of cracks is the fact that this is only limited to very fine cracks. Therefore, more and more attention is paid by researchers to autonomous healing, for example by the addition of superabsorbent polymers (SAPs) in concrete. In Figure 3 it can be seen that research on concrete healed by SAPs is only recently conducted.

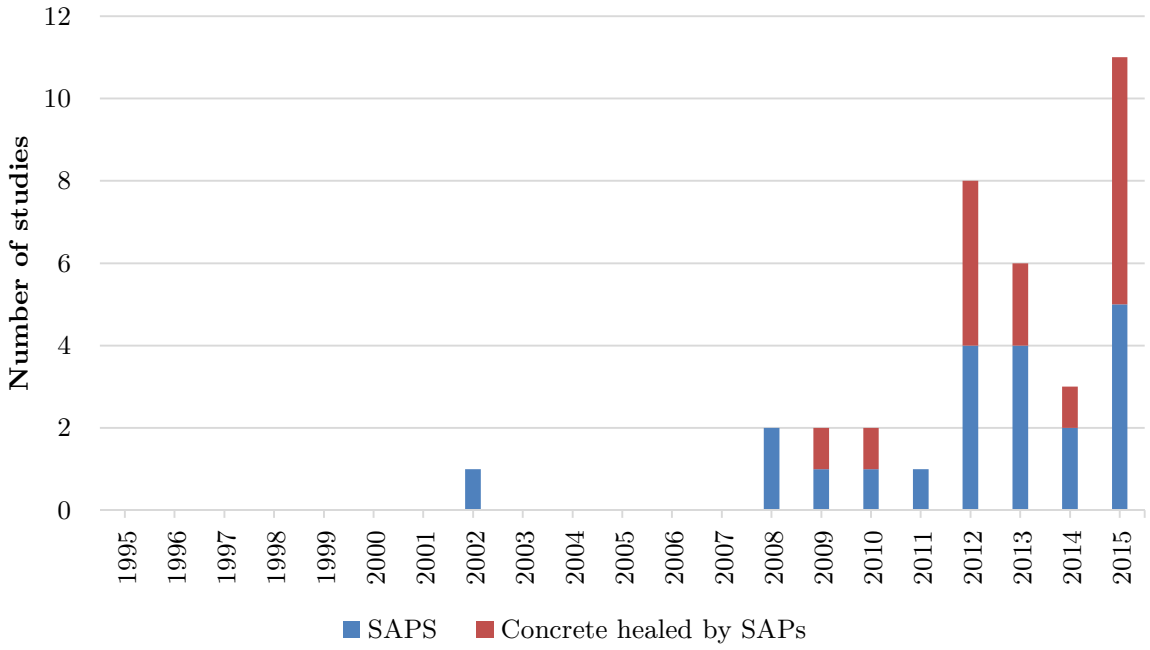

Figure 3: Evolution in time of the number of studies dealing with concrete healed by SAPs

SAPs are already used for several reasons in concrete, as stated in a report by Mechtcherine and Reinhardt [52] on the applications of SAPs in concrete. During preparation of the concrete mixture, SAPs will take up part of the mixing water and form water-filled inclusions. As SAPs act in this way as water reservoirs, they can provide efficient internal curing of concrete [52], reducing autogenous shrinkage ([11],[52]) and promoting further hydration of cement [38]. SAPs will gradually release their water and shrink, leaving empty macro pores in the concrete increasing the porosity of the matrix [53].

With regards to compressive strength, Jensen et al. [16] found an increase of the 28 days compressive strength of concrete with SAPs due to the improved curing conditions that compensate for the increased porosity. Sherir et al. [51] obtained similar results. Mignon et al. [43], Snoeck et al. ([13],[15]) and Mechtcherine and Reinhardt [52] however found a significant reduction of both bending and compressive strength when SAPs are added, due to the formation of macro pores

due to the shrinkage of the SAPs. However, these macro pores are beneficial for the freeze/thaw resistance of concrete as it increases the air entrainment ([16],[54]).

SAPs are added to the concrete during mixing and by this the rheology of the fresh concrete is altered, e.g. change in w/c ratio, plastic viscosity, thickening of the concrete [52]. As the SAPs absorb part of the mixing water, this has a negative effect on the workability and therefore additional water (possibly in combination with super plasticizer) needs to be added to compensate for the loss in workability ([43],[53]).

As already mentioned earlier, SAPs can promote autogenous self-healing and self-sealing of cracks. SAPs at the crack faces swell in contact with water and seal the cracks. This water can be released towards the cementitious matrix to stimulate the autogenous healing. Snoeck and De Belie [49] found that concrete healed with SAPs was able to regain up to 75% of their mechanical properties after the first reloading and up to 66% after second reloading.

When liquid enters a crack, the SAPs along the crack face will swell and block the crack. This self-sealing of the crack is reflected in a decrease of water permeability through the crack and is already studied by several authors ([2],[13],[33],[43]). In this way, harmful substances dissolved in water will penetrate the concrete to a lower extent which is beneficial for the durability of the concrete structure.

The abovementioned studies differ from each other not only in their research subjects, but also in the examined parameters like for example the type of SAPs, the added amount of SAPs (expressed in mass-% of binder or cement), concrete mixtures and testing methods. Due to this, it is not always possible to compare the results of different studies.

2.2.6 Summary

From the literature study concerning self-healing concrete with SAPs, it is clear that this research mainly focuses on the general concepts, mechanical properties and water permeability. The addition of SAPs has a beneficial influence on both the autogenous and autonomous crack healing and sealing. Due to the swelling of SAPs upon contact with water, cracks are blocked. This absorbed water can be released later on to stimulate the autogenous healing, by further hydration of unhydrated cement particles and the precipitation of $CaCO_3$. The addition of SAPs also has a positive influence on some properties of the hardened concrete: an increase in freeze/thaw resistance and a reduction in water permeability. However, no consensus is found on the influence of SAPs on the strength of concrete. A lot of research on the addition of SAPs in concrete is still ongoing or needs to be done in the future in order to obtain more insights in this subject.

2.3 Testing of chloride penetration in concrete

Research question 1b "What is already known about testing of chloride penetration in concrete?" is further split up in following topics:

- Chloride penetration in concrete;
- Influence of cracks on chloride penetration;
- Testing of chloride penetration.

From Table 22 in the appendix, it is clear that there are a lot of studies dealing with chloride penetration and testing of chloride penetration in concrete. A reason for this can be found in the purpose of these studies: providing more insight in the dangerous and severe chloride-induced corrosion of steel reinforcement in concrete structures. However, not all of these studies are dealing with the influence of cracks on this phenomenon (see Figure 4). In the following paragraphs this extensive amount of information is summarized and categorized, in order to find out whether these studies discuss the same topics and whether results from different studies are consistent with one another or inconsistent.

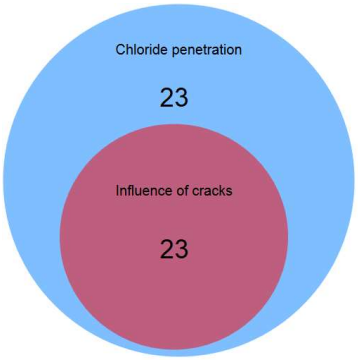

Figure 4: Primary studies dealing with chloride penetration and the influence of cracks on chloride penetration

2.3.1 Chloride penetration in concrete

The main external sources of chlorides in concrete are seawater and deicing salts. However chlorides inherently present in components of the concrete mix, like for example calcium chloride or contaminated aggregates dredged from sea, are possible sources as well.

The transport of chlorides in fully saturated hardened concrete is due to two different mechanisms, acting at the same time: diffusion and migration [55]. The most governing mechanism is diffusion. This transport mechanism is due to the leveling out of concentration differences and is described by means of Fick's first and second law [8]. The second transport mechanism, migration, has as driving force the presence of an external electrical field, which in field conditions is not

present. Due to this electrical field, the chlorides in solution will migrate towards a positive electrode in a very fast way, with the result that no chloride binding can take place. This mechanism is described by the Nernst-Planck equation [27]. It is however stated by Zhou et al. [56], Ŝavija et al. [57], Lu et al. [58] and Boddy et al. [59] that in some cases, other transport mechanisms like absorption, capillary suction or convection can become more dominant than the diffusion mechanism. This is especially the case for non-saturated concrete, for example in tidal zones. However, research on this complex topic is still on-going to provide more insight on these topics.

A distinction is made between total chloride content, free chloride content and bound chloride content in the concrete [55]. The last one is a measure for the capacity of the concrete to bind chlorides to the formed hydration products. A high chloride binding capacity is favorable concerning the resistance against chloride-induced corrosion for several reasons [55]: as it reduces the total amount of free chlorides in the concrete, it reduces both the risk for and the rate of chloride-induced corrosion. Another positive effect of a high binding capacity is the production of Friedel's salts, which reduce the porosity of the microstructure [60].

After a certain time, a critical chloride content will reach the steel reinforcement in the concrete, resulting in the local destruction of the protective passivation layer around the rebars that was formed in the highly alkaline environment of the concrete [55]. This event marks the start of the so called chloride-induced corrosion, also called the corrosion initiation. This type of corrosion is called pitting corrosion and has a detrimental effect on the durability and integrity of the structure, as it leads to cracking and spalling of the concrete as well as a reduction of the cross section of the steel reinforcement and a loss of bond between steel and concrete [56].

When looking in literature, a lot of different critical chloride contents are mentioned. Alonso and Sanchez [61] and Angst et al. [62] both made an extensive study on different critical chloride contents in literature. The reason for this variety in values can be due to several reasons: different definitions of critical chloride content (free chlorides versus total chlorides), the test method used to determine this content, different testing conditions and last but not least the extensive amount of factors that can have an influence on this critical content, as summarized by Angst et al. [62]: steel-concrete interface, concentration of hydroxide ions in the pore solution, electrochemical potential of the steel, binder type, surface conditions of the steel, moisture content of the concrete, oxygen availability at the steel surface, w/b ratio, degree of hydration, temperature, chloride source, chemical composition of the steel etc. To make it even more complex, some of these influencing factors are interrelated. According to Angst et al. [62] the corresponding range for the free critical chloride content amounts to 0.07 to 1.16 m% binder. According to Maes et al. [8] the most common values for

the critical chloride content are ranged between 0.40 and 2.50 % compared to the mass of the binder or 0.06–0.37 % compared to the mass of concrete. From this it is clear that defining one unique value for the critical chloride content is not feasible.

Summarizing the main influencing factors on chloride penetration in concrete mentioned by different authors ([10],[56],[61],[63],[64]): surface chloride concentration, chloride source, temperature, relative humidity, carbonation, always immersed versus wet-dry cycles (e.g. tidal zone), moisture content of concrete, exposure time, curing conditions and time, age of the concrete, cover thickness, initial chloride content within the concrete, chloride binding capacity, chloride resistivity, concrete mixture, cement type, replacement of cement by additions, w/b ratio, alkalinity of the concrete, loading of the concrete, self healing of the concrete… Remark that this is not a finite list.

2.3.2 Influence of cracks on chloride penetration

Chloride migration and diffusion coefficients derived for uncracked concrete should only be used in the case the concrete is indeed uncracked, which is in reality mostly not the case due to different causes such as shrinkage, thermal effect, loading etc. [23]. The effect of cracking on chloride permeability of concrete is already studied by several authors and is summarized in the literature review of Ŝavija and Schlangen [10] and Gu [21]. Cracks are preferential pathways for the penetration of chlorides into concrete, resulting in chloride-induced corrosion of the steel reinforcement which endangers the durability and service-life of the concrete structure. Microstructure, permeability, cracking and durability are thus inseparably connected with each other and should be considered together to achieve a durable concrete structure [31].

A lot of studies were done by several authors, with different studied parameters concerning cracks: crack width, crack depth, crack density and artificial versus realistic cracks together with other influencing parameters like concrete mixtures with and without supplementary cementitious materials, w/b ratio, curing conditions, age of the concrete and self-healing of the cracks. In the following paragraphs some of the most remarkable results are summed up. A general observation that was found by almost all researchers was that in the case of cracked concrete, the penetration of chlorides happens much faster than in uncracked concrete, resulting in a reduction of time to corrosion initiation.

The crack width is considered to be the most important factor that influences the chloride transport in cracked concrete. Therefore, many studies are dealing with this topic. Ismail et al. [5] studied the influence of different crack widths on chloride penetration in concrete. He found that for cracks bigger than 205 µm the

chloride penetration perpendicular to the crack wall is similar to that for the surface. Fine cracks in the range of 80 – 100 µm showed that diffusion still occurs, but at a lower level, whereas for cracks smaller than 30 µm all chloride diffusion is blocked along the crack. Another observation concerning crack widths is made by Jang et al. [30]: the diffusion coefficients do not increase with an increase of crack width up to about 80 µm. Over 80 µm in crack width however, the diffusion coefficients start to increase in a linear way. Other authors also did research concerning the crack width below the cracked concrete showed a similar behavior as sound, uncracked concrete. Aldea et al. [65] concluded that concrete with cracks < 200 µm has a similar behavior as sound, uncracked concrete. Van den Heede et al. [23] performed a similar study, but stated that uncracked behavior exists for crack widths below 50 µm. Audenaert et al. [66] and Djerbi et al. [27] found a bilinear relation between chloride migration and a crack width in the range of 100 to 300 µm, whereas Maes et al. ([9],[24]) found a quadratic relationship in this range. Marsavina et al. [25] however did not find a pronounced influence of the crack widths on the chloride penetration depth. The effect of cracking on the chloride diffusion can be divided in three cases according to Jin et al. [7]: 1) when the width is less than 30 µm, its effect can be neglected due to self-healing; 2) when the width is more than 100 µm, two-dimensional diffusion will happen in the cracking zone; 3) when the crack width is between 30 and 100 µm, chloride diffuses into concrete along and perpendicular to the crack surface simultaneously.

Win et al. [3], Maes et al. [24] and Djerbi et al. [27] found that the chloride penetration at the crack tip is higher than from the exposed surface, because of the combined effect of horizontal and vertical chloride penetration and the existence of microcracks along the crack surface.

Only a few studies consider the effect of crack density on the chloride transport in cracked concrete. Jacobsen et al. [6] measured crack densities by counting the number of cracks traversing parallel lines of approximately 5 mm distance. He found that internal cracking increased the chloride penetration rate up to 7.9 times, but could be reduced up to 35% due to self-healing of the cracked specimens when stored in water. Mu et al. [26] also studied the influence of multiple cracks rather than one single crack on the chloride penetration. It was found that for samples with more than three cracks, the effect on the chloride diffusion coefficient was not remarkable. For less than four cracks an almost linear relationship between the diffusion coefficient and number of cracks is found. Also Win et al. [3] studied the effect of adjacent cracks by inducing two cracks in the same sample using a four-point bending test.

Ismail et al. [5], Jacobsen et al. [6], Van den Heede et al. [23] and Maes et al. ([9],[24]) stated that autogenous self-healing can significantly reduce the rate of chloride migration and the chloride penetration depth in cracked concrete, but

further research on this topic is recommended as this was not the main topic of their research.

A lot of formulae and numerical models to predict the chloride penetration depth in concrete can be found in literature for both cracked and uncracked concrete ([56],[57],[58],[66],[67]), but as the focus in this thesis lies on experimental testing, this falls beyond its scope.

2.3.3 Testing of chloride penetration

When testing chloride penetration in laboratory conditions, three kinds of chloride source are mostly used: actual sea water, simulated sea water solution that has the same ion proportioning as actual sea water or an artificial solution that has approximately the same chloride concentration as actual seawater with use of only one salt, e.g. NaCl [55].

A lot of different tests exist to determine the chloride content in concrete. An overview of tests can be found in the Round-Robin test on chloride analysis in concrete, carried out by the Technical Committee RILEM TC 178-TMC [68] or in the literature review of Stanish et al. [69]. A major distinction can be made between tests that determine the total chloride content (extracted by means of an acid-solution) and tests that determine the free chloride content (by measuring the water-soluble chloride content) [70]. Another way of classifying chloride tests is looking at the transport mechanism of chlorides that is used in the test: diffusion or migration. Sometimes a distinction is made on the basis whether time has an effect on the results or not. In the case the studied parameter changes in time, this is called a non-steady-state test, whereas in the case the parameter stays unchanged in time, this test is called steady-state. In the following paragraphs the most frequently used techniques are briefly discussed.

One of the easiest methods to apply in order to get an indication of the chloride penetration depth is the colorimetric method using $AgNO_3$. In this test, a 0.1 mol/l $AgNO_3$ solution is sprayed onto the surface of the split sample. By means of a color change boundary the free chloride penetration front is visualized: black in the case no chlorides are penetrated into this zone, white if the zone is penetrated by chlorides. As this test is cheap, easy and quick, it is often used in practice in both laboratory conditions and in field conditions ([71],[72]). However, no consensus can be found in literature concerning the chloride concentration corresponding to this color change boundary ([63],[72],[73]). There exist few other colorimetric procedures that are less frequently used, but similar to the one described in this paragraph. More information on these tests can be found in [71].

A test to determine the free chlorides in concrete embodies squeezing the hardened pastes under high pressure. As this is quite difficult and complex to do on concrete samples, another technique called leaching is more often used in this case [74].

The principle of the Rapid Chloride Test (RCT) ([55],[63]) is easy: a calibrated electrode is submerged into a prepared solution containing chloride ions. The voltage readings during the test are recorded and by means of a predetermined calibration curve, these voltages are converted into chloride content in percentage by concrete weight. This test can be done for both acid soluble chloride and water soluble chloride concentration, the only difference is the preparation of the solutions. The main advantage of this test is that it can be performed quickly and easily.

Rapid chloride migration test (non-steady-state test) in accordance with NT Build 492 [75]: An external electrical potential is applied axially across the cylindrical specimen which forces the chloride ions to migrate into the specimen. After a certain test duration (e.g. 24 hours), the specimen is axially split and a silver nitrate solution is sprayed on the freshly split sections. The chloride penetration depth can then be measured from the visible white silver chloride precipitation, after which the non-steady-state chloride migration coefficient can be calculated from this penetration depth. An advantage of this test is that results are obtained within a few hours.

Accelerated chloride diffusion test according to NT build 443 (non-steady-state test) [76]: The test specimen is immersed in a saturated $Ca(OH)_2$ solution until a constant mass of the specimen is obtained. Next, all the faces of the specimen except the one to be exposed are coated with epoxy. When the coating has hardened, the test specimen is again immersed in a $Ca(OH)_2$ solution until a constant mass of the specimen is obtained. In the next step, the specimens are immersed in an aqueous NaCl solution with a concentration of 165 g per dm^3 solution during the whole exposure time (e.g. 5 weeks). The chloride profile is measured immediately after exposure by grinding off material in layers parallel to the exposed surface, preparation of an acid-soluble extraction or water-soluble extraction and followed by a potentiometric titration with silver nitrate [8]. From this test the chloride diffusion coefficient can be obtained, which can be used to determine the chloride concentration in time and depth. Diffusion tests take much more time (several weeks) compared to chloride migration tests (hours), but provide a more realistic chloride ingress situation.

Rodriguez and Hooton [22] used Scanning Electron Microscopy (SEM) combined with Energy Dispersive X-ray analysis (EDX) to determine the concentration of chlorides present in the concrete. This technique makes use of the fact that X-rays emitted by a specific chemical element (e.g. Cl) has its own characteristic energy,

which can be applied for element identification. As the intensity of the emitted radiation is proportional to the concentration of the element, an estimation of the total chloride content can be made.

Ferreira and Makkonen [64] describe some other techniques that are sometimes used to determine the chloride content: X-ray fluorescence spectrometry (XRF), the inductively coupled plasma mass spectrometry (ICP-MS) and electron probe micro-analyzer (EPMA) which was also used by Win et al. [3], Mori et al. [77] and Ye et al. [78]. Electron Probe Micro Analysis can be used to extract accurate chloride concentrations through scanning of the surface of the specimen. The element distribution measurement results are displayed as colored maps using a color scale, which makes this technique very suitable for the visualization of chloride concentrations.

Another innovative technique to determine chloride distributions in cracked concrete is Laser Induced Breakdown Spectroscopy (LIBS), described in the paper of Ŝavija et al. [79]. It is an optical technique that can be used for the accurate detection of trace elements (in this case chlorides) present in a solid, liquid or gaseous sample, as all elements emit characteristic frequencies.

2.3.4 Summary

Summarizing the findings of the selected studies on the topic of chloride penetration, it can be concluded that already a lot of research is done on this topic. This research is mostly done for the purpose of acquiring insight in the chloride-induced corrosion and the implementation of experimental results in numerical models and formulae. Several studies have also been conducted with regards to chloride penetration in cracked concrete. However, a wide range of different results are obtained and some aspects, for example the effect of crack density and healing of cracks on chloride penetration, are not yet investigated thoroughly. These topics could be a main interest of future research. With regards to test methods, a lot of different techniques exist, however the colorimetric method using $AgNO_3$ and the accelerated diffusion and migration test according to the NT-Build standards are the most frequently used nowadays.

2.4 Testing of carbonation in concrete

Research question 1c "What is already known about testing of carbonation in concrete?" is further split up in following topics:

- Carbonation in concrete;
- Influence of cracks on carbonation;
- Testing of carbonation.

From Table 22 in the appendix it is clear that there are much less studies dealing with carbonation in concrete in comparison to the large amount of studies dealing with chloride penetration in concrete. A possible reason for this can be found when looking at the purpose of these studies: acquiring more insight in two important corrosion phenomena, namely chloride-induced corrosion and carbonation-induced corrosion of steel reinforcement in concrete. When comparing both corrosion phenomena, it is stated by Vantyghem [46] that carbonation-induced corrosion leads to a more uniform corrosion of the reinforcement compared to the more locally harmful pitting corrosion in the case of chloride-induced corrosion. As the latter will lead to a faster and more severe degradation of the reinforcement, possibly ending in sudden failure of the structure, more research is done on this topic.

When investigating the studies from this systematic literature review, only two studies that examine carbonation in cracked concrete are identified (see Figure 5). This clearly illustrates the need for further research on this topic.

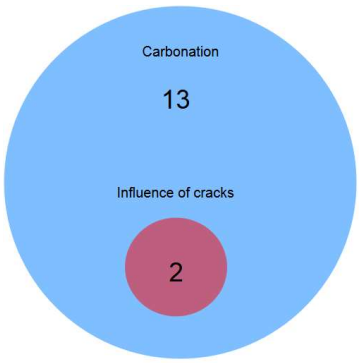

Figure 5: Primary studies dealing with carbonation and the influence of cracks on carbonation

2.4.1 Carbonation in concrete

Besides the abovementioned chloride-induced corrosion, the ingress of carbon dioxide CO_2 into the concrete can induce another type of corrosion, called carbonation-induced corrosion. Due to this, expansive products are formed at the concrete - reinforcement interface, resulting in spalling and cracking of the

concrete. Due to this degradation mechanism, the durability and integrity of the concrete structure are jeopardized.

The carbonation reaction of $Ca(OH)_2$ involves different steps as can be seen in following chemical reaction formulae (1) and (2) [63]:

$$CO_2 + H_2O \rightarrow H_2CO_3 \quad (1)$$

$$Ca(OH)_2 + H_2CO_3 \rightarrow CaCO_3 + 2\ H_2O \quad (2)$$

In the first step, gaseous CO_2 present in the air dissolutes in the pore water to form carbonic acid H_2CO_3. In the second step, H_2CO_3 on its turn can react with calcium hydroxide $Ca(OH)_2$ present in the concrete, resulting in the precipitation of calcite $CaCO_3$ and the formation of water. At high concentrations of CO_2, the amount of produced water can be very high, resulting in blocking of the carbon dioxide and slowing down the carbonation [80]. Sometimes these 2 steps are combined in the following overall chemical reaction (3) [81]:

$$Ca(OH)_2 + CO_2 \rightarrow CaCO_3 + H_2O \quad (3)$$

However, $Ca(OH)_2$ is not the only compound present in the concrete that can react with CO_2: calcium silicate hydrates (C-S-H) can also react with CO_2, resulting in the formation of $CaCO_3$ and a silica gel. With this reaction carbonation shrinkage is accompanied [81]. These two types of carbonation occur simultaneously, but at different rates. The carbonation of $Ca(OH)_2$ is initially faster than the carbonation of C-S-H, but because of the formation of a layer $CaCO_3$ around $Ca(OH)_2$, the $Ca(OH)_2$ is no longer accessible for the CO_2, resulting in a decreased rate of carbonation of $Ca(OH)_2$ in favor of the carbonation of C-S-H [81].

Because the reaction products of these carbonation processes have higher molar volumes than $Ca(OH)_2$ and C-S-H, a decrease in porosity of the cement matrix is obtained and the further ingress of CO_2 is prevented. This is described by several authors based on the examination of water sorption tests or mercury intrusion porosimetry (MIP) ([63],[81]). However, this is countered by Van den Heede [55] and Gruyaert et al. [4] in the case of cement blended with mineral admixtures (for example fly ash, silica fume or blast furnace slag) where a higher porosity is obtained due to carbonation shrinkage, facilitating the penetration of carbon dioxide even further and thus resulting in ongoing carbonation of the concrete.

The aforementioned carbonation reactions will lower the pH of the concrete (that was initially higher than 13, i.e. highly alkaline) because of the consumption of hydroxide ions OH^- and the production of water [60]. This decrease in pH (below 9) has a detrimental effect on the steel reinforcement in concrete, as it destroys the

passive protection layer around the rebars, the so called depassivation of the reinforcement, resulting in carbonation-induced corrosion [81].

A lot of factors have an influence on the carbonation depth in concrete and are discussed and summarized by Zhou et al. [56] and Van den Heede and De Belie [80]: cover thickness, age, curing conditions, cement type and composition, temperature, relative humidity, CO_2 concentration, CO_2 diffusion coefficient, calcium oxide content in cement and carbonation resistivity as well as some environmental conditions such as sheltered versus exposed.

A lot of formulae and numerical models to predict the carbonation depth can be found in literature ([56],[60],[81]), but as the focus in this thesis lies on experimental testing, this falls beyond its scope.

Glasser et al. [60] suggests that chloride ingress and carbonation are related. In the presence of CO_2, Friedel's salts formed during the reaction between chlorides and hydrated cement paste (as discussed in research question 1b) can react, leading to free Cl^- ions, which on their turn can initiate chloride-induced corrosion.

2.4.2 Influence of cracks on carbonation

Despite the fact that the effect of cracks and crack widths on carbon dioxide penetration in concrete is only investigated in few studies ([46],[82]), it is shown by all of them that these parameters have a significant influence on the ability of carbon dioxide to diffuse through cracks, resulting in possible additional and deeper penetration of carbon dioxide into the concrete. As in existing structures concrete is almost always cracked, not taking into account cracks would lead to results that are not in accordance with reality and could underestimate the consequences regarding durability and integrity.

Alahmad et al. [82] studied the influence of different crack widths on carbon dioxide diffusion through the crack, for both artificial and realistic cracks. The distinction between artificial and realistic cracks is made in order to study the potential effect of the so called interlocking between fracture surfaces in case of realistic cracks. The effect of this interlocking phenomenon increases when the crack width decreases, resulting in the blocking of carbon dioxide in very fine cracks (less than 9 µm). For crack widths of 60 µm or more, the carbonation depth perpendicular to the crack wall is similar to the surface carbonation depth. For crack widths of 41 µm or less, carbon dioxide along the crack path is limited, resulting in small carbonation depths perpendicular to the crack wall. Similar observations were also confirmed in the research of Vantyghem [46].

As to this date few research is performed concerning the influence of cracks on carbonation, further research is recommended as it can provide more insights or deepen the existing ones.

2.4.3 Testing of carbonation

In reality, the CO_2 concentration of air is situated in the range of 0.03% - 0.3%, with a maximum of 1% [4]. As at these low CO_2 concentrations the evolution of carbonation depth in time would be extremely slow, carbonation tests are mostly executed in an accelerated way by applying (non-realistic) high CO_2 concentrations. These accelerated carbonation tests are executed in a carbonation chamber in order to predict the carbonation depth in a concrete structure after several years (e.g. 50 years). When looking at several studies applying these tests, not much uniformity regarding the testing method is found: different CO_2 concentrations, relative humidities (RH), temperatures and exposure times are used (see Table 2). When performing carbonation tests at CO_2 concentrations above 3%, it is stated by Van den Heede [55] that depending on the dominating mechanism of carbonation, an increase of permeability in case carbonation shrinkage versus the blocking effect of the water released during carbonation, the carbonation of C-S-H can be over- or underestimated, as well as the related carbonation depths and rates. As an overestimation of carbonation depths is rather conservative, this will lead to safe, but uneconomical design of concrete structures. In the other case however, an underestimation of the carbonation depth can have detrimental consequences for the concrete structure. Taking this into account, an accelerated carbonation test with maximum 3% CO_2 is favored as it represents reality in a better way.

Table 2: Overview of accelerated carbonation tests

Reference	**CO_2 concentration** [%]	**Relative Humidity** [%]	**Temperature** [°C]	**Time of exposure**
Van den Heede [55]	1	60	20	3 – 6 – 10 – 14 – 18 weeks
Van den Heede [55]	10	60	20	3 – 6 – 10 – 14 – 18 weeks
Alahmad [82]	50	65	23	65 days
Vantyghem [46]	10	60	20	2 – 9 weeks
Glasser [60]	5	50	25	14 – 28 days
Gruyaert [4],[83],[63]	10	60	20	2 – 4 – 8 – 16 – 24 weeks
Mönnig [84]	10	60	20	800 days
Thiery [81]	50	53	21	3 – 7 – 14 – 28 days

When looking at the used relative humidities, it can be seen that they all lie in the range of 50-70%, as these are optimal conditions for carbonation ([63],[81]). The diffusion speed of CO_2 is strongly decreased for climates with a relative humidity higher than 70% [83] and are therefore not applied in accelerated carbonation tests. As carbonation increases in time, it is interesting to do long duration tests to investigate the effects on the long-term.

The carbonation depth is usually estimated by spraying a phenolphthalein indicator on sawn or broken surfaces of the sample. Gruyaert et al. [4] however have found that the preparation method (sawing versus splitting) has no significant influence on the obtained carbonation depths. This technique is sometimes called a colorimetric technique, as it makes use of a color change boundary depending on the pH of the concrete: in the carbonated part of the sample no change in color occurs (pH below ~9), whereas in the non-carbonated part a purple color is obtained (pH above ~9) [4]. As this technique is easy and quick, it is often used, even in field conditions [71]. However, recent measurements show that this technique only gives an approximate estimation of the carbonation depth and does not provide the depth of maximum ingress of CO_2 [81]. This observation implies that in reality carbonation depths extend beyond the depth indicated by phenolphthalein [60]. It is shown by several authors ([60],[81]) that spraying phenolphthalein will not indicate the presence of partially carbonated areas and by this the risk of carbonated-induced corrosion can be underestimated.

In a few studies, some other techniques to measure the carbonation depth are used: use of $AgNO_3$ spray (same technique as for chloride penetration, but with less pronounced color contrast) [71], X-ray diffraction (XRD) ([55],[81]) and the use of optical microscopy on thin sections by using crossed-polarized light ([4],[55]). This last technique results in general in higher and more precise carbonation depths than colorimetric measurements with phenolphthalein ([4],[55]).

Snoeck et al. [53], Van den Heede [55] and Thiery et al. [81] discuss another technique to study the carbonation of concrete, namely thermogravimetry, also called thermogravimetric analysis (TGA). This technique can be used to quantify both the mass loss in the range of 400-500°C due to the decomposition of $Ca(OH)_2$ in CaO and H_2O and the mass loss around 680°C due to the decarbonation of $CaCO_3$ (i.e. the decomposition of calcite to CaO and CO_2). By using this technique, it can be identified whether the concrete shows carbonation or not.
Thiery et al. [81] also use another method to evaluate carbonation depth profiles: the gamma-densitometry method. This method monitors the evolution of the density of the sample in time and depth. By doing this, the local density increase in the case of carbonation can be observed, especially in partially carbonated regions.

2.4.4 Summary

Summarizing the findings of the selected studies on the topic of carbonation, it can be concluded that most of the current research is done on the general phenomenon of carbonation in concrete. This research is mostly done for the purpose of acquiring insight in the carbonation-induced corrosion and the implementation of experimental results in numerical models and formula. However, when looking at studies dealing with carbonation in cracked concrete, only two studies are obtained in this systematic literature review. It clearly illustrates the need for further research on this topic in order to provide more insight to obtain results that are in accordance with reality. Regarding to test methods, accelerated carbonation tests in combination with a colorimetric method using phenolphthalein are traditionally used. However, in most cases no information is provided about the used CO_2 concentration or the influence of this concentration on the obtained results. Despite the fact that other, more accurate methods are already available, they are not often used by researchers. A critical comparison of different techniques to measure the carbonation depth and the amount of carbonation in concrete concerning accuracy, advantages, disadvantages and ease of use could be the scope of future research.

The answers on the three sub questions can now be summarized to provide a general answer to research question 1.

2.5 Testing of chloride penetration and carbonation of concrete healed by superabsorbent polymers

From the literature study concerning self-healing of concrete with SAPs, it is clear that literature mainly focuses on the general concepts, mechanical concepts and water permeability. Influence of SAPs on carbonation and chloride penetration is only discussed by two authors: Mönnig [84] and Vantyghem [46]. Mönnig did a few experiments on chloride penetration and carbonation in concrete healed by SAPs, but as the results showed a lot of scatter, he decided not to make a conclusion. Vantyghem only briefly mentions the influence of SAPs as this is not the main focus of his thesis. It clearly illustrates the need for further research on this topic.

2.6 Fit with current research and knowledge

The studies on chloride penetration as well as those on carbonation mention a range of critical crack widths underneath which the deterioration mechanism is only limited and should not be feared. The healing of concrete by SAPs should therefore preferably decrease the crack widths under this limit. In this case, stimulated autogenous healing of the cracks could stop or at least delay the ingress of these aggressive substances and hence reducing the risk of corrosion. This will lead to an increase of the durability and service life of concrete structures. However, it should be noted that the swelling effect of SAP particles depends upon the type of liquid. Lee [85] noticed complete sealing when tap water, synthetic groundwater or sodium chloride solution entered into the crack, while the swelling of the SAP particles was only limited when synthetic seawater intruded. This effect should be taken into account when trying to heal concrete in marine environments. In this case, it could be that the healing efficiency of the SAPs is lower compared to their behavior in fresh water.

3 Materials and Methods

3.1 Materials

The discussion of the materials used in this master dissertation is divided into three parts. In the first part, the used superabsorbent polymers are discussed. In the second part, the components that can be found in traditional concrete are treated. In the third and final section, the various test samples and their composition are summed up.

3.1.1 Superabsorbent polymers (SAPs)

The superabsorbent polymers used in this thesis were commercially available synthetic SAPs, produced by SNF Floerger. The used SAPs were of the type SAP A and were cross-linked copolymers of acrylamide and acrylate, obtained through bulk polymerization. In this method, the undiluted and pure monomer was polymerized without the use of a solvent. After the polymer melt came from the reactor and was cooled down, it was finely ground and sieved to obtain the desired diameter. This method also accounted for the irregular shape of the SAP-particles [86], see Figure 6.

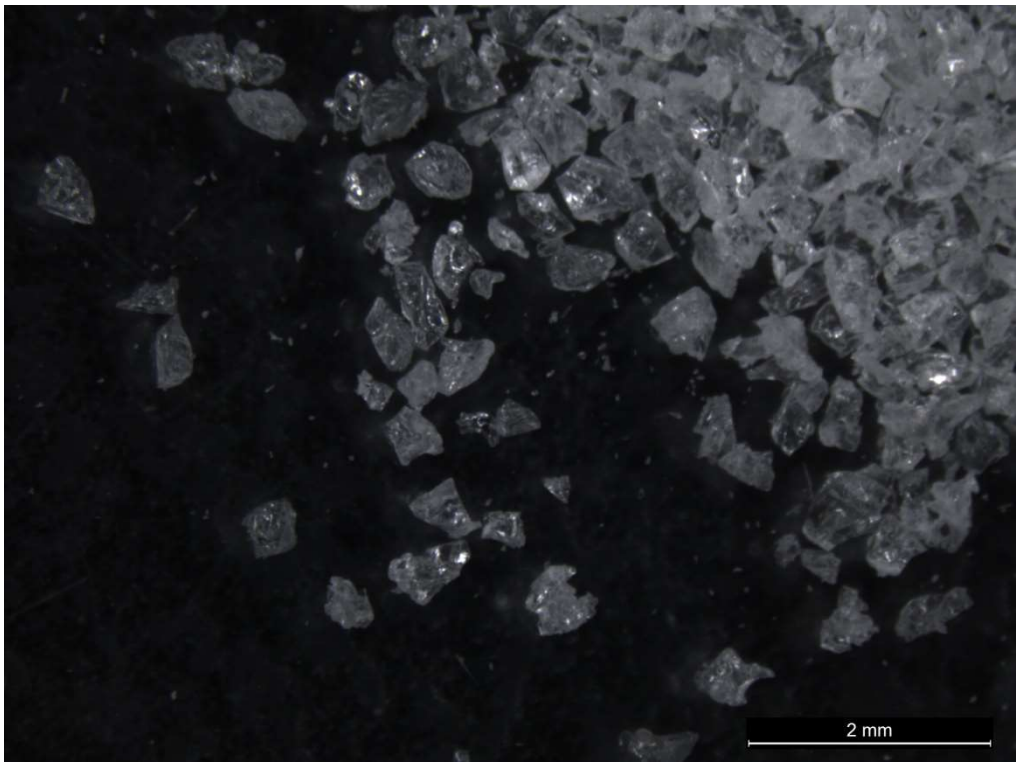

Figure 6: Microscopic picture of SAP A

The SAPs were perceived as a white, odorless powder with a bulk density of 700 kg/m^3 and particle sizes around 600 µm.
The amount of SAPs used in the concrete mixtures was expressed as mass% (m%) of the cement weight. In Figure 7, a picture of a dry SAP particle made by an optical Leica S8 microscope is shown. In Figure 8, a saturated swollen SAP particle is shown after the addition of some drops of water. The difference in dimension between a dry and swollen particle is clearly visible. More information on the microscopic analysis of SAP particles can be found in section 3.2.1.2.

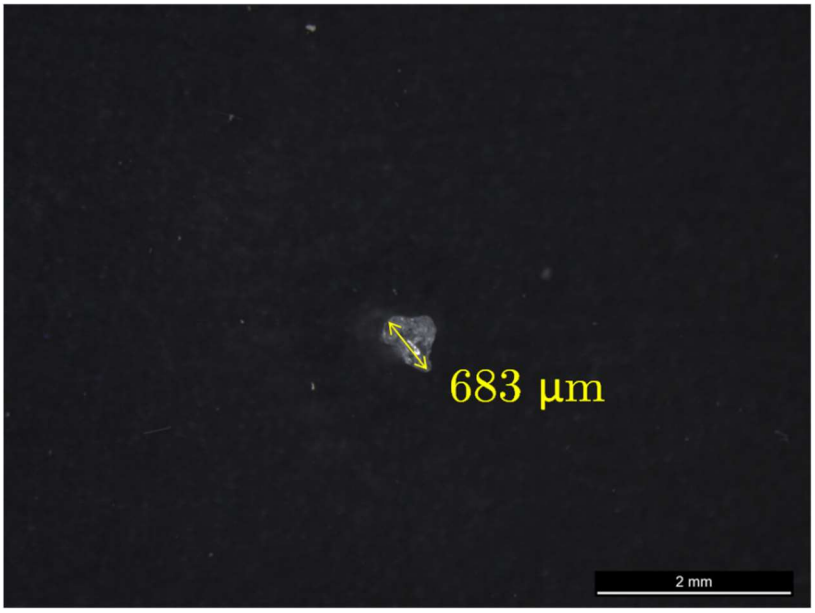

Figure 7: Microscope image of a dry SAP particle

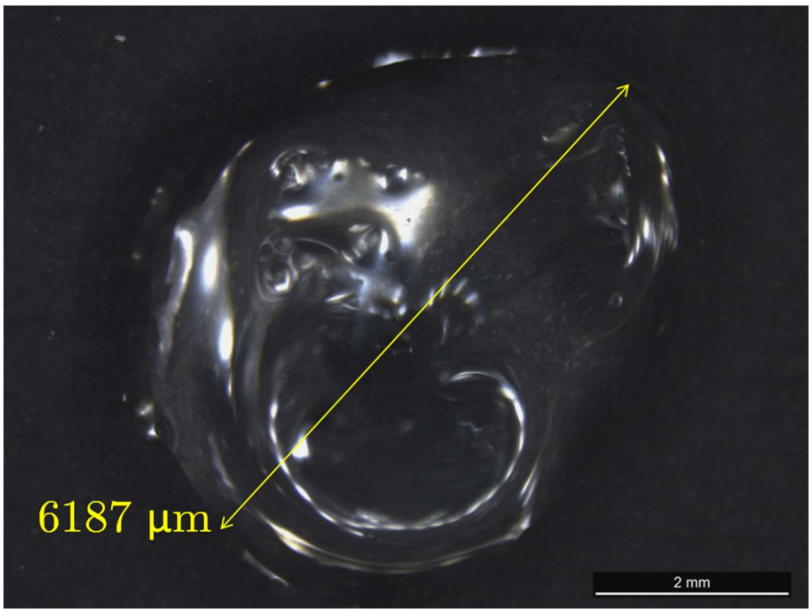

Figure 8: Microscope image of a saturated, swollen SAP particle

3.1.2 Traditional materials

The traditional materials used in the studied mixtures were: Ordinary Portland Cement (OPC) CEM I 52.5 N (HOLCIM), fly ash ASTM type F (OBBC), fine silica sand 0/4, gravel 2/8, gravel 8/16 and tap water. A polycarboxylate super plasticizer, Glenium 51, conc. 35% (BASF) was added to improve the workability.

3.1.3 Mixtures

3.1.3.1 Mixtures for the determination of self-healing and chloride penetration

For the determination of self-healing and chloride penetration, three different concrete mixtures were used: a reference mixture without SAPs (REF) and two mixtures with varying amount of SAPs, expressed as mass% (m%) of the cement weight: SAP 0.5 m% and SAP 1 m%. As already mentioned in the literature review (see section 2.2.5) the SAPs will absorb part of the mixing water, resulting in a negative effect on the workability. Therefore, additional water needs to be added to compensate for this loss in workability. The amount of additional water was determined by comparing the flow values of mixtures with and without SAPs on one hand and the results obtained with the filtration method on the other hand, see section 3.2.1.1. For the latter, it was also taken into account that the swelling of the SAPs will be hindered by the surrounding concrete matrix. Furthermore, a dosage of 2 ml super plasticizer per kg binder was added to all mixtures to improve the workability. Table 3 gives an overview of the used concrete compositions.

Table 3: Composition of the concrete mixes

		REF	**SAP 0.5**	**SAP 1**
Sand 0/4	[kg/m³]	696.0	666.5	639.3
Gravel 2/8	[kg/m³]	502.0	480.7	461.1
Gravel 8/16	[kg/m³]	654.0	626.3	600.7
CEM I 52.5 N	[kg/m³]	317.6	304.2	291.7
Fly ash	[kg/m³]	56.0	53.6	51.4
SAP	[kg/m³]	-	1.5	2.9
Water	[kg/m³]	153.0	146.5	140.5
Additional water	[kg/m³]	-	40.7	78.1
SP	[ml/kg binder]	2.0	2.0	2.0

In Table 4 the additional water-to-binder ratio $(w/b)_{add}$, the total water-to-binder ratio $(w/b)_{tot}$ and the effective water-to-binder ratio $(w/b)_{eff}$ are given. These ratios take into account respectively the additional water, the total water and the amount of water disregarding the additional water, all with respect to the binder (i.e. cement + fly ash). A $(w/b)_{eff}$ of 0.41 is maintained for all mixtures.

Table 4: Studied concrete mixtures with their water-to-binder ratios (additional, total and effective)

	REF	**SAP 0.5**	**SAP 1**
$(w/b)_{add}$	0	0.11	0.23
$(w/b)_{tot}$	0.41	0.52	0.64
$(w/b)_{eff}$	0.41	0.41	0.41

3.1.3.2 Mixtures for the determination of carbonation

For the determination of carbonation, three different mixtures were used: a cement paste (CEM), a concrete mixture without SAPs (CON) and a concrete mixture with 1m% of cement weight SAPs (SAP). As concrete with fly ash is more susceptible to carbonation [55], no fly ash was added. In the case SAPs were present in the mixture, extra water was added to compensate for the loss in workability. Table 5 gives an overview of the compositions of the used mixtures.

Table 5: Compositions of the different mixtures

		CEM	**CON**	**SAP**
Sand 0/4	[kg/m³]	-	715	660
Gravel 2/8	[kg/m³]	-	516	476
Gravel 8/16	[kg/m³]	-	672	620
CEM I 52.5 N	[kg/m³]	300	300	277
SAP	[kg/m³]	-	-	2.77
Water	[kg/m³]	142.6	165	152
Additional water	[kg/m³]	-	-	74
SP	[ml/kg cement]	2	2	2

In Table 6 the additional water-to-cement ratio $(w/c)_{add}$, the total water-to-cement ratio $(w/c)_{tot}$ and the effective water-to-cement ratio $(w/c)_{eff}$ are given. These ratios take into account respectively the additional water, the total water and the amount of water disregarding the additional water, all with respect to the amount of cement. Although the concrete mixtures CON and SAP had a slightly higher $(w/c)_{eff}$ than the cement paste CEM, the same amount of water was available for the reaction with the cement particles. After all, part of the water was absorbed by the granulates in the concrete mixtures and was thus not available for the hydration reaction.

Table 6: Studied mixtures with their water-to-cement ratios (additional, total and effective)

	CEM	**CON**	**SAP**
$(w/c)_{add}$	0	0	0.27
$(w/c)_{tot}$	0.475	0.55	0.82
$(w/c)_{eff}$	0.475	0.55	0.55

3.2 Methods

3.2.1 Swelling behavior SAPs

A very important characteristic of superabsorbent polymers is the swelling capacity. This is frequently expressed as the ratio of the swollen wet polymer volume or mass to that of the dry state. As already mentioned in the literature review section 2.2.1, this swelling capacity will be depending on the type of fluid, amongst other parameters like pH and temperature, and can be determined in several ways. In this thesis, the filtration method for the determination of the swelling capacity in different solutions was used. Another interesting characteristic of SAPs is the swelling time, which can be obtained by the so-called vortex test [19]. Both tests are explained in the following sections.

3.2.1.1 Filtration method

The filtration method is a gravimetric method to determine the swelling capacity of SAPs in different solutions. A certain amount of fluid was added to dry SAP particles. After 24 hours the SAP particles definitely reached their equilibrium swelling and everything was filtered using filter paper with particle retention 12-15 µm. In order to exclude possible absorption of the fluid by the filter paper, the latter was first saturated with the fluid. To minimize evaporation during the test, the test setup was covered with a lid. A picture of the used test setup is showed in Figure 9.

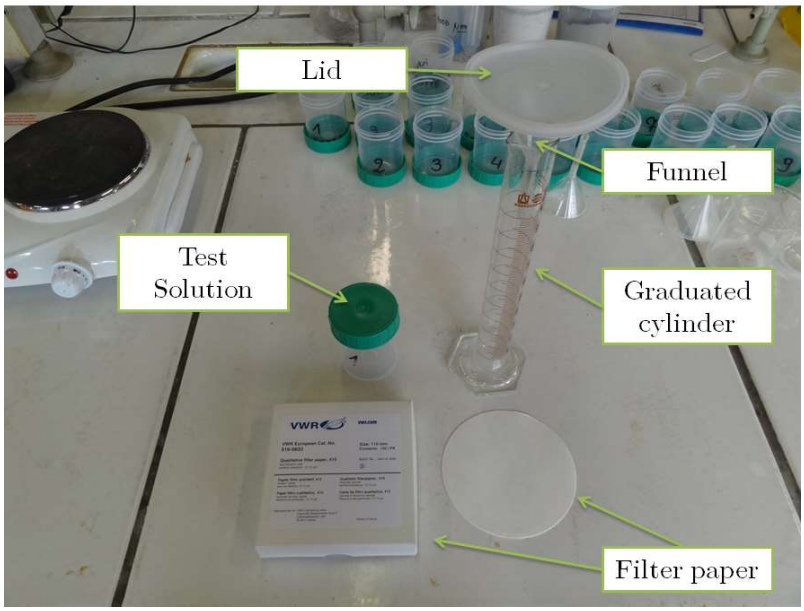

Figure 9: Test setup filtration method

After filtering, the amount of fluid that was not absorbed by the SAPs was recorded. The swelling ratio, i.e. the amount of fluid that can be absorbed by 1 g of SAPs can be calculated by formula (4):

$$\text{Swelling ratio [g fluid/g SAP]} = \frac{w_{\text{fluid added}} - w_{\text{fluid not absorbed}}}{w_{\text{dry SAP}}} \quad (4)$$

With

- $w_{\text{fluid added}}$ [g]: the amount of fluid before filtration;
- $w_{\text{fluid not absorbed}}$ [g]: the amount of fluid that was not absorbed by the SAPs;
- $w_{\text{dry SAP}}$ [g]: the amount of dry SAPs.

In this research, tests were carried out in four different solutions. These include demineralized water, cement filtrate solution (obtained by mixing 100 g of ordinary Portland cement CEM I 52.5 N in 1 liter of demineralized water for 24 hours, followed by filtration), artificial seawater (containing 24 g NaCl, 5 g $MgCl_2$, 4 g Na_2SO_4 and 0.7 g $CaCl_2$ for 1 liter seawater) and a chloride solution (with 165 g NaCl for 1 liter). The filtration test was executed three times for each solution.

3.2.1.2 Microscopic analysis

A second, more visual method that was used to investigate the swelling behavior of SAPs, was the microscopic analysis of an individual SAP particle. In this method, a single, dry SAP particle was placed under an optical microscope (Leica S8 APO mounted with DFC 295 camera), a picture was taken and its maximum initial dimension r_0 was determined using the ImageJ software. The maximum dimension was used as the particle had an irregular shape due to its production process. By using a needle and a 1 ml syringe, drops of demineralized water were added one by one to the SAP particle. After each addition of water, a picture was taken with the microscope. This procedure was continued until the particle was fully saturated with water and did not take up any additional water. At this moment a last picture was taken and the maximum dimension r_{max} of the fully saturated, swollen SAP particle was again determined using the ImageJ software. By doing this, the dimensions of the initial dry SAP particle and the swollen saturated SAP particle could be compared to serve as in indicator of the swelling behavior of a SAP particle. In order to simplify the calculations, it is assumed that the SAP particles are spheres with radius equal to the measured maximum dimensions. The following formula is used:

$$\text{Swelling ratio [g fluid/g SAP]} = \frac{1}{\rho} * \frac{\frac{4}{3}\pi\,(r_{max}^3 - r_0^3)}{\frac{4}{3}\pi\,r_0^3} \quad (5)$$

with $\rho = 1400$ kg/m³, the density of the SAP particle.
This procedure was repeated for five individual SAP particles.

3.2.1.3 Vortex method

The vortex method is an easy and quick test to determine the swelling time of SAPs in different solutions. To do so, 100 g of the fluid of interest was added to a beaker. Using a magnetic stirrer of 2 mm at 400 rpm, a vortex was created, see Figure 10. From the aforementioned filtration method, the amount of SAPs to absorb 100 g of the fluid was calculated and added to the beaker. The time until the vortex disappeared was recorded.
This test was executed with the same solutions as used for the filtration method. For the test with demineralized water, three repetitions were executed. For the other solutions however, only one test was executed due to the limited amount of fluid available. The vortex method was not executed in cement filtrate, as not enough solution was available.

Figure 10: Vortex created by magnetic stirrer

3.2.2 Sample preparation

3.2.2.1 Cylindrical samples

For the determination of self-healing and chloride penetration, cylindrical samples with a height of 50 mm and a diameter of 100 mm were used. The moulds were made by cutting a cylindrical PVC tube with inner diameter 100 mm into pieces with a length of 50 mm.

3.2.2.2 Cubes

For the determination of carbonation, cubes with sides 100x100x100 mm^3 were used. The moulds were made in a similar way as for the cylindrical samples, but now using a prismatic PVC tube with inner dimensions of 100 mm.

3.2.2.3 Mixing procedure

Before mixing, all traditional components were weighed with an accuracy of 1 gram. The SAPs were weighed with an accuracy of 0.01 gram.
The mixing procedure was as follows:

- 0 – 30 s dry mixing of gravel and sand;
- 30 – 60 s addition of cement, fly ash and SAP and further mixing;
- 60 – 150 s addition of water while mixing;
- 150 – 210 s addition of super plasticizer (SP) while mixing.

After mixing the slump, flow, density and air content of the mixture were determined, see section 3.2.3. Subsequently the moulds were filled and compacted by means of a poker-vibrator (Figure 11) and/or vibrating table (Figure 12).
If needed, extra material was added in the moulds to obtain the desired height of the samples. During casting and compaction, the PVC moulds were clamped on a wooden base, see Figure 13, in order to prevent the moulds from lifting up due to vibrations and prevent leakage of the concrete from the bottom. Finally, the surface of the samples was flattened, see Figure 14.
The samples were demoulded after 24 h and the outer layer of both upper and lower face of the cylinders was cut off by water-cooled sawing to obtain a flat test surface. Afterwards, the samples were stored at a relative humidity of more than 90% and a temperature of 20 ± 2 °C.

Figure 11: Compaction with poker-vibrator

Figure 12: Compaction with vibrating table

Figure 13: PVC moulds clamped on wooden base

Figure 14: Flattening of the sample surface

3.2.2.4 Coating

In order to obtain carbonation or chloride penetration from one exposure surface only and hence to achieve a uni-directional flow, the other, non-exposed sides were coated with a two-component epoxy (SikaCor-277), see Figure 15. The coating was applied in two layers, with a drying time of 24 hours in between each layering. Afterwards, the samples were again stored at a relative humidity of more than 90% and a temperature of 20 ± 2 °C until their testing age.

Figure 15: Coating of the non-exposed sides with a two-component epoxy

3.2.3 Fresh concrete characteristics

3.2.3.1 Slump

The consistency of fresh concrete was determined by the slump test as described in the standard EN 12350-2.
A truncated cone with height 300 mm was filled with fresh concrete in three equal layers. Each layer was compacted uniformly over the cross section with 25 strokes with a normalized steel tamping rod. After compacting the top layer, the surface was struck off and the mould was carefully removed in a vertical direction. Immediately after the removal of the mould, the slump was determined to the nearest 10 mm as the difference between the height of the mould and the highest point of the slumped test specimen. A picture of the apparatus and an example of a slumped test specimen are shown in Figure 16. Depending on the measured slump, the fresh concrete was classified according to specific slump consistency classes, see Table 7.

Table 7: Slump consistency classes

Consistency Class	Slump [mm]
S1	10 - 40
S2	50 - 90
S3	100 - 150
S4	160 - 210
S5	≥ 220

a) b)

Figure 16: a) apparatus for the determination of the slump b) slumped test specimen

3.2.3.2 Flow

Besides the classification of the consistency based on the slump, the consistency of fresh concrete was also determined using the flow table test as described in the standard EN 12350-5.
A truncated cone with height 200 mm was placed on a flow table and filled with fresh concrete in two equal layers. Each layer was compacted ten times with a wooden tamping bar and the top layer was struck off at the edge of the cone, see Figure 17a. Next, the mould was carefully removed in vertical direction (see Figure 17b) and the table was subjected to 15 drops where each cycle lasted for minimum two seconds and maximum five seconds. Finally, the length of two mutually perpendicular diameters of the concrete spread parallel to the edge of the table was measured to the nearest 10 mm, see Figure 17c. The average of these two diameters is called the flow and was used to classify the concrete in a specific flow consistency class, see Table 8.

Table 8: Flow consistency classes

Consistency Class	**Flow [mm]**
F1	≤ 340
F2	350 - 410
F3	420 - 480
F4	490 - 550
F5	560 - 620
F6	≥ 630

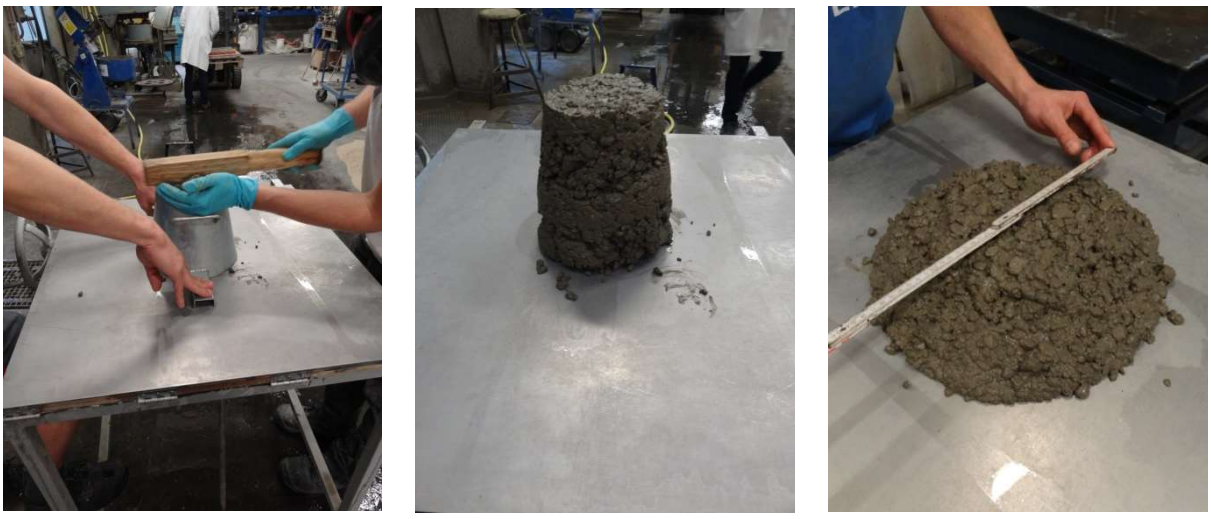

a) b) c)

Figure 17: a) Striking off the top layer at the edge of the cone b) test specimen after removal of the mould c) measuring the diameter of the concrete spread

3.2.3.3 Density

The density of the fresh concrete in kilograms per cubic meter was determined according to NBN EN 12350-6. A container with known volume V_c and weight W_c was filled with fresh concrete. The fresh concrete was compacted with a vibrating needle according to NBN EN 12350-4. The surface of the fresh concrete was flattened with a palette knife.
Subsequently, the weight of the container filled with fresh concrete W_{all} is recorded. The density of the fresh concrete [kg/m^3] was calculated with formula (6):

$$\rho = \frac{W_{all} - W_c}{V_c} \quad (6)$$

With

- W_{all}: the weight of the container filled with fresh concrete [kg];
- W_c: the weight of the container [kg];
- V_c: the volume of the container [m^3].

3.2.3.4 Air content

The air content of the fresh content was determined with the pressure gauge method according to NBN EN 12350-7.
The used pressure meter consisted of an upper part initially filled with air and a lower part filled with fresh concrete. The fresh concrete was compacted with a vibrating needle according to NBN EN 12350-4. The surface of the fresh concrete was made even with a palette knife.
After closing the air valve between the upper air chamber and the lower sample container, the air space under the cover and above the fresh concrete was filled with water. Subsequently, air was pumped into the sealed air chamber until a certain pressure was reached. Next, the valve between the air chamber and the sample container was opened. The pressure gauge on top of the meter indicated the change in pressure as the water was forced into the concrete, displacing air from the pores. The measured pressure change is correlated to the air content of the concrete.

3.2.4 Compressive strength

In order to test the compressive strength of the concrete according to NBN EN 12390-3, three cubes with side 150 mm were cast per mixture and cured at 20 ± 2 °C and a relative humidity (RH) higher than 90%. These cubes were demoulded after 24 h and cured under the same conditions until the age of 28 days. The cubes were tested by a compression testing machine. A load was applied gradually at the rate of 0.6 ± 0.2 MPa/s until the specimen failed. The maximum load that could be resisted by the specimen was recorded.

The compressive strength of the concrete is calculated with formula (7):

$$f_c = \frac{F}{A_c} \tag{7}$$

With

- f_c: the compressive strength in MPa (N/mm²);
- F: the maximum load at failure in N;
- A_c: the area of the cross-section of the specimen where the load was applied in mm²

3.2.5 Open porosity

The open porosity was determined by means of a vacuum saturation test according to EN 1936.
After 28 days of storage in a room with a relative humidity of more than 90% and a temperature of 20 ± 2 °C, three samples of each test series were weighed and put in a vacuum tank. The pressure was lowered gradually to 2.0 ± 0.7 kPa and this pressure was maintained for at least two hours in order to eliminate the air contained in the open pores of the specimen. Then, with the vacuum pump still running, demineralized water was slowly introduced into the tank until the specimens were fully immersed. After 24 hours of submersion, the samples were taken out of the vacuum tank and the mass of the sample under water (m_w) and the surface-dry saturated sample (m_a) were recorded. For the latter, the surfaces of the specimen were wiped with a wet cloth. Subsequently, the samples were dried in an oven at 105 °C for at least 72 hours until constant dry mass (m_d) was reached. Constant mass was reached if two successive weighings with a time interval of 24 hours, showed a difference in mass smaller than 0.1 %.

The open porosity is expressed by the ratio (as a percentage) of the volume of the open pores and the apparent volume of the specimen by formula (8):

$$p_o = \frac{m_a - m_d}{m_a - m_w} \times 100 \tag{8}$$

With

- m_a: the mass of the saturated sample [g];
- m_d: the mass of the oven-dried sample [g];
- m_w: the mass of the saturated sample measured under water [g].

3.2.6 Crack formation

In this master dissertation, both realistic and artificial cracks were used. As already explained in section 2.2.2 of the literature review, both type of cracks have their advantages and disadvantages and several methods exist to create these cracks in the specimens. In the following sections, the methods used in this research are discussed.

3.2.6.1 Realistic crack formation

Realistic cracks were induced in the cylindrical samples by means of a crack-width controlled splitting test at the age of 28 days. The intended crack widths were 100 µm and 300 µm.
At both sides of the cylinder a Linear Variable Differential Transformer (LVDT) with a measuring range of 1 mm and an accuracy of 1 µm, was installed by means of a steel block and a steel plate which were glued to the specimen. The LVDT measured the crack width at the surface, also called the crack opening displacement (COD) and the mean of the registered crack widths was used to control the splitting test. Between the cylinder and the loading plate, a thin piece of plywood was placed in order to create a uniform distributed line load instead of a high concentrated point load which could locally damage the sample. The applied coating, see section 3.2.2.4, together with extra duct tape and a clamping screw acted as a kind of reinforcement during crack formation so the specimen would not suddenly split into two pieces.
Figure 18 shows a schematic representation of the test setup for a crack-width controlled splitting test and a photograph of a specimen during the test.

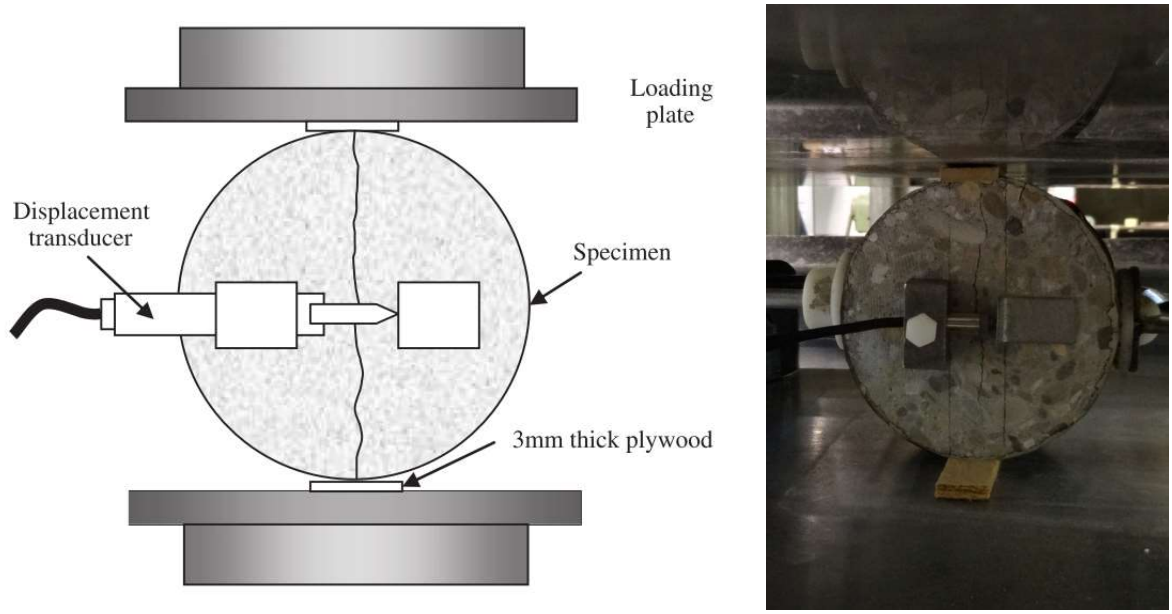

a) b)

Figure 18: a) Schematic representation of test setup of the crack-width controlled splitting test, by Jang et al. [30] b) photograph of a specimen during the test

In case a crack of 100 µm was desired, the crack width was increased at a constant speed of 0.3 µm/s, until the average of the two CODs reached a value of 180 µm. At this moment, the specimen was unloaded automatically. Due to the unloading, the crack partially closed to a final crack width of approximately 100 µm. In case a crack width of 300 µm was needed a similar procedure was used: the crack width was increased at a constant speed of 0.8 µm/s until a crack width of 600 µm was reached. After unloading a crack width of approximately 300 µm was obtained.
The realistic cracks were propagating over the entire diameter and through the total height of the specimen. Hence, there was a crack at both sides of the cylinder. As only one side was analyzed, a choice must be made: which side will be studied and which one will be coated. The choice of the test surface was based on the average crack width and is explained in section 3.2.6.3. An example of a realistic crack of 100 µm obtained with this method can be seen in Figure 19.

Figure 19: Example of a realistic crack of 100 µm obtained with the crack-width controlled splitting test

3.2.6.2 Artificial crack formation

Artificial cracks were created by putting thin brass plates in the PVC moulds before casting. By using different sizes of plates, varying crack parameters such as crack width, length and depth can be obtained and their influence can be studied. In the case of cylindrical samples, brass plates with a nominal thickness of 0.1 and 0.3 mm were used. In this case, the crack depth was kept constant at 25 mm and the crack length was 60 mm. In case cubes were used, the thickness of the plates was 0.5 mm, the crack depth was kept constant at 50 mm and the crack length was 95 mm. Figure 20 shows a schematic representation of the mould setup with the brass plate fixed at the desired crack depth, for both cylinders and cubes.

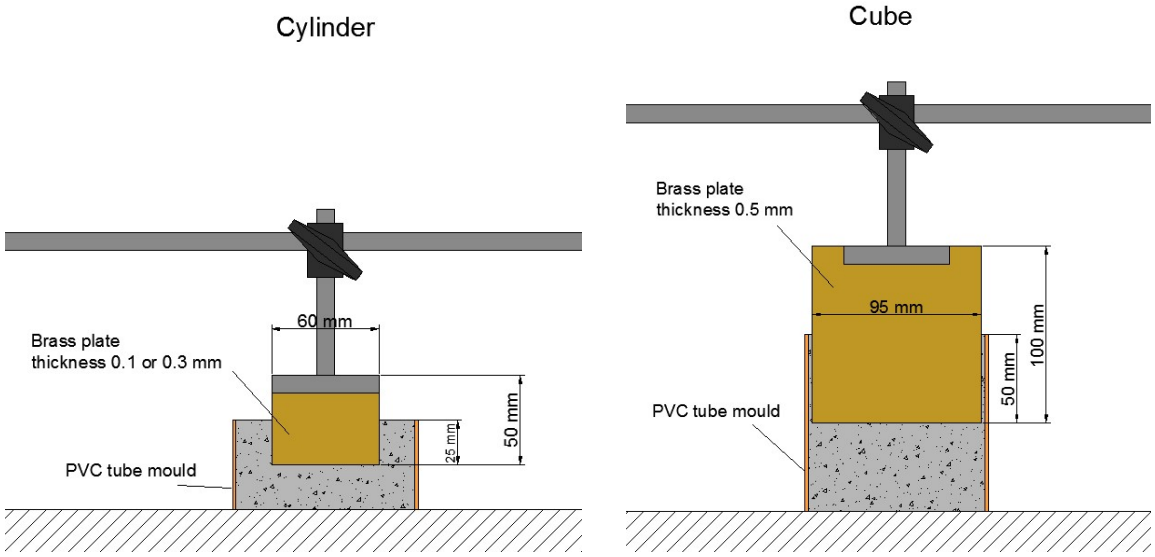

Figure 20: Schematic test setup for creating artificial cracks for both cylinders and cubes

The plates were positioned in the center of the samples and at the correct depth using metal rods, which were fixed by means of magnets. The preparation of the setup for the creation of artificial cracks, the resulting concrete samples and an example of a cracked specimen are shown in Figure 21.

a) b) c)

Figure 21: a) Positioning of the brass plates b) Casting of the samples c) Resulting artificial crack

Compaction of these samples was executed with extra care in order to keep the metal plates in the intended position. It could happen that due to the vibrations of the vibrating table, the magnets switch off, resulting in undesired movements of the rods and thus also the plates. In case of touching the plates with the vibrating needle, the plates could loosen from the rods and will no longer be in the correct position. This was not the case and the plates remained in the right position.

The plates were carefully removed from the samples after 24 hours and the formed crack was cleaned by pulling a thinner brass plate through the crack and with compressed air.
Before testing, the crack widths were measured with a microscope, see section 3.2.6.3.

3.2.6.3 Crack width measurements

Before exposing the specimens to wet-dry cycles, chlorides or carbon dioxide, crack widths were measured by means of an optical stereo microscope (Leica S8 Apo mounted with a DFC camera). By means of the camera, a picture was taken every cm along the crack at the surface and these pictures were analyzed using the ImageJ software. Subsequently, the average crack width and standard deviation could be calculated for each sample.

In case of realistic crack formation, a crack was made at both sides of the sample and one side must be chosen as the test side. To determine which side is 'the best choice', both the calculated mean and standard deviation were taken into account. The method followed is explained based on an example, see Figure 22. In this example, side A had an average crack width of 91.2 µm with a standard deviation of 21 µm, whereas side B had an average crack width of 100.8 µm with a standard deviation of 27 µm. The target crack width was 100 µm.
It was assumed that the crack widths were normally distributed. The probability density functions (PDF) of both sides A and B, based on the calculated average and standard deviation, were plotted on the same graph. In the next step, the target crack width, in this example 100 µm was visualized on the graph as well.
The side which had the highest probability density for the target crack width, was chosen as the test side and will be used in further research, whereas the other side was coated and no longer studied. In this case, side A had the highest probability density for a crack width of 100 µm and was chosen as test side.

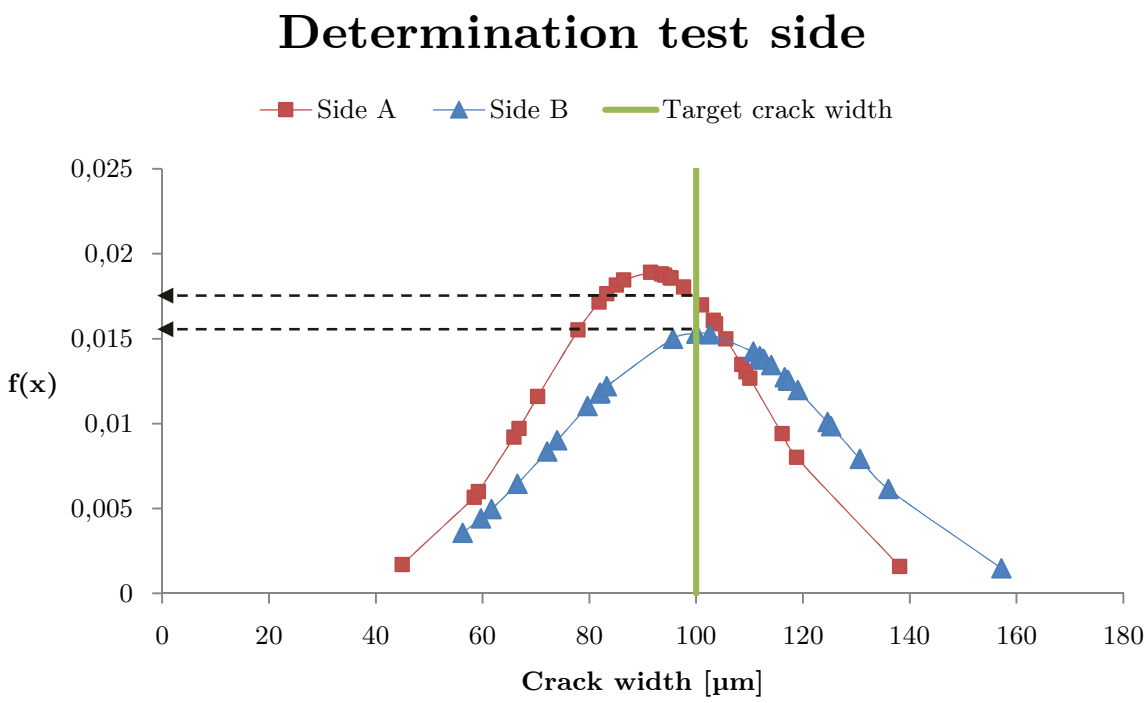

Figure 22: Determination of test side, example

Despite the fact that side B had an average crack width closer to the target value, this side was not chosen due to the larger standard deviation and as a consequence smaller probability density for a crack width of 100 µm. This example shows that the average crack width as well as the standard deviation should be taken into account when selecting the test side.

To test whether the crack widths were indeed normally distributed, a Kolmogorov-Smirnov normality test (significance level = 0.05) was executed, together with a Q-Q plot. In case of normal distributed crack widths, the measurement points are located on a straight line in a Q-Q plot, like in Figure 23a. Figure 23b shows a histogram of the measured crack width together with the normal distribution line.

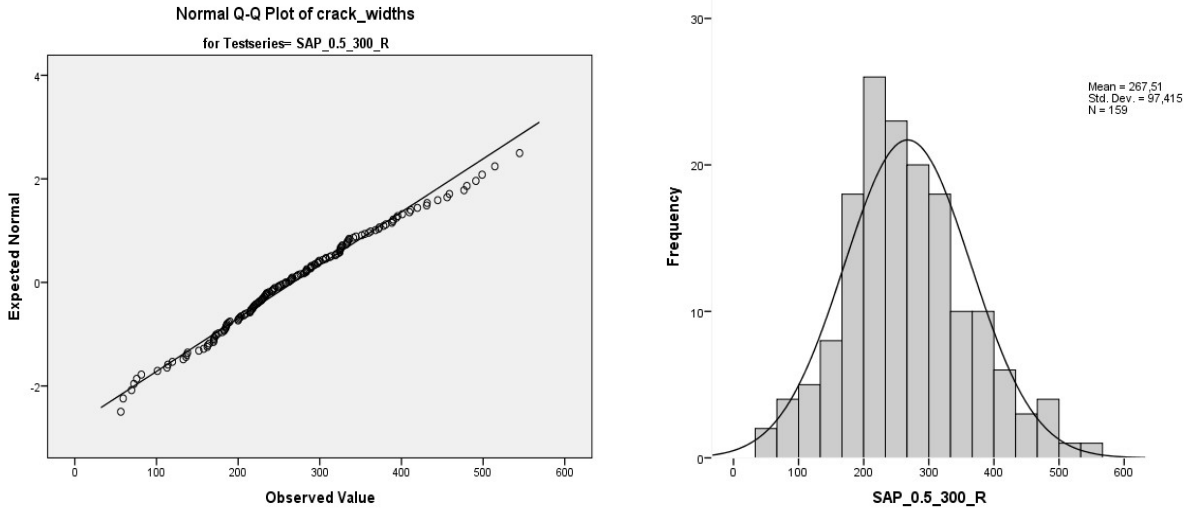

a) b)

Figure 23: a) Q-Q plot of crack widths b) histogram of crack widths together with normal distribution line

3.2.7 Self-healing

3.2.7.1 Wet-dry cycles

One of the three necessary conditions for autogenous crack healing, is the exposure to humid conditions [35]. In this case, the specimens were subjected to wet-dry cycles. Compared to storage in 60% RH or 90% RH, this condition stimulates the autogenous healing by SAPs the most [13].

One wet-dry cycle took 24 hours: 12 hours of immersion in demineralized water, followed by a drying period of 12 hours at 60 ± 5% RH and 20 ± 2 °C. The cycles were automated by a timer that activated a pump at certain times, so water was pumped from one basin to another one. The samples were placed with the cracked faces upwards, see Figure 24. In order to assure that the specimens were not in

contact with any residual water in the basin during the dry periods, they were placed on steel platform with holes. The water was refreshed every week.

Figure 24: Test setup for wet-dry cycles

3.2.7.2 Microscopy

Autogenous healing was investigated by monitoring the crack width in time. By means of the Leica S8 Apo stereo microscope with DFC camera, see Figure 25, pictures of the crack at the surface were taken at five points in time: just before the start of the wet-dry cycles (i.e. the initial crack width) and after 3, 7, 14 and 28 days in wet-dry cycles. In order to obtain clear pictures, the pictures were made during the dry periods.

Figure 25: Leica S8 Apo stereo microscope mounted with DFC camera

The crack closing ratio (percentage) was expressed as the difference between the initial average crack width and the remaining average crack width compared to the initial average crack width:

$$\text{crack closing ratio } [\%] = \frac{w_{initial} - w_{remaining}}{w_{initial}} \times 100 \quad (9)$$

3.2.8 Chloride diffusion tests

The chloride diffusion test used in this master dissertation is based on the NT Build 443 [76]. For this test, cylindrical samples with a height of 50 mm and a diameter of 100 mm were used. All sides of the cylinder, except the one to be exposed to chlorides, were coated with an epoxy coating. In this way, one-dimensional penetration of chlorides from one side of the sample was assured. More information on the sample preparation and coating can be found in section 3.2.2.
After immersion of the specimens in a 165 g/ℓ NaCl solution for seven weeks, the chloride penetration was investigated in two ways: by means of color change boundary by spraying $AgNO_3$ and by means of chloride profiles resulting from chloride titrations. Both techniques are discussed in the following paragraphs.

3.2.8.1 Continuous immersion

After four weeks of wet-dry cycles, see section 3.2.7.1, at a sample age of 56 days, the cylinders were immersed in a 165 g/ℓ NaCl solution at 20°C. The samples were placed with their free surface facing upwards, so chlorides could only penetrate via this non-coated surface. In order to prevent evaporation of the water, resulting in an unwanted increase of the concentration of NaCl, the solutions with the immersed samples were stored in a closed box. After 7 weeks of immersion, all test specimens were taken out of the solution.

3.2.8.2 Spraying $AgNO_3$

Four samples per test series were split orthogonally to the crack and the free chloride penetration was visualized by means of spraying 0.1 Mol/ℓ $AgNO_3$ on both halves of the split specimens. The chloride-affected zone appeared to turn out white, whereas the chloride-free zone turned black/brown.
The depth of the white penetration front from the exposed surface was measured to the nearest millimeter at 10 positions along the surface. The chloride penetration in the direction perpendicular to the crack was measured in a similar way, but only at depths larger than the average penetration depth from the exposed surface.
A schematic representation of the measurement points for the determination of chloride penetration from the surface and perpendicular to the crack is shown in Figure 26 for both artificial and realistic cracks.

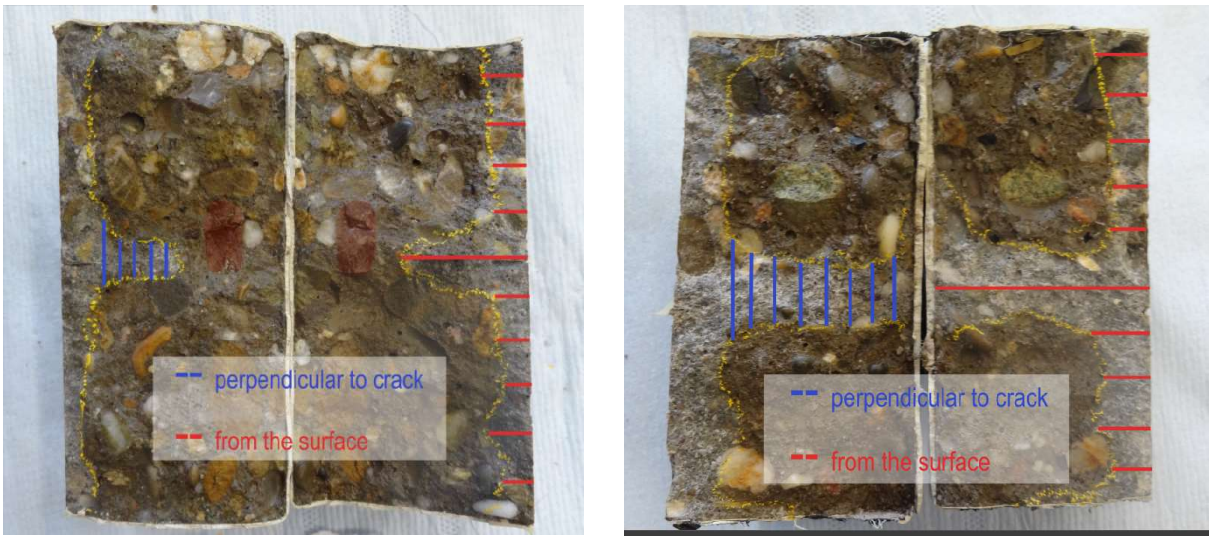

a) b)

Figure 26: Schematic representation of the measurement points for chloride penetration from the surface and perpendicular to crack in case of a) artificial crack and b) realistic crack

Besides the abovementioned chloride penetration depths, the ratio of the area in which chlorides were penetrated to the total surface of the test piece could also be determined with the ImageJ software. This was achieved by analyzing the ratio of the number of pixels in the area affected by chlorides to the number of pixels of the test piece.

An example of the determination of the area affected by chloride penetration for one half of a test specimen using ImageJ is depicted in Figure 27.

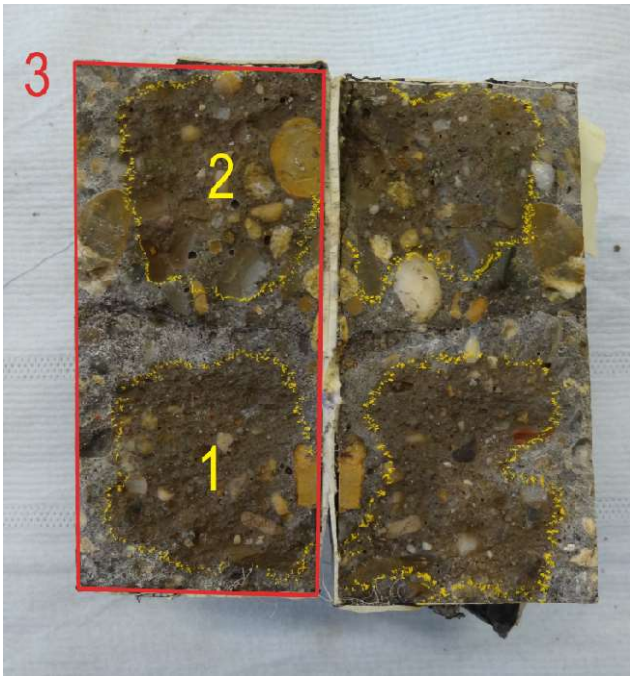

Results

File Edit Font Results

	Area	Mean	Min	Max
1	895058	64.013	8	193
2	904795	69.238	6	225
3	3033090	75.478	2	225

(area 3 – area 1- area 2)/ area 3 = 0,407

40,7% of the area shows chloride penetration

Figure 27: Example of the determination of the area affected by chloride penetration using ImageJ

3.2.8.3 Chloride titrations with potentiometric indication

Chloride profiles

Three samples of each series were used for potentiometric titrations to obtain chloride profiles. The first step consisted of collecting powders from the cylinders. This was done by grinding layers of 2 mm thickness parallel to the exposure surface, in a zone of 10 mm wide and 65 mm long around the crack. Figure 28 shows a schematic representation of the grinding zone around the crack.

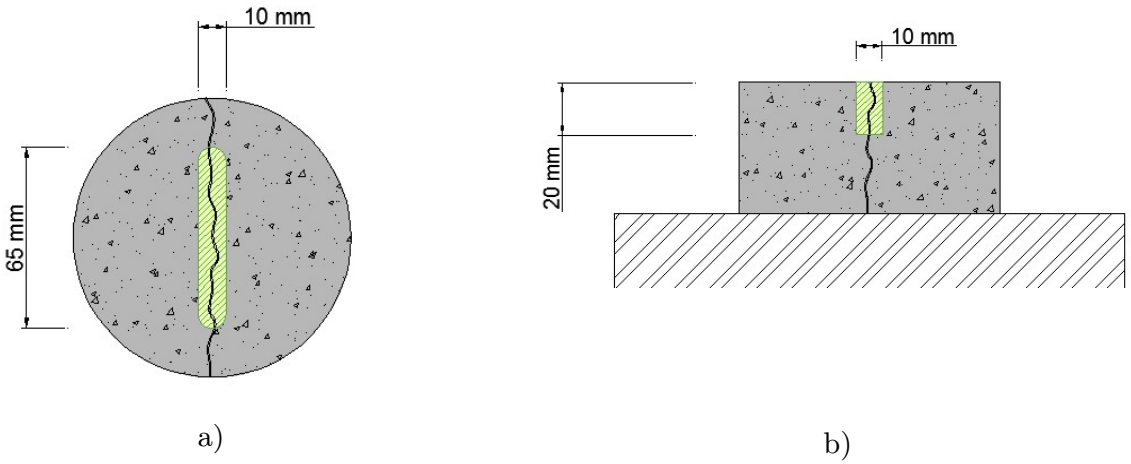

Figure 28: Schematic representation of grinding in a zone around crack; a) top view b) side view

The grinding was executed with a diamond drill head with diameter 10 mm, mounted on a column drill, see Figure 29. By grinding up to a depth of 20 mm, 10 powders were obtained. These powders were collected in small aluminum cups and dried in an oven at 100°C for at least 7 days. Figure 30 shows an example of a ground sample and some powders stored in small aluminum cups.

Figure 29: Grinding using diamond drill head mounted on column drill

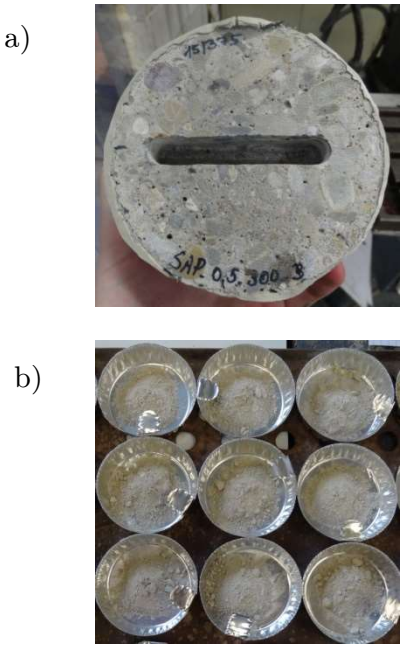

Figure 30: a) example of a ground sample b) powders in aluminum cups

The determination of the total chloride concentration of each layer consisted of an acid-soluble extraction in a nitric acid (HNO_3) solution, followed by a potentiometric titration using silver nitrate as titration solution. As an acid-soluble extraction was used to determine the chloride concentration, it is identified as the acid-soluble chloride concentration.

First, 2 ± 0.001 g of each powder was weighed with a scale with an accuracy of 0.0001 g and put in a glass beaker. At this beaker, 5 ml of nitric acid HNO_3 with a concentration of 0.3 mol/ℓ and 40 ml demineralized water were added. Subsequently, the solution was stirred manually for at least one minute and placed onto a hot plate until boiling. After cooling the solutions down to room temperature, they were filtered in a 100 ml volumetric flask using filter paper with particle retention 12-15 µm. The glass beaker was rinsed with demineralized water and poured over the filter paper. The solution in the flask was further filled up with demineralized water to 100 ml and shaken manually. From these 100 ml solutions, 10 ml was obtained using a pipette. Together with 10 ml demineralized water and 40 ml HNO_3 with a concentration of 0.3 mol/ℓ, this pipetted 10 ml extract formed the test solution. With this test solution, the total chloride concentration of each layer could be determined using a Metrohm MET 702 automatic titration apparatus with 0.01 mol/ℓ silver nitrate as titration solution. The automatic titrator adds $AgNO_3$ to the test solution, until the point of equivalence of the reaction $Ag^+ + Cl^- \rightarrow AgCl \downarrow$ is reached. The moment at which this point of equivalence is reached, is characterized by a sudden change in the potential of the solution. This potential was measured by means of an electrode.
Figure 31 shows some steps in the preparation of the test solution and the Metrohm MET 702 automatic titration apparatus.

a) b) c) d)

Figure 31: a) Weighing of 2 g powder with an accuracy of 0.001 g b) Heating of the solutions until boiling c) Filtering of the solutions using filter paper with particle retention 12-15 µm d) Metrohm MET 702 automatic titration apparatus

Before calculating chloride profiles, the exact concentration of the $AgNO_3$ titration solution (~ 0.01 mol/ℓ $AgNO_3$) needed to be determined by means of a calibration. First, a manual titration was executed using a calibration solution of 15 ml demineralized water, 5 ml 0.01 M NaCl and 40 ml 0.3 M HNO_3.
The potential was read after each addition of 0.5 ml $AgNO_3$ until 0.5 ml before the estimated inflexion point of the ml-mV curve. This inflexion point can be estimated using formula (10):

$$\text{Conc } AgNO_3 * \text{Vol } AgNO_3 = \text{Conc NaCl} * \text{Vol NaCl} \quad (10)$$

Assumed that the concentration NaCl is equal to 0.01 mol/ℓ, the volume NaCl in the calibration solution is 5 ml and the concentration $AgNO_3$ is approximately equal to 0.01 mol/ℓ. From formula (10) it is found that the estimated inflexion point is situated at 5 ml titrated $AgNO_3$.
In the vicinity of the equivalence point (in this case after 4.5 ml $AgNO_3$ was added), the potential was read after each addition of 0.1 ml $AgNO_3$ until 5.5 ml $AgNO_3$ was added in total. Afterwards $AgNO_3$ was again added in steps of 0.5 ml until 2 extra ml had been added (i.e. 7.5 $AgNO_3$ ml in total). From the obtained data, a ml-mV graph could be plotted using Excel. An example of such a graph is depicted in Figure 32. From the titration with the calibration solution, the equivalence point could be obtained. The equivalence point corresponded with the inflexion point of the ml-mV graph, located at 5.07 ml $AgNO_3$ added (green line in Figure 32). In the example of Figure 32, the equivalence point lies around -192 mV (yellow line in Figure 32).

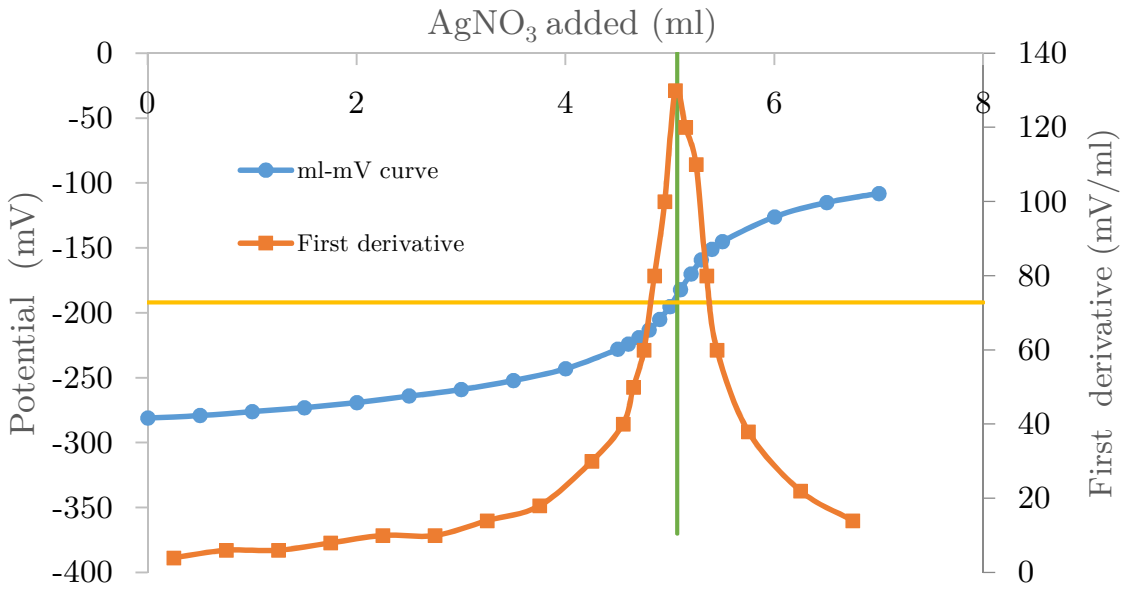

Figure 32: Example of calibration curve

The potential corresponding with the inflexion point was then used as an input for a second titration with the same calibration solution. During this second titration, $AgNO_3$ was automatically added until the point of equivalence was reached. The total volume of $AgNO_3$ added was read from the apparatus. By means of formula (10), the exact concentration of the $AgNO_3$ titration solution was determined.

After calibration, the test solutions were titrated. The resulting acid-soluble chloride content for each layer, expressed in mass% concrete, can be calculated using formula (11):

$$[Cl^-] = \frac{10 \text{ x } 100 \text{ x } 35.45 \text{ x exact } [AgNO_3] \text{ x titrated volume } AgNO_3}{1000 \text{ x mass powder}} \qquad (11)$$

With

- $[Cl^-]$: the acid-soluble chloride content, expressed as mass% concrete;
- 10: the dilution factor;
- 35.45: the atomic mass of chloride [g/mol];
- exact $[AgNO_3]$: the exact concentration of the $AgNO_3$-solution, resulting from the calibration [mol/l];
- titrated volume $AgNO_3$: the amount of volume $AgNO_3$ titrated during the test [ml];
- 1000: a factor taking into account consistency of units;
- mass powder: 2 g of concrete powder in the extraction solution.

In a next step, the acid-soluble chloride content expressed as mass% concrete is converted to mass% binder. Furthermore, in this thesis, the total chloride content was equated with the acid-soluble chloride content [63]. When plotting the measured acid-soluble chloride concentration versus the depth below the exposed surface, the total chloride profile was obtained.

Diffusion coefficient

In a next stage, the diffusion coefficient was calculated according to the method described in NT Build 443 [76].

The values of the chloride surface concentration C_s and the non-steady-state diffusion coefficient D_{nssd} are obtained by fitting equation (12) to the measured chloride contents by means of a non-linear regression analysis in accordance with the method of least squares fit. The first point of the determined chloride profile is omitted in the regression analysis, as the measured chloride content in this first layer is considered not representative.

$$C(x,t) = C_s - (C_s - C_i)\ \mathrm{erf}\left(\frac{x}{\sqrt{4\,D_{nssd}\,t}}\right) \qquad (12)$$

With

- C(x,t): the chloride concentration at depth x and time t [m% binder];
- C_s: the chloride concentration at the surface [m% binder];
- C_i: the initial chloride concentration [m% binder];
- erf: error function;
- x: the distance from the exposed surface until the middle of the layer [m];
- t: the exposure time to NaCl solution [s];
- D_{nssd}: non-steady-state diffusion coefficient [m²/s].

In order to simplify equation (12), the error function erf was replaced by an approximate cumulative normal distribution. The final formula used was:

$$C(x,t) = C_s - 2\,(C_s - C_i)\left[\Phi\left(\frac{\sqrt{2}\,x}{\sqrt{4\,D_{nssd}t}}\right) - \frac{1}{2}\right] \qquad (13)$$

In Figure 33 an example of both the measured chloride profile and the fitted mathematical model is shown. This figure clearly shows the reason why the first measuring point is omitted in the regression analysis, as this point is not in line with the results from the mathematical fit.

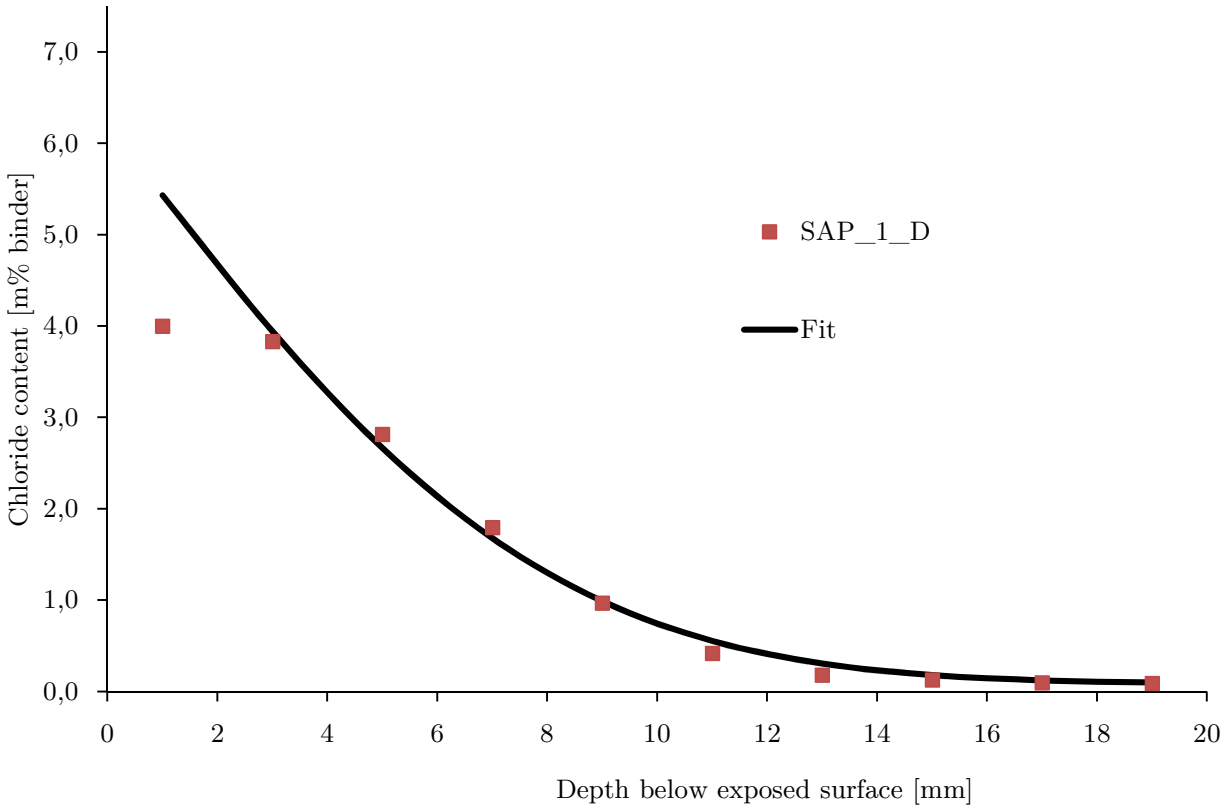

Figure 33: Measured chloride profile (red dots) and fitted model (black line) for an uncracked specimen with 1 m% SAP

3.2.8.4 Research plan

For the determination of the chloride penetration, three different concrete mixtures were used: a reference mixture without SAPs (REF) and two mixtures with varying amount of SAPs, expressed as mass% (m%) of the cement weight: SAP 0.5 m% and SAP 1 m%. The latter made it possible to see the influence of different amount of SAPs added to the concrete. Part of the samples remained uncracked, whereas in the other part cracks were made. Both artificial and realistic cracks were used. In order to see the influence of the crack width, two different crack widths were used: 100 µm and 300 µm.

By varying the different studied parameters (i.e. amount of SAPs, type of crack and crack width) a total of 15 test series was obtained. Per test series, seven samples were made. For each test series, four test pieces were used for spraying $AgNO_3$. The chloride titrations were carried out on three test pieces per series, but only for crack widths of 100 µm due to time limitations.

Each test series has a unique identification, consisting of

- the amount of SAP: REF (0 m% SAP), SAP_0.5 (0.5 m% SAP) or SAP_1 (1 m% SAP);
- the crack width (in the case the sample is cracked): 100 or 300 µm;
- the type of crack: R for realistic crack and A for artificial crack.

The test series SAP_1_300_A for example stands for samples with 1 m% SAP with artificial cracks of 300 µm. A sample with the identification REF stands for an uncracked sample with no SAPs.

An overview of the test series with their identification, number of samples and use is shown in Table 9.

Table 9: Overview of test series for chloride penetration tests

Amount of SAP	Cracked or uncracked	Type of crack	Crack width [µm]	Identification	# of samples		
					Total	Spraying AgNO3	Titrations
REF	uncracked	/	/	REF	7	4	3
	cracked	realistic	100	REF_100_R	7	4	3
	cracked	realistic	300	REF_300_R	7	4	0
	cracked	artificial	100	REF_100_A	7	4	3
	cracked	artificial	300	REF_300_A	7	4	0
SAP 0.5	uncracked	/	/	SAP_0.5	7	4	3
	cracked	realistic	100	SAP_0.5_100_R	7	4	3
	cracked	realistic	300	SAP_0.5_300_R	7	4	0
	cracked	artificial	100	SAP_0.5_100_A	7	4	3
	cracked	artificial	300	SAP_0.5_300_A	7	4	0
SAP 1	uncracked	/	/	SAP_1	7	4	3
	cracked	realistic	100	SAP_1_100_R	7	4	3
	cracked	realistic	300	SAP_1_300_R	7	4	0
	cracked	artificial	100	SAP_1_100_A	7	4	3
	cracked	artificial	300	SAP_1_300_A	7	4	0

Figure 34 shows the followed research plan. First, the samples were made and demoulded the day after. The exposed surface was polished and the non-exposed sides were coated. Subsequently, the samples were cured at a relative humidity of more than 90% and a temperature of 20 ± 2 °C for 28 days. At the age of 28 days, the realistic cracks were formed using a crack-width controlled splitting test and a first microscopical investigation of the cracks (both artificial and realistic) was executed. Next, the samples were exposed to wet-dry cycles (12 hours wet, 12 hours dry) in demineralized water for 4 weeks. During this period, the cracks were investigated microscopically after 3, 7, 14 and 28 days in order to see the visual closure of the cracks in time. The next step in the research plan was placing the samples in a NaCl-solution for 7 weeks, followed by spraying with $AgNO_3$ and the chloride titrations.

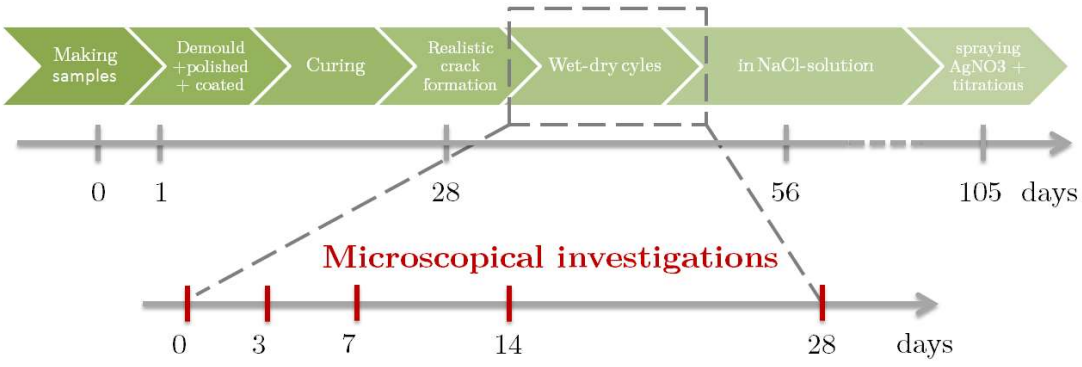

Figure 34: Schematical representation of research plan for chloride tests

3.2.9 CO_2 diffusion tests

For the CO_2 diffusion tests, cubes with sides 100x100x100 mm^3 were used. All sides of the cubes, except the one to be exposed to CO_2, were coated with an epoxy coating. In this way, one-dimensional penetration of CO_2 from one side of the cube is assured. More information on the sample preparation and coating can be found in section 3.2.2.
At the age of 12 days, the specimens were placed in a carbonation chamber containing 1 vol% CO_2 at a temperature of 20 ± 2°C and relative humidity of 60 ± 5%. After 2, 4, 6 and 12 weeks, the carbonation depth was determined by spraying phenolphthalein on the broken surfaces of the samples.

3.2.9.1 Spraying Phenolphtalein

Three samples per test series were split orthogonally to the crack, see Figure 35a. The carbonation depth was visualized by means of spraying a 1% phenolphthalein pH-indicator on both halves of the broken specimen. Non-carbonated zones turned out purple, whereas the carbonated zone stayed colorless, see Figure 35b.

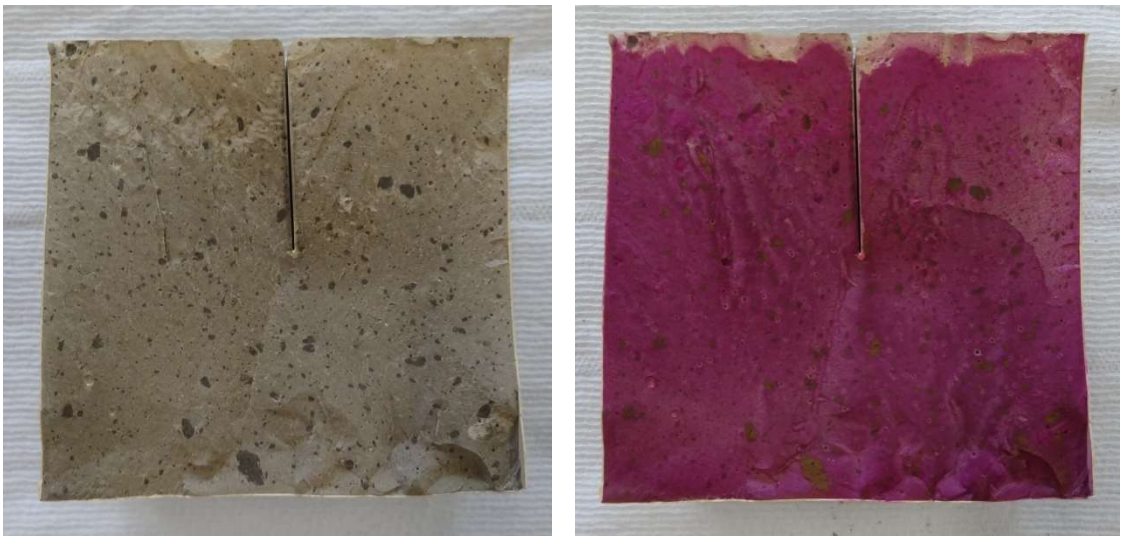

a) b)

Figure 35: a) sample split orthogonally to crack b) visualization of carbonation depth by spraying phenolphthalein: non-carbonated depths are purple, carbonated zones are colorless

The carbonation depth from the exposed surface was measured to the nearest millimeter at 18 positions along the surface (5 mm distance between the measurements). In the case there was carbonation in the direction perpendicular to the crack, this was measured in a similar way.

3.2.9.2 Research plan

To determine the carbonation, three different mixtures were used: a cement paste (CEM), a concrete mixture without SAPs (CON) and a concrete mixture with 1 m% of cement weight SAPs (SAP). Some of the samples remained uncracked, whereas in the other part artificial cracks of 500 µm were made. To investigate the influence of different curing conditions, part of the cracked samples is submersed in water for 24 hours every four weeks.

By varying the different studied parameters (i.e. type of mixture, cracked versus uncracked and curing condition) a total of nine test series was obtained. Per test series, 18 samples were made and demoulded the day after. The exposed surface was polished and the non-exposed sides were coated. Subsequently, the samples were cured at a relative humidity of more than 90% and a temperature of 20 ± 2°C for 12 days. At the age of 12 days, the specimens were placed in a carbonation chamber containing 1 vol% CO_2 with a temperature of 20°C and relative humidity of 60%, except for the samples that will be periodically immersed in water. These samples were first immersed in water for 24 hours before placing them in the carbonation chamber. After 2, 4, 6 and 12 weeks of exposure to 1% CO_2, three samples of each series were split and sprayed with phenolphthalein.
In case the sample was cured with water, the sample was immersed in demineralized water for 24 hours every four weeks.

A schematic representation of the research plan is depicted in Figure 36.

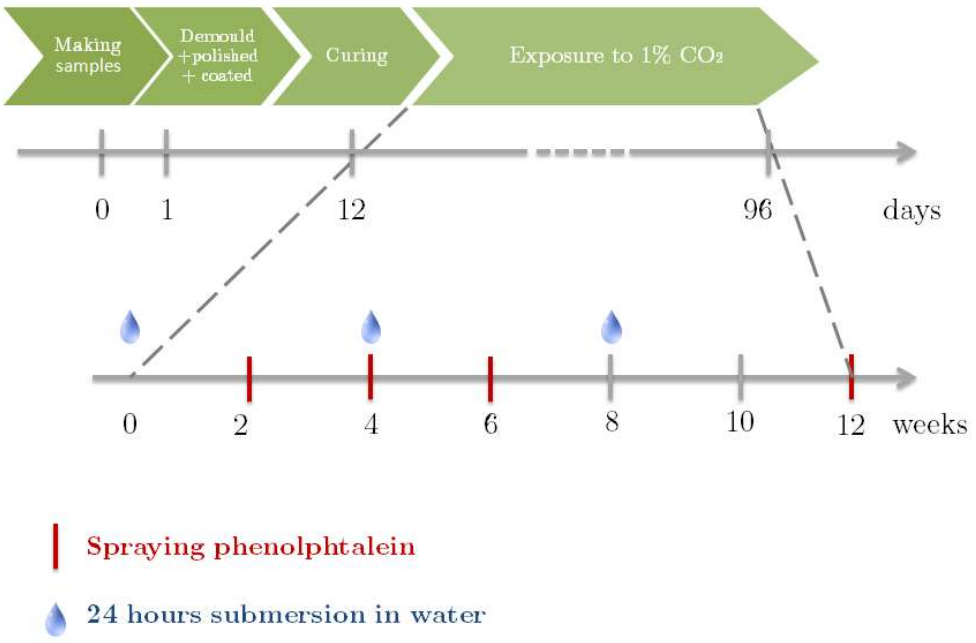

Figure 36: Schematical representation research plan for carbonation tests

Each test series has a unique identification, consisting of

- The type of mixture: CEM, CON or SAP;
- The letter 'C' in the case a crack is present;
- 'Water' in the case the cracked sample is cured with water.

An overview of the test series with their identification, number of samples and use is tabulated in Table 10.

Table 10: Overview of test series for carbonation tests

Type of mix	Cracked or uncracked	Curing condition	Identification	# of samples spraying phenolphtalein
CEM	uncracked	/	CEM	18
	cracked	/	CEM_C	18
	cracked	water	CEM_C_Water	18
CON	uncracked	/	CON	18
	cracked	/	CON_C	18
	cracked	water	CON_C_Water	18
SAP	uncracked	/	SAP	18
	cracked	/	SAP_C	18
	cracked	water	SAP_C_Water	18

After 18 and 24 weeks, two extra test series will also be tested by spraying phenolphthalein on three samples Every four weeks, part of the samples will be immersed in demineralized water for 24 hours. As these tests will be executed after the deadline of this thesis, the results are not included in this thesis. Nevertheless, a schematic representation of the complete research plan is depicted in Figure 37.

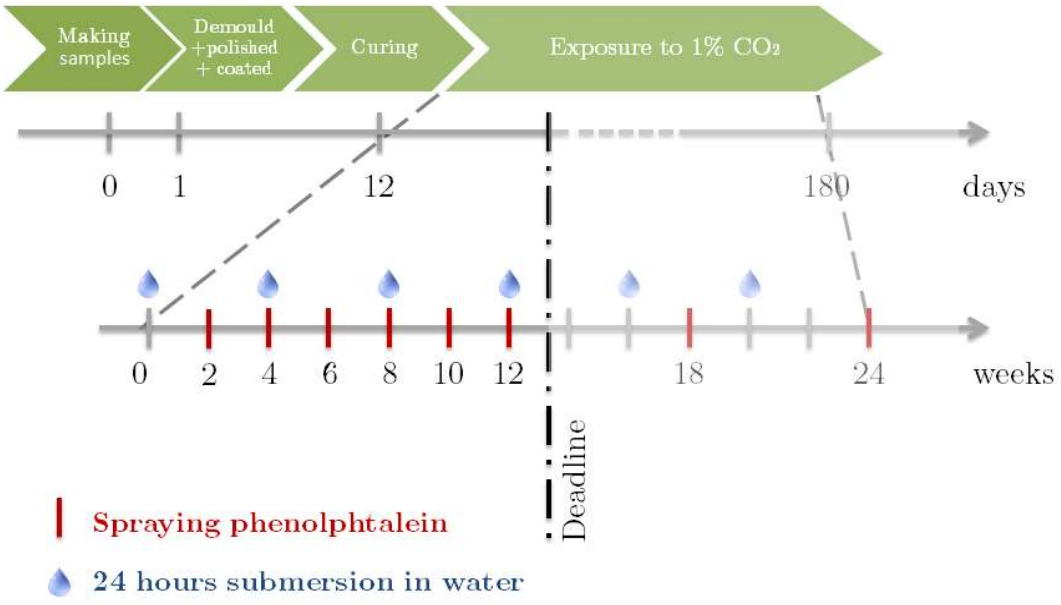

Figure 37: Complete research plan for carbonation tests

3.2.10 Statistical Analysis

The obtained results were statistically analyzed by means of the software SPSS Statistics 22.
Two means were compared by performing an independent samples t-test. When comparing multiple means, an Analysis of Variance (ANOVA) was performed.
The homogeneity of the variances was studied on the basis of a Levene's test. In the case of homogeneous variances, the multiple comparison test of Student-Newman-Keuls was performed. In the case the variances were not homogeneous, a Dunnett's T3 test was performed. On the basis of one of these two tests, it could be concluded whether the average values were significantly different or not. A significance level of 5% was used for all tests, unless specified otherwise.

All graphs in chapter 4 Results and Discussion represent average values, unless explicitly stated otherwise. The error bars represent the standard deviations of the individual measurements.

4 Results and Discussion

4.1 Swelling behavior of SAPs

In this section, the swelling behavior of the used SAPs is discussed into more detail. When dry SAP particles come in contact with a fluid, the cross-linked copolymers will straighten, resulting in a swelling of the SAPs. The amount of fluid that a single SAP particle can absorb, depends on different parameters like the temperature, relative humidity, pressure and ionic composition of the exposure liquid ([17],[18]).

4.1.1 Filtration method

The average absorption [g fluid/g SAP] with the standard deviation for different types of fluid is depicted in Figure 38. The SAPs have an absorption capacity of 240.0 ± 9.3 g fluid/g SAP in demineralized water, 21.2 ± 1.2 g fluid/g SAP in a chloride solution, 21.4 ± 1.3 g fluid/g SAP in sea water and 39.8 ± 1.1 g fluid/g SAP in cement filtrate.

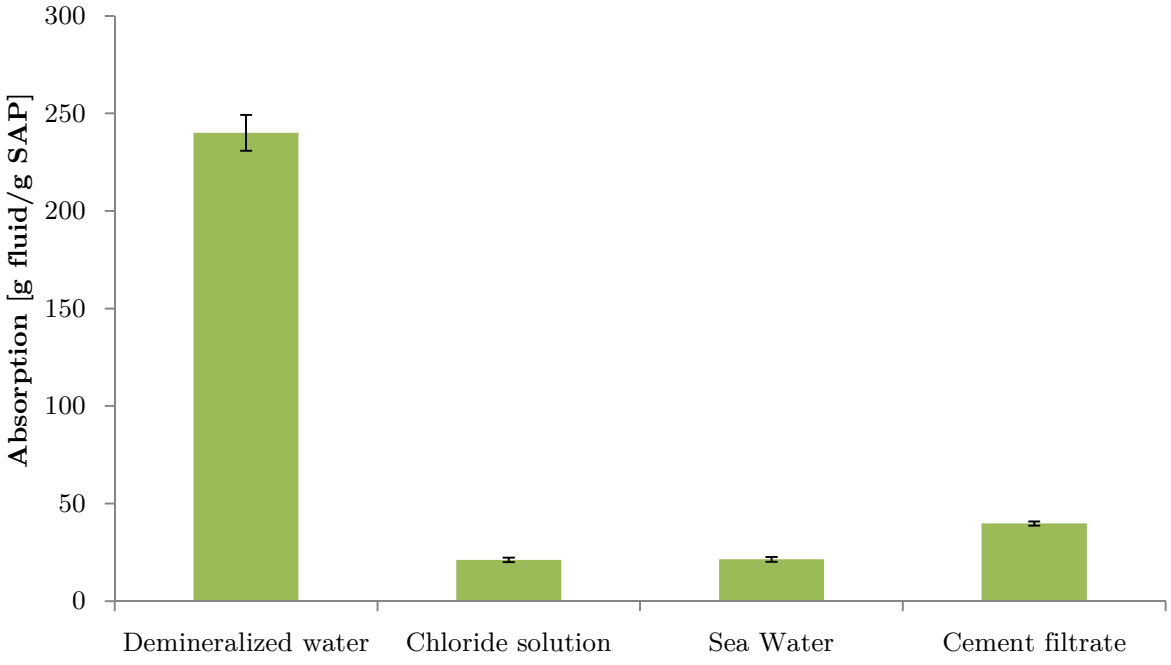

Figure 38: Average absorption in different fluids with their standard deviation [g fluid/g SAP]

The average absorption is not significantly different for chloride solution and sea water, but is significantly different for all other combinations of fluids.

Cations like K^+, Na^+, Mg^{2+} or Ca^{2+} give rise to a so-called charge screening effect of the negatively charged polymer chains, resulting in a lowered absorption and less swelling of the SAP particles. This phenomenon is the reason for the low absorption in the case of chloride solution (Na^+), sea water (Na^+, Mg^{2+} and Ca^{2+}) and cement filtrate (K^+, Na^+, Ca^{2+}). Demineralized water gives the highest absorption as there is no or only a limited shielding effect due to the absence or limited amount of cations present. Furthermore, the presence of divalent cations (Mg^{2+} and Ca^{2+}) gives rise to an additional reduction of the swelling properties as these cations form strong complexes with the carboxylate groups and can therefore act as cross-linkers. Due to the latter, there is less opportunity for the repelling negative charges to increase the volume of the swollen SAP, which results in a lower swelling degree [43].

It is important to note that the absorption of SAP particles in concrete is even smaller than in cement slurry because of the weight exerted by the surrounding material and because the fluid inside concrete may differ from the artificial cement slurry [2]. Brüdern and Mechtcherine [87] state that the swelling capacity in a concrete mixture is about half the one in filtered cement slurry.

As already mentioned in the literature review (see section 2.2.5) the SAPs will absorb part of the mixing water, resulting in a negative effect on the workability. Therefore, additional water needs to be added to compensate for this loss in workability. Based on the results of the filtration method in cement slurry and the aforementioned statement of Brüdern and Mechtcherine, the amount of additional water that should be added approximates 20 g/g SAP. However, in the used mixtures the amount of additional water was increased to 27 g/g SAP to obtain a similar workability as mixtures without SAPs.

4.1.2 Microscopic analysis

Based on the measurements of the maximum dimension of five randomly chosen SAP particles in the dry state, an average maximum dimension of 638 ± 61 µm was found. After addition of drops of demineralized water until the particle was fully saturated, the average swollen dimension amounts 5933 ± 450 µm, indicating a magnification with a factor 9.
An example of the swelling behavior of an individual SAP particle where demineralized water is gradually added, is depicted in Figure 39 a-e.
The investigated particle had an initial maximum dimension of 561 µm and was found to have a maximum dimension of 5155 µm after absorption, which is 9 times greater.

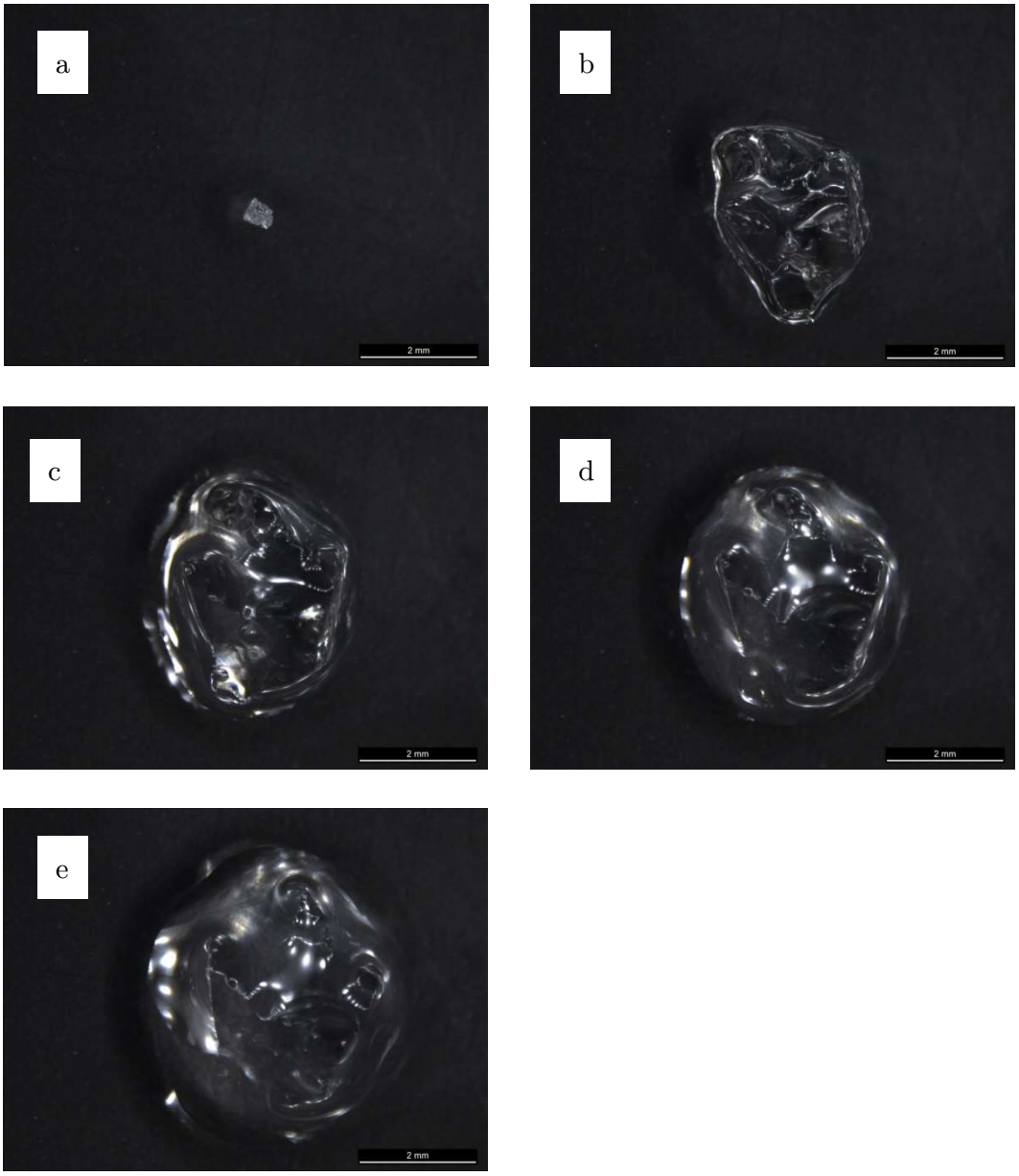

Figure 39 a-e: Gradual growth of an individual SAP particle when moistened with demineralized water

This microscopic analysis can also be used to determine the absorption capacity of an individual SAP particle in another way, namely by using formula (5). This method can give very accurate results in the case of spherical SAP particles, as the swelling of an individual particle is studied without taking into account possible water present in between the particles as could be the case in the filtration method. However, this type of SAP does not have spherical particles, hence the radius to be used in formula (5) needs to be estimated.
In a first calculation, the maximum dimension of the swollen particle was used as the radius of the spherical swollen particle. This led to an overestimation of the

absorption capacity as in reality the volume of the swollen SAP is much smaller. The found average absorption capacity is 928.3 ± 233.3 g fluid/g SAP.
In order to get more realistic values, it was decided to redo the calculations with a radius equal to the average of the maximum and minimum dimension of the swollen particle. In this way, the obtained average absorption capacity was found to be 200.0 ± 40.0 g fluid/g SAP. This result is closer to the value of 240 g/g SAP obtained in the filtration method with demineralized water.
It is clear that this method is not very suitable in this case, as the SAP particles are not spherical and thus a radius needed to be estimated. As the five studied particles differed a lot in shape and dimensions, the obtained standard deviations are also quite large in comparison to the standard deviations obtained with the filtration method.
Although this method is quite time-consuming, it provides an estimation of the expected order of magnitude of the absorption capacity of an individual SAP particle. When applying the filtration method, it is possible that extra water is present in between the SAP particles due to adhesive effects, resulting in larger calculated absorption capacities than in reality. With this microscopic method, one SAP particle is studied, so this phenomenon will not occur.
However, as the influence of capillary forces is limited, the filtration test can serve to determine the correct absorption capacity.

4.1.3 Vortex method

The swelling time for the SAPs is 38 ± 2 s in demineralized water, 36 s in chloride solution and 28 s in sea water. All obtained swelling times are lower than the mixing time with water (150 s) when making concrete, so it can be assumed that the SAPs will already swell to their maximum dimensions during mixing and settlement of the concrete. Nevertheless, this method is quite subjective, as different people will judge the disappearance of the vortex at different times.

4.2 Concrete properties

The measured concrete properties of the mixtures that are used for the determination of self-healing and chloride penetration are summarized in Table 11.

Table 11: Properties of the concrete mixtures: self-healing and chloride penetration

		REF	**SAP_0.5**	**SAP_1**
Slump	[mm]	150	150	155
Flow	[mm]	440	430	430
Compressive strength	[MPa]	65.5 ± 1.3	49.2 ± 0.8	38.2 ± 1.2

The mean compressive strengths of the three test series are significantly different from one another (level of significance = 0.05). When the amount of added SAPs is increased, a lower compressive strength at 28 days is found due to the formation of macro pores upon shrinkage of the SAPs. These findings are comparable to the findings of Mechtcherine and Reinhardt [52], Snoeck et al. ([13],[15]) and Mignon et al. [43].
From the almost identical obtained values for the slump and flow of the three different mixtures, it can be concluded that the amount of additional water, namely 27 g/g SAP, indeed results in the intended similar workability.
The measured concrete properties of the mixtures for the determination of carbonation are summarized in Table 12.

Table 12: Properties of the concrete mixtures: carbonation (- not applicable)

		CON	**SAP**	**CEM**
Slump	[mm]	165	150	-
Flow	[mm]	500	430	-
Air content	[%]	2.6	4.2	-
Density (fresh state)	[kg/m³]	2345	2220	-
Open porosity	[%]	11.9 ± 0.4	17.4 ± 0.4	41.9 ± 0.3

As the cement paste CEM had a very low viscosity, no fresh concrete properties could be determined in this case.
Due to the addition of SAPs, the air content of the fresh mixture increases. This higher amount of entrained air causes a lower fresh concrete density compared to the reference concrete mixture without SAPs.
The mean open porosities of the three test series are significantly different from one another (level of significance = 0.05). An increase in open porosity has a significant influence on both chloride penetration and carbonation, as will be discussed in section 4.5 and 4.6 respectively.

4.3 Crack formation

4.3.1 Artificial cracks

Artificial cracks with intended widths of 100 µm, 300 µm and 500 µm are created by putting thin brass plates with a thickness corresponding to the desired crack width in the fresh concrete.

In Figure 40 the obtained mean crack widths of each sample for artificially created cracks are shown. The target crack width is 100 µm. For test series REF_100_A, mean crack widths in between the interval [85 µm – 154 µm] are found. For test series SAP_0.5_100_A and SAP_1_100_A, mean crack width intervals of [98 µm – 139 µm] and [97 µm – 182 µm] respectively are found.

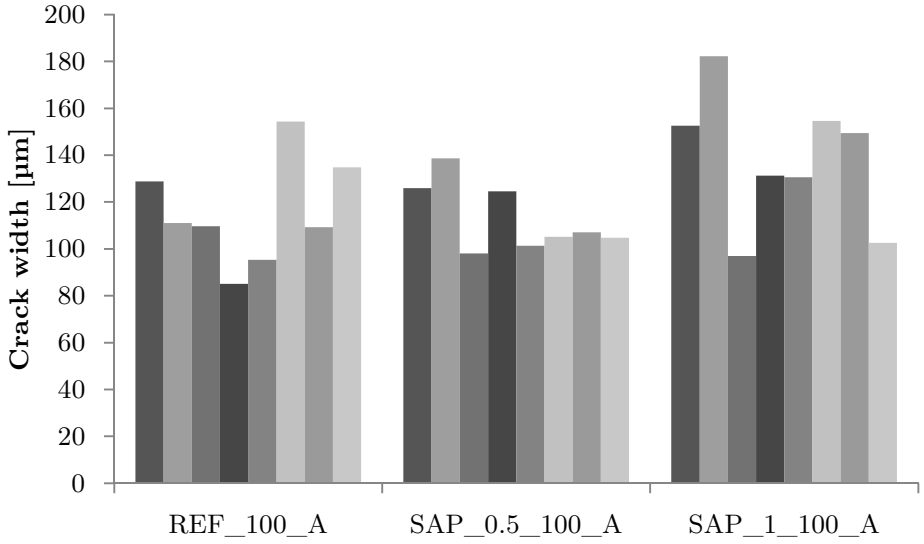

Figure 40: Crack width measurements artificial cracks, target crack width 100 µm

The mean crack widths of test series REF_100_A and SAP_0.5_100_A are not significantly different from each other, whereas the mean crack width of test series SAP_1_100_A is found to be significantly higher than the means of the two other test series (level of significance = 5%).

In Figure 41 the obtained mean crack widths for artificially created cracks with target crack width of 300 µm are shown. For test series REF_300_A, mean crack widths in between the interval [291 µm – 303 µm] are found. For test series SAP_0.5_300_A and SAP_1_300_A, mean crack width intervals of [286 µm – 307 µm] and [299 µm – 332 µm] respectively are found.

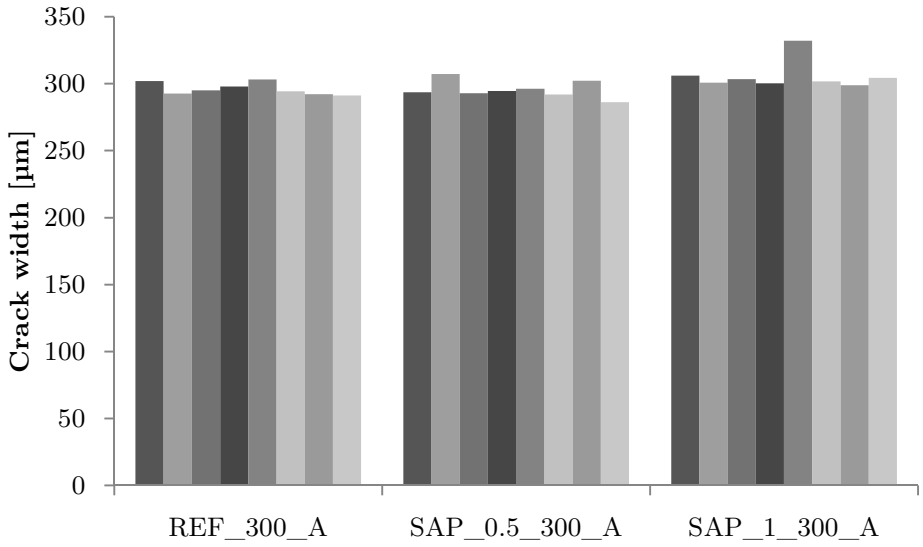

Figure 41: Crack width measurements artificial cracks, target crack width 300 µm

A similar conclusion as for artificial 100 µm cracks is found: the mean crack widths of test series REF_300_A and SAP_0.5_300_A do not differ significantly, whereas the mean crack width of test series SAP_1_300_A is significantly higher than the other two test series. Even if the fifth sample of SAP_1_300_A is omitted from the ANOVA-analysis, as it can be considered an outlier, a significant difference between the different test series is still found.

Table 13 shows the amount of tested samples, the mean crack width, the standard deviation on the individual measurements as well as the measured minimum and maximum crack width for the two used target crack widths 100 and 300 µm for the three different test series.

Table 13: Microscopic crack width measurements artificial cracks

Test series	# samples	Mean [µm]	St.dev. [µm]	Minimum [µm]	Maximum [µm]
REF_100_A	8	116	29	28	197
SAP_0.5_100_A	8	113	26	62	189
SAP_1_100_A	8	138	44	58	317
REF_300_A	8	296	9	272	318
SAP_0.5_300_A	8	296	12	271	375
SAP_1_300_A	8	306	16	263	394

For both 100 µm and 300 µm artificial cracks, the mean crack width created in samples containing 1 m% SAP is significantly larger than for the other two test series. Also the corresponding standard deviation is found to be larger. A possible explanation could be found in a less pronounced bond between the concrete and the brass plate in case of a high amount of SAPs. The water from the SAPs can

create a thin film of water around the brass plates, resulting in somewhat larger crack widths. It was also observed that the higher the amount of SAPs, the easier it was to remove the brass plates, possibly due to the lubricating effect of the SAPs and the thin water layer around the plates.

The measurements of the 100 µm crack widths show that the observed crack widths at the surface are generally somewhat larger than the thickness of the brass plates. In case of 300 µm crack widths however, the crack widths are almost the same as the thickness of the plates. A reason for this can be found in the more difficult intact removal of 100 µm plates from the hardened concrete. A lot of wiggling was needed to pull out the very thin plates, whereas the thicker 300 µm plates could easily be removed. A similar observation can be made about the mean crack width intervals: in case of 100 µm cracks the intervals are found to be more broad than in case of 300 µm cracks.
Nonetheless, the produced crack widths are considered to satisfactorily represent the intended crack widths of 100 and 300 µm.

For the carbonation tests, artificial cracks of 500 µm were created. As these cracks were not made to investigate self-healing and were as a consequence not further investigated under the microscope, crack widths of only three samples of each test series were recorded in order to have an indication of the initially created crack widths. The three samples were chosen randomly and are assumed to be representative for all created cracks.
The measured crack widths are shown in Figure 42.

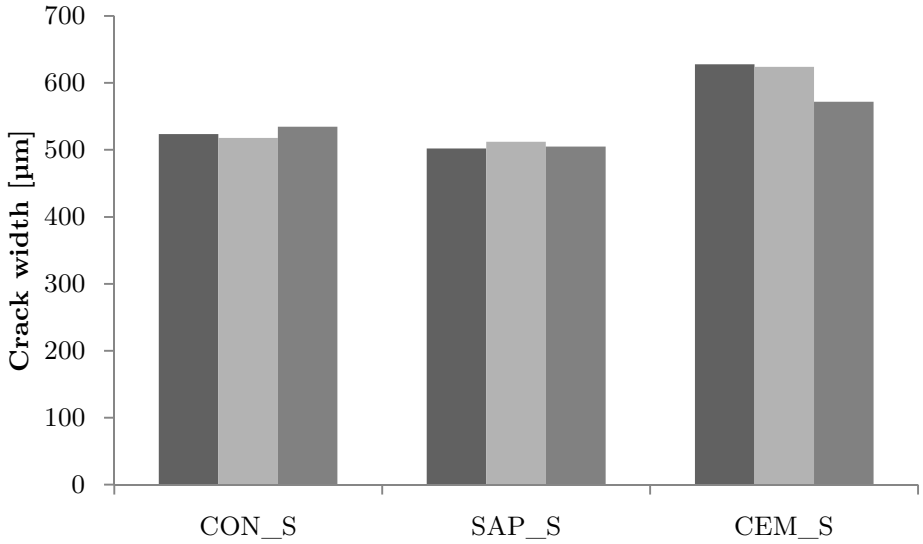

Figure 42: Crack width measurements artificial cracks, target crack width 500 µm

For test series CON_S, mean crack widths in between the interval [518 µm – 535 µm] are found. For test series SAP_S and CEM_S mean crack width intervals of [502 µm – 512 µm] and [572 µm – 628 µm] respectively are found.

The mean crack widths for the three test series are significantly different (level of significance = 0.05). In this case, the mixture composition has a significant influence on the created artificial crack widths. Although this topic was not treated in more detail in this thesis, it could be interesting to investigate what happens exactly at the interface mixture-steel plate and which components are found at the crack walls as this can have an influence on carbonation depths, chloride penetration and self-healing of the artificial cracks.

Table 14 summarizes some descriptive statistics of the measured microscopic crack widths for samples with artificial 500 µm cracks. However, these results should be treated with caution, as only three samples per test series were investigated.

Table 14: Microscopic crack width measurements artificial cracks, 500 µm

Test series	**# samples**	**Mean [µm]**	**St.dev. [µm]**	**Minimum [µm]**	**Maximum [µm]**
CON_S	3	525	24	466	593
SAP_S	3	506	23	462	578
CEM_S	3	608	32	544	666

The realized cracks in cement paste are on average wider than the thickness of the plate, especially in comparison to the two other test series. This is probably due to a difference in bonding between the plates and the mixture and/or the presence of fines at the interface that create a lubricating layer around the plates. This results in larger crack widths and a more easy removal of the plates.

4.3.2 Realistic cracks

In case of realistic cracks, the intended crack widths were 100 µm and 300 µm and are formed by a crack-width controlled splitting test, see section 3.2.6.1.

As a first test series of 100 µm cracks did not show any healing, a second test series with cracks of 100 µm was made and tested, see also section 4.4. As this part focuses on the initially made crack widths and the crack formation methods, it is interesting to mention and compare the results of both test series.

The obtained mean crack widths for realistic created cracks with a targeted crack width of 100 µm are depicted in Figure 43 and Figure 44 for test series one (1) and two (2) respectively.

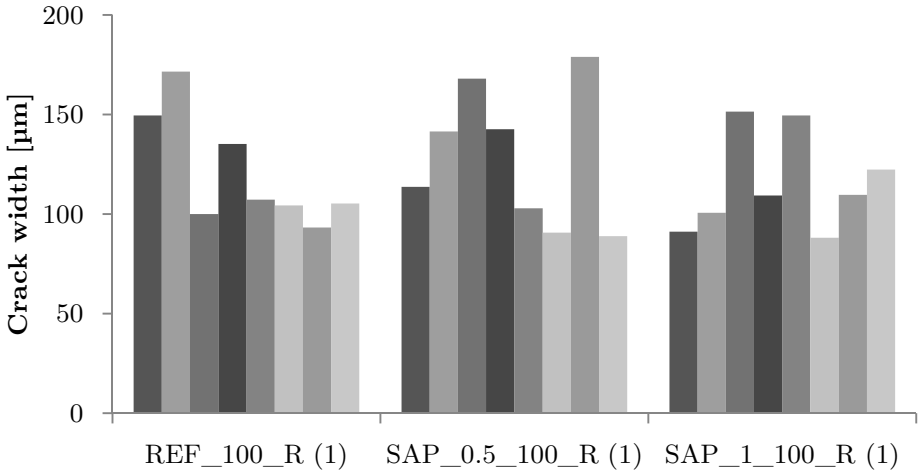

Figure 43: Crack width measurements realistic cracks, target crack width 100 µm, test series 1

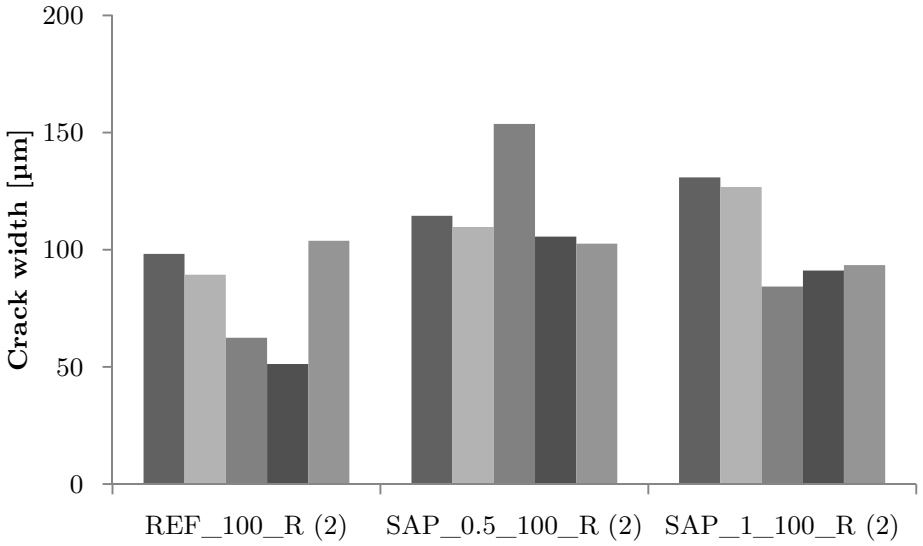

Figure 44: Crack width measurements realistic cracks, target crack width 100 µm, test series 2

For test series REF_100_R the intervals for the obtained mean crack widths vary from [93 µm – 172 µm] and [51 µm – 104 µm] for series 1 and 2 respectively. In case of test series SAP_0.5_100_R ranges of [89 µm – 179 µm] for series 1 and [103 µm – 154 µm] for series 2 are noticed. For SAP_1_100_R the intervals were situated in between [88 µm – 151 µm] and [84 µm – 131 µm] for series 1 and 2 respectively.

To compare the obtained results, a one-way ANOVA with a Dunnett's T3 test (level of significance = 0.05) is performed for series 1 and 2 separately. Secondly, the results of series 1 and series 2 are compared with an independent samples t-test.
When looking at the results of series 1, the obtained average crack width of test series SAP_0.5_100_R is significantly higher than the average crack width of series SAP_1_100_R, but no significant difference was found between other combinations. For test series 2 however, it was found that the average crack widths of all three test series were significantly different from each other.

In theory, there should be no significant difference between the results obtained from test series (1) and (2), as the followed method as well as the used materials are the same. It was found that in case of a significance level of 5%, the means between corresponding test series from series (1) and (2) are significantly different. However, in case of a lowered significance level of 1%, the mean crack widths between series (1) and (2) for test series SAP_0.5_R and SAP_1_R are no longer significantly different, whereas the means of REF_100_R_(1) and REF_100_R_(2) are still significantly different. The latter is probably mainly due to personal influences when executing the test, like for example placing of the sample in the middle of the apparatus, placing of the LVDT's etc.

In Figure 45 the obtained mean crack widths for realistic created cracks with target crack width of 300 µm are shown. For test series REF_300_R, mean crack widths in between the interval [218 µm – 371 µm] are found. For test series SAP_0.5_300_R and SAP_1_300_R mean crack width intervals of [173 µm – 315 µm] and [244 µm – 532 µm] respectively are found.

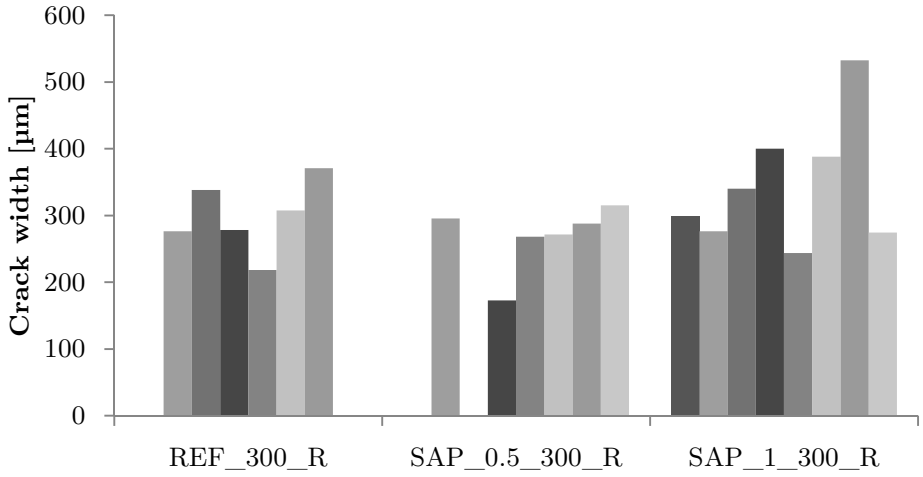

Figure 45: Crack width measurements realistic cracks, target crack width 300 µm

In the case of REF_300_R and SAP_0.5_300_R the results of only six samples are shown. This is due to the fact that two samples of each series were broken during the execution of the test.

A one-way ANOVA with a Dunnett's T3 test (level of significance = 0.05) showed that all three test series were significantly different from each other.

In Table 15, the amount of tested samples, the mean crack width, the standard deviation of the individual measurements as well as the measured minimum and maximum crack width for the two used target crack widths 100 µm (series 1 and 2) and 300 µm for the three different test series REF, SAP_0.5 and SAP_1 are summarized.

Table 15: Microscopic crack width measurements realistic cracks

Test series	**# samples**	**Mean [µm]**	**St.dev. [µm]**	**Minimum [µm]**	**Maximum [µm]**
REF_100_R (1)	8	121	47	23	252
SAP_0.5_100_R (1)	8	129	52	34	281
SAP_1_100_R (1)	8	116	42	45	231
REF_100_R (2)	5	81	34	20	219
SAP_0.5_100_R (2)	5	116	42	31	274
SAP_1_100_R (2)	5	106	34	29	190
REF_300_R	6	298	118	72	659
SAP_0.5_300_R	6	268	97	56	545
SAP_1_300_R	8	342	158	46	809

When investigating the results for 100 µm cracks, it can be seen that the crack widths of series 2 are a closer match to the predefined crack width than series 1. As the method as well as the used materials are the same for both test series, this difference is probably due to the more experienced level of the executor, as it was the second time this kind of tests were performed.

The used mixture has a significant influence on the obtained realistic crack widths, as all the other parameters were kept constant for the different series. This is probably due to their different compressive strength, see also section 4.2. It is quite difficult to obtain the intended crack width by applying this method. Several reasons can contribute to this phenomenon: crack recovery during unloading, the heterogeneity of the samples as well as personal influences of the executor.
The crack width varies a lot along the crack, resulting in large standard deviations. Nevertheless, the measured ranges per intended crack width are still acceptable.

From the Kolmogorov-Smirnov normality test with significance level 0.05, it was found that all test series except for SAP_1_100_R and SAP_1_300_R were

normally distributed. The assumption made in section 3.2.6.3 for the selection of the test side, is therefore justified in most cases.

4.3.3 Comparison crack formation method

Apart from the advantages and disadvantages of the methods for creating artificial or realistic cracks mentioned in section 2.2.2 of the literature review, there exist some other differences between both methods. The most remarkable differences are summarized in the next paragraphs.

In case of the formation of realistic cracks, personal influences (for example the eccentric placing of the sample in the apparatus) have a larger influence on the obtained results in comparison to the formation of artificial cracks. A proper execution of the method is therefore even more important in the case of realistic cracks, as it will influence the results to a large extent. In case of artificial cracks, the personal influences on the results are very limited.
The obtained realistic cracks are situated in much broader ranges than in case of artificial cracks, as the crack widths are less consistent along the crack length. The formed realistic cracks also deviate more from the intended crack width due to (uncontrollable) parameters like heterogeneity of the specimens, crack closure upon unloading and the level of experience of the executor.

In case of artificially made cracks, the type of mixture has an influence on the obtained crack width. A possible explanation could be a difference in bonding between the plates and the mixture and/or the presence of fines at the interface that create a lubricating layer around the plates. Also in the case of realistic cracks, a significant difference in mean crack width was obtained for the different studied mixtures. As the formation of realistic cracks is done with a splitting test, the difference in compressive strength between series REF, SAP_0.5 and SAP_1 is probably the governing factor. Further research is needed to verify these hypotheses.

Micrographs taken with an optical microscope during crack width measurements are depicted in Figure 46 a and b for artificial and realistic cracks respectively.
In Figure 46b, a second smaller crack can be observed next to the intended main crack, this is in contrast with artificial cracks where no secondary cracks were observed. The presence of these micro-cracks can have an influence on the chloride penetration. However, this was not further investigated in this thesis as it is assumed that their influence is rather limited because they will probably heal autogenously due to their small crack width.

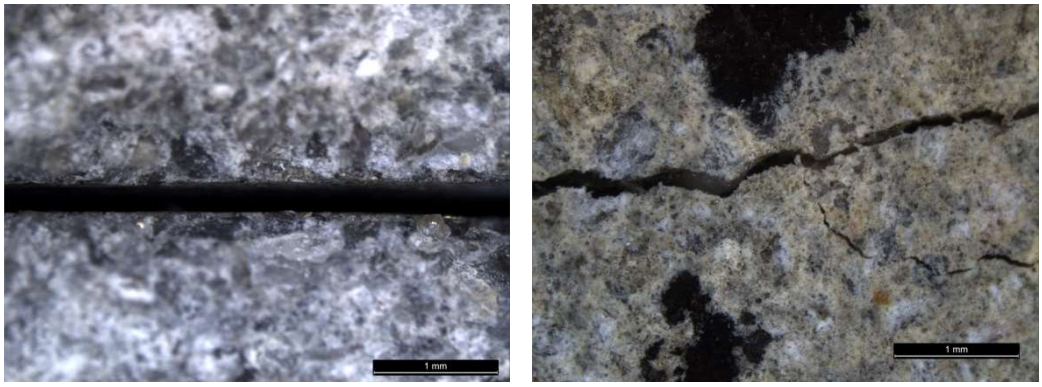

a) b)

Figure 46: Pictures taken with optical microscope of a) artificial crack and b) realistic crack

4.4 Self-healing of the cracks

A first test series was made to study the effect of SAPs on the self-healing of cracks. Therefore three different mixtures were studied: REF (0 m% SAP), SAP_0.5 (0.5 m% SAP) and SAP_1 (1 m% SAP). Both artificial and realistic cracks of 100 and 300 µm were made in order to examine the influence of the crack formation method as well as the crack width on the self-healing properties. The samples were subjected to wet-dry cycles and microscopically investigated after 3, 7, 14 and 28 cycles. However, none of the studied samples showed healing at the surface. The lack of visible crack healing at the surface is probably due to the sample preparation: after demoulding the samples, the surfaces were wet polished with an excess of water by means of a circular saw in order to obtain a smooth surface. This operation might result in a very low amount of unhydrated cement particles and SAPs at the surface, which are both needed in order to stimulate self-healing. Furthermore, the crack was extensively rinsed and cleaned, removing most of the building blocks needed for a sufficient autogenous healing. In that way, these specimens can be considered unhealed. A second test series was therefore made without saw cutting of the surface nor cleaning of the cracks. Furthermore, the samples were not coated in order to eliminate any possible influence of the coating.

Although the samples of the first test series did not show any healing at the surface, they were further examined to see the influence of SAPs on the chloride penetration, see section 4.5.

In case of artificially made cracks of 100 µm, the cracks were almost fully blocked with impurities, probably originating from the polishing of the surface, see Figure 47. This phenomenon was not observed in the case of larger 300 µm artificial cracks, neither in the case of realistic cracks as these cracks were made after saw

cutting of the surface. It was tried to clean the cracks by pulling a thinner brass plate through the crack and by means of compressed air, but this made no significant difference. As the crack is blocked in this case, this could have an influence on for example the chloride penetration through the crack. This is further investigated in section 4.5.

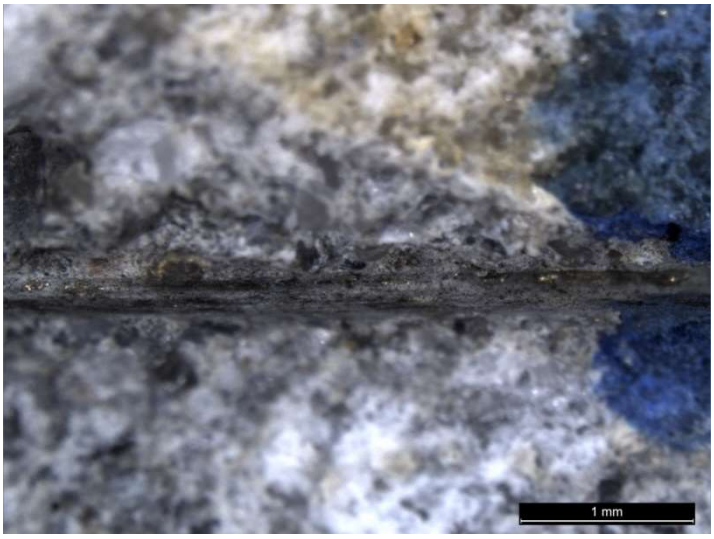

Figure 47: Blocking of 100 µm artificial cracks by impurities

The second series was made of the same mixtures as series 1, namely a reference mixture without SAPs (REF), a mixture with 0.5 m% SAPs (SAP_0.5) and a mixture with 1 m% SAP (SAP_1). Per mixture, five samples were made and investigated microscopically after 3, 7, 14 and 28 days in wet-dry cycles. The difference with series 1 is that the surface was not polished this time, the sides were not coated and only the self-healing of realistic cracks of 100 µm was studied due to time limitations.

The results of the microscopic investigation are depicted in two ways. In a first graph A, the remaining average crack width after n wet-dry cycles for all five samples per test series are depicted. A second graph B depicts the average crack closure ratio after n wet-dry cycles for all five samples per test series. In the latter, the crack closure ratio after 0 cycles is not depicted, as this is by definition 0%.
In order to increase the readability of the graphs, the error bars are not depicted. However, it is important to mention that the results showed a lot of scatter and some of the samples could be considered outliers, namely REF_100_R_D, SAP_0.5_100_R_D and SAP_1_100_R_C. Yet, as their influence seemed to be only limited and because of the limited sample size, it is decided to include them in the analysis.

Figure 48, Figure 49 and Figure 50 show the abovementioned graphs for mixtures REF, SAP_0.5 and SAP_1 respectively.

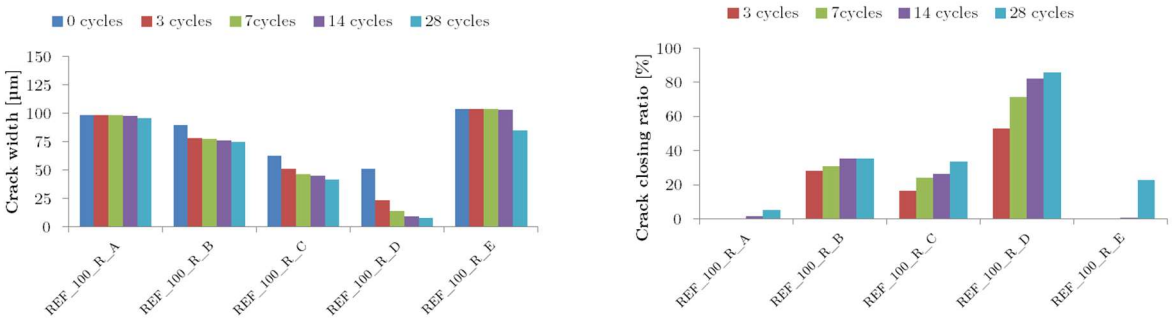

A) B)

Figure 48: Self-healing of cracks, REF; A) Remaining crack width B) crack closing ratio

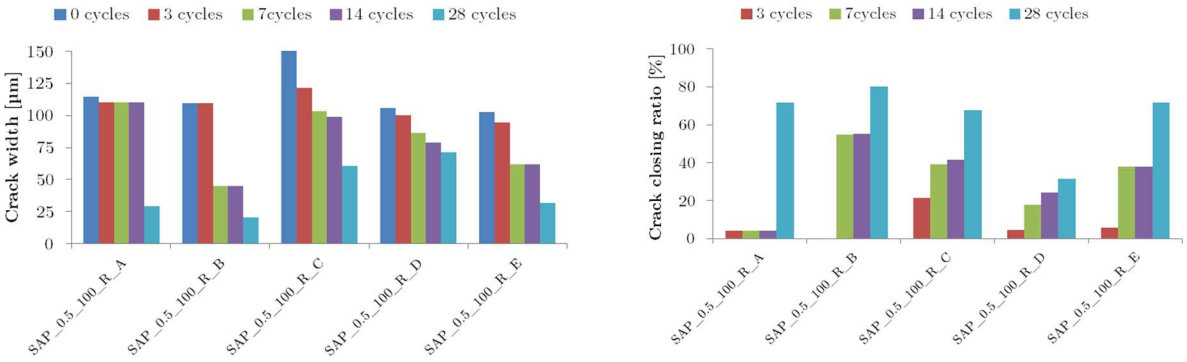

A) B)

Figure 49: Self-healing of cracks, SAP_0.5; A) Remaining crack width B) crack closing ratio

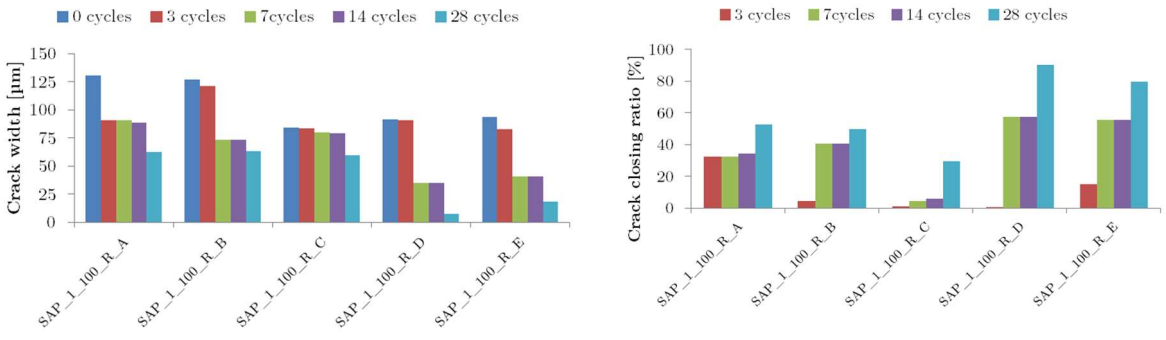

A) B)

Figure 50: Self-healing of cracks, SAP_1; A) Remaining crack width B) crack closing ratio

There is quite some scatter between the samples of the same mixture. In the case of the reference mixture REF, some samples show almost no healing, whereas other samples show 40% to even 80% of healing. The main cause of this scatter is the heterogeneity of the material and the variety in obtained crack widths. Furthermore, the presence of granulates at the surface can play a role as in that case less $Ca(OH)_2$ is present for healing.

In order to compare the results of the different test series REF, SAP_0.5 and SAP_1 and to make general conclusions, the average crack width and average crack closing ratio of the five samples of each series are used. Figure 51 A shows the average remaining crack widths after 0, 3, 7, 14 and 28 cycles for the three different mixtures, whereas the corresponding crack closing ratio is depicted in Figure 51 B.

A)

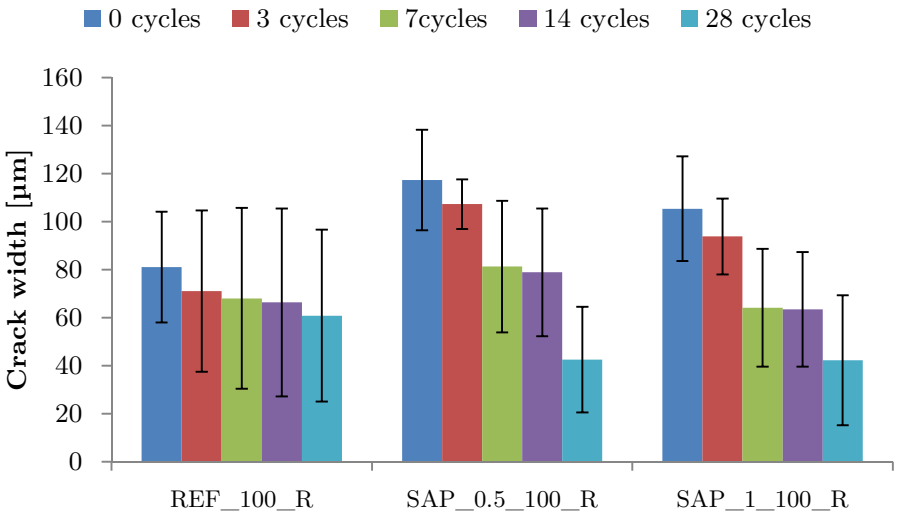

B)

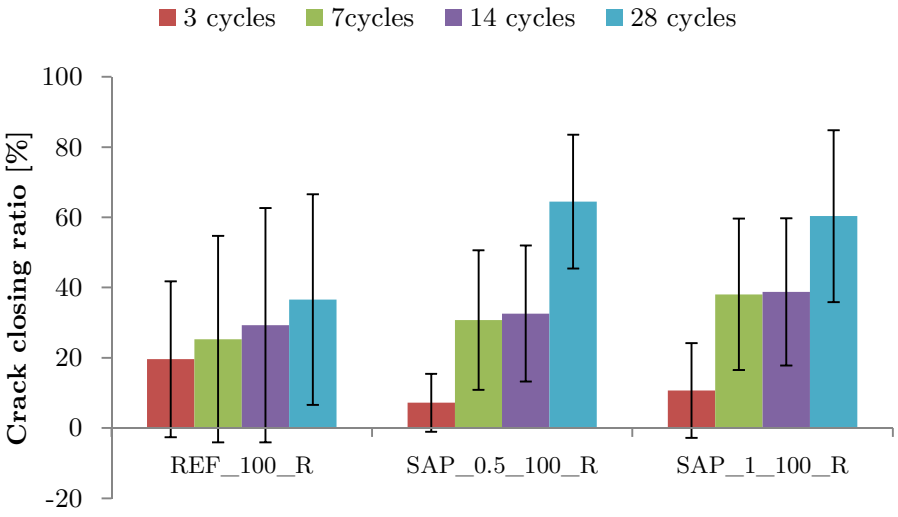

Figure 51: A) average remaining crack width B) average crack closing ratio

First, the results are analyzed visually based on these graphs. In a second step, it is checked whether the observed differences are significant or not using a one-way ANOVA (level of significance = 0.05).

The crack closing ratio after 3 cycles is the highest for the REF mixture (20%), whereas the ones for SAP_0.5 and SAP_1 are approximately half this value (7 and 10% respectively). However, this difference is found not to be significant. An explanation for this can be found when looking at the initial crack widths of the individual samples of the REF mixture, see Figure 48 A. Sample D only has an initial crack with of 51 µm, whereas the initial crack widths of the test series SAP_0.5 and SAP_1 are higher and lie in range of [85 – 154 µm]. Due to the limited width, healing products formed at both sides of the crack will encounter each other faster and close the crack more rapidly, resulting in a crack closing ratio of 100%. This is in accordance with the findings of Snoeck and De Belie [35] and Li and Yang [37] who have observed that cracks smaller than 30 µm can show complete closure due to autogenous healing.
This example shows the importance of not only making conclusions based on average values, but also keeping the individual results in mind as they can have a large influence, especially when the sample size is small and the scatter is high.

After 7 cycles, the crack closing ratio of SAP_0.5 and SAP_1 is increased significantly from 7% to 30% and from 10% to 38 % respectively, which is approximately four times higher than the value after 3 cycles. For the REF mixture, the increase amounts only 5% and is found not to be significant. From this, the beneficial effect of SAPs on the stimulated autogenous healing can be seen: the SAPs are working as water reservoirs that gradually release their absorbed water. This will lead to a further hydration of unhydrated cement particles on the one hand and will also stimulate the precipitation of calcium carbonate on the other hand as the CO_2 will dissolve in water and will react with Ca^{2+} present in the concrete.

Between 7 and 14 cycles, almost no crack reduction is observed for neither of the mixtures. No clear explanation is found for this observation.

The average crack closing ratio obtained after 28 cycles amounts 37% for the REF mixture. This high value is mainly due to the large healing of the small crack widths of sample D. When sample D is omitted, an average crack closing ratio of 24% is obtained, meaning that the cracks are only partially healed. These findings are in accordance with literature, as it is stated by several authors ([35],[37],[38]), that crack widths >50 µm are not able the heal completely due to autogenous healing and a similar amount of crack closing ratio is obtained (De Belie et al. [33], Van Tittelboom et al. [88]).

In between 14 and 28 cycles, the cracks in mixtures containing SAPs, show an extra crack width reduction of 31% and 21% for SAP_0.5 and SAP_1 respectively. When examining the final crack closing ratios after 28 cycles, it was found that they are significantly higher than the one of the reference mixture REF. The values are 64% with a maximum of 80% and 60% with a maximum of 90% in the case 0.5 m% and 1 m% SAPs are added respectively. These values have the same order of magnitude as found in literature (De Belie et al. [33], Van Tittelboom et al. [88]).
None of the samples showed 100% healing at the surface, as none of the cracks was closed over the full crack length.
As a large percentage of the crack healing only occurred after 28 cycles, it could be interesting to investigate whether the self-healing capacity would increase significantly after more than 28 wet-dry cycles and whether 100% crack closure would be reached.

The difference between the ratios for SAP_0.5 and SAP_1 is found not to be significant, after neither amount of cycles. This result seems counterintuitive at first sight and is in contrast to findings in literature (Snoeck et al. [13], Mignon et al. [43]) as it would be expected that the more SAPs are added, the more water is available for further hydration and the better the self-healing will be.
From this result however, it can be concluded that increasing the amount of SAPs from 0.5 to 1 m% has no significant influence on the self-healing. This conclusion could be taken into account when trying to find the optimal amount of SAPs to be added. However, one should bear in mind that if more SAPs are added, the strength of the concrete will decrease due to the more porous matrix. In the case of 1 m% SAP, it could be that there is in general better healing as more water is available, but this effect is probably overshadowed by the healing of the weaker matrix.

An example of complete crack healing in the case 1 m% SAP is added is shown in Figure 52. In each corner, the number of cycles is depicted. As no visible healing occurred between 7 and 14 cycles, the picture of 14 cycles is omitted.

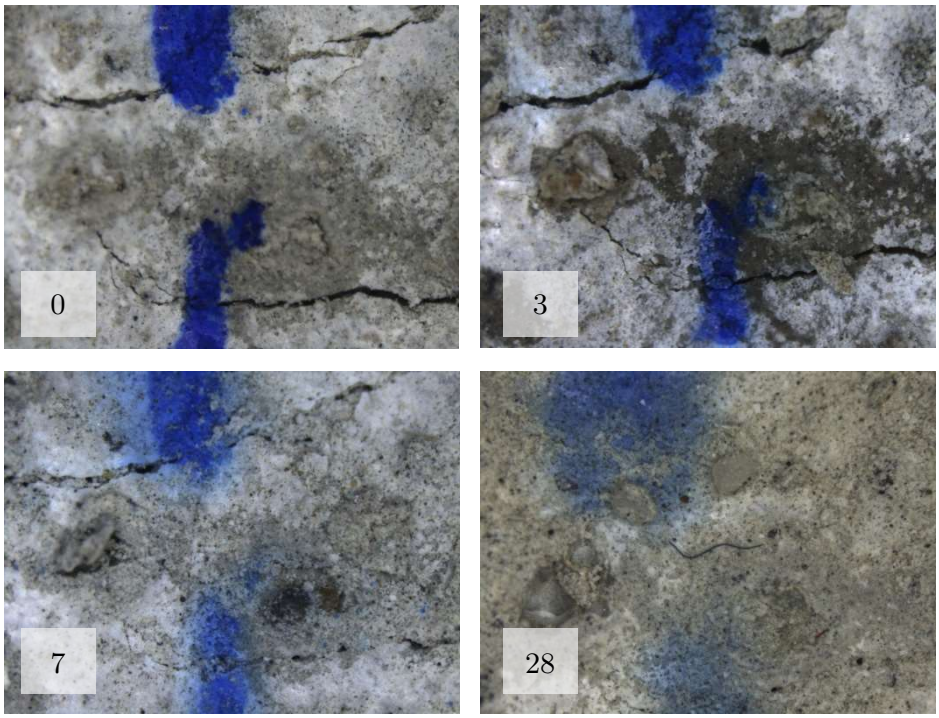

Figure 52: Example of complete crack healing, SAP_1_100_R_D

In Figure 53 an example of a partially closed crack in a reference mixture is shown. The amount of cycles is depicted in the corner. In the first picture, the initial crack width is depicted as well. Although there are no SAPs present, it can be seen that autogenous healing can (partially) close fine cracks. However, this autogenous healing is limited to very fine cracks (<30 µm). In the case fibers are added together with a sufficiently high amount of cement, larger crack widths could also heal autogenously. Though this is not further investigated in this thesis ([34],[35]).

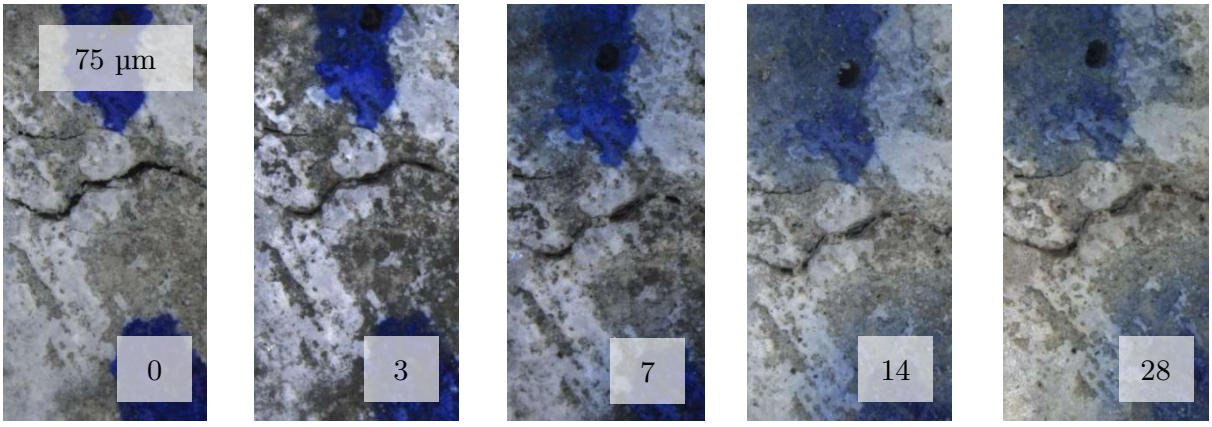

Figure 53: Example of partially closed crack, REF_100_R_B

Figure 54 shows an example of the complete self-healing of a crack in a mixture with 0.5 m% SAP.

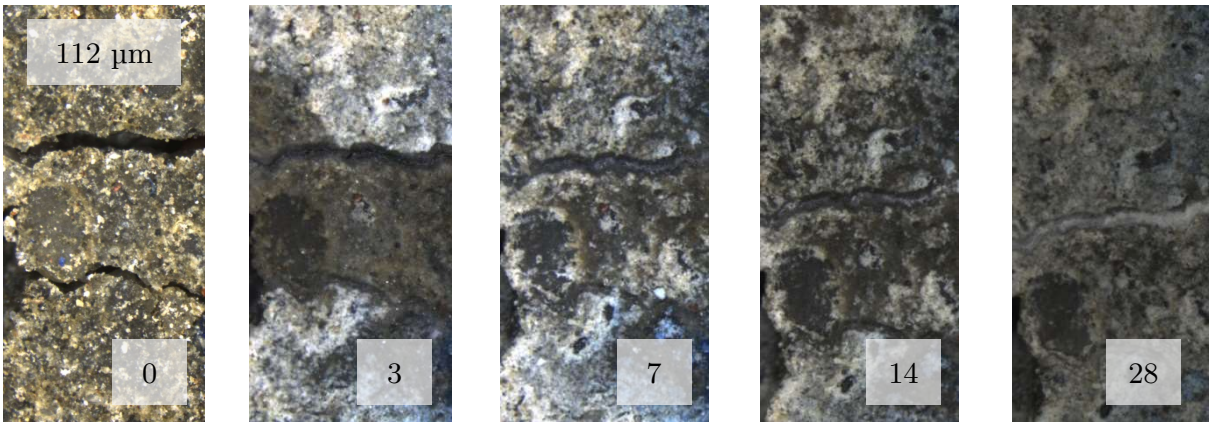

Figure 54: Example of complete crack healing, SAP_0.5_100_R_C

The crack steadily closes in time as it is filled with white healing products. The formation of these whitish calcium carbonate crystals is the main mechanism for the stimulated autogenous healing, together with the further hydration of unhydrated cement particles. In this example, also a secondary micro-crack is visible. This smaller crack also healed completely. The addition of SAPs can lead to higher crack closing ratios, even in the case of cracks that are too wide to close autogenously.

The addition of SAPs has a beneficial influence on the self-healing of cracks with a crack width of 100 µm due to the combined effect of further hydration and the stimulated precipitation of calcium carbonate. The samples with SAPs showed a significantly higher crack closing ratio (60-64%) than the reference samples (crack closing ratio of 24% by autogenous healing).
As the studied crack widths of 100 µm are still limited and in reality larger crack widths occur frequently, it would be interesting to examine the efficiency of SAPs for self-healing in the case of larger crack widths as well.

It should be mentioned that the crack healing in this section is only based on measurements and observations at the surface of the samples. Possible healing at the inside of the crack is not studied in this thesis, but as this could have a beneficial effect on the resistance against chloride penetration and carbonation, this would be an interesting topic for future research.

In the next sections, the healed specimens of the second test series were not studied as there was not enough time left in between the end of the self-healing tests and the deadline of this thesis. Therefore only the unhealed specimens of the first test series could be studied to investigate the influence of the addition of SAPs to the concrete on chloride penetration and carbonation.

4.5 Chloride diffusion tests

Chloride profiles were obtained after seven weeks of immersion in NaCl solution, by means of potentiometric titrations and investigating the color change boundaries by spraying 0.1 M $AgNO_3$ solution. In case of the latter, the free chloride concentration is visualized whereas in case of the former, the total chloride concentration is obtained.

4.5.1 Spraying $AgNO_3$

In the next paragraphs, the total area penetrated by chlorides and the average chloride penetration depth from both the surface and perpendicular to the crack are discussed.

4.5.1.1 Chloride penetration areas

After the samples were split perpendicularly to the crack and sprayed with $AgNO_3$, all the obtained chloride profiles could be classified in four different classes. An example of each class is shown in Figure 55 A – D.
Class A is characterized by a homogeneous, equidistant penetration over the entire width of the sample. Samples belonging to class B show an increased local penetration of chlorides around and into the crack. Samples that are classified in class C show chloride penetration up to the opposite coated surface. In class D, samples are also characterized by chloride penetration up to the opposite coated surface, accompanied by an accumulation of chlorides at this surface. In case of through-going realistic cracks, a piece of tape was applied over the crack at the non-studied side before coating, in order to avoid possible ingress of epoxy. A poor adhesion of the coating to the tape could lead to chloride diffusion in the zone in between the coating and the tape, resulting in the chloride penetration profile of class D.

A)

B)

C)

D)

Figure 55: Classification of the chloride penetration profiles in four classes: A) equidistant penetration from the surface B) local penetration around crack C) chloride penetration up to the opposite coated side D) chloride penetration up to the opposite coated side accompanied by accumulation of chlorides at the coated side; The chloride penetration is from the top of the picture

In Table 16, the percentage of test specimens of each test series that belongs to a specific class is summarized.

Table 16: Percentage of test specimens of each test series belonging to a specific class

	class A	class B	class C	class D
REF	100%			
REF_100_R				100%
REF_100_A		100%		
REF_300_R				100%
REF_300_A		100%		
SAP_0.5	100%			
SAP_0.5_100_R				100%
SAP_0.5_100_A	25%	75%		
SAP_0.5_300_R				100%
SAP_0.5_300_A		50%	25%	25%
SAP_1	100%			
SAP_1_100_R			40%	60%
SAP_1_100_A		100%		
SAP_1_300_R				100%
SAP_1_300_A		75%	25%	

As expected, all uncracked specimens belong to class A. In the case of specimens with artificial cracks, the chloride penetration is restricted to a local zone around the crack and therefore these specimens are classified in class B. Few exceptions are found: only in 25% of specimens belonging to test series SAP_0.5_100_A no influence of the crack was visible and these samples were therefore classified in class A. As it is unlikely that this was due to healing of the crack, a more plausible explanation is the blocking of the crack by impurities. Some specimens with artificial cracks are classified in class C or D as they show penetration up to the opposite coated side. However, this was only observed in test series with artificial cracks of 300 µm that contain SAPs. A reason for this can be found in the combination of both a large crack width, together with a more porous structure due to the presence of SAPs, leading to an increase in chloride penetration.
As the realistic cracks are through-going over the entire height of the sample, chloride penetration up to the opposite coated side is observed for all specimens. In most cases, also accumulation of chlorides at the coated side is observed (class D). This is possibly due to the poor adhesion between concrete and tape, see supra.
In the case of SAP_1_100_R, 40% of the samples are classified in class C. This could be due to partial healing at the inside of the crack. However, when looking at the data of the realistic cracks created at the non-studied side of the samples that are classified in class C, it was found that these samples did not have a crack at the opposite side. As a consequence no tape was used at this side, resulting in a good bonding between concrete and coating.

Aside from the absence of visible healing at the surface for these test series, see section 4.4, these results are a second proof of the lack of healing for these specimens. In case there would be healing at the inside of the cracks, more samples with artificial cracks should be classified in class A, as chlorides can no longer penetrate along the healed crack. Also in the case of healed realistic cracks, the majority of these specimens should be classified in class A or B, as the healing products would obstruct chloride penetration up to the opposite side.

According to the method described in section 3.2.8.2, the ratio of the area in which chlorides were penetrated to the total surface of the test piece was calculated for each specimen. Subsequently, the average ratios for each test series, together with the standard deviations for the individual measurements were calculated. The results are depicted in Figure 56.

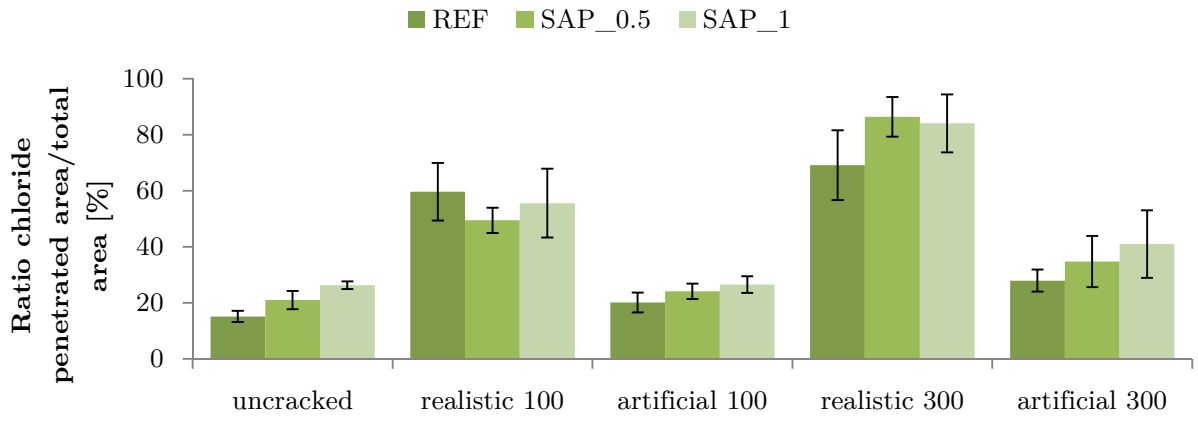

Figure 56: Ratio of chloride penetrated area to the total area, expressed in percentage

In case of uncracked, artificial 100 and artificial 300 the average area ratio increases when the amount of SAPs is increased, leading to a higher porosity and thus a larger area penetrated by chlorides. This phenomenon is not observed for realistic cracks, due to the larger variation of created crack widths and thus larger variation in the area affected by chlorides. The latter makes it impossible to make similar conclusions as in the case of uncracked or artificially cracked samples. However, in case of realistic cracks, the affected area was significantly larger than in case of artificial cracks with the same intended crack width. The main reason for this is that the realistic cracks are through-going where the artificial cracks are only limited in depth. As stated earlier, in case of realistic cracks secondary micro-cracks can be formed, which might increase the chloride penetration as well. However, the latter was not further investigated in this thesis.
Another significant difference is found when looking at the crack widths. In the case of 300 µm cracks, the mean area ratio is found to be significantly larger than the ones obtained for 100 µm cracks, for both artificial and realistic cracks. This result can be explained because in the case of wider cracks, a larger amount of chlorides can more easily penetrate into the crack and further into the concrete.

4.5.1.2 Chloride penetration depth from the exposed surface & perpendicular to the crack

For each half specimen, the chloride penetration depth from the exposed surface was measured at 10 places with an interval of 10 mm and an accuracy of 1 mm. However, it was observed that in the vicinity of the crack, larger penetration depths were measured due to the combined effect of penetration from the surface and perpendicular to the crack. As the interest in this first part lies on the penetration depth from the surface only, the measurement points in a zone around the crack equal to the average penetration perpendicular to the crack were not taken into account. By doing this, the possible influence of penetration via the crack on the surface penetration was excluded. The obtained results are grouped based on the studied mixture. Finally, the average penetration depths and the standard deviations on the individual measurements are calculated. The results for penetration from the exposed surface are depicted in Figure 57.

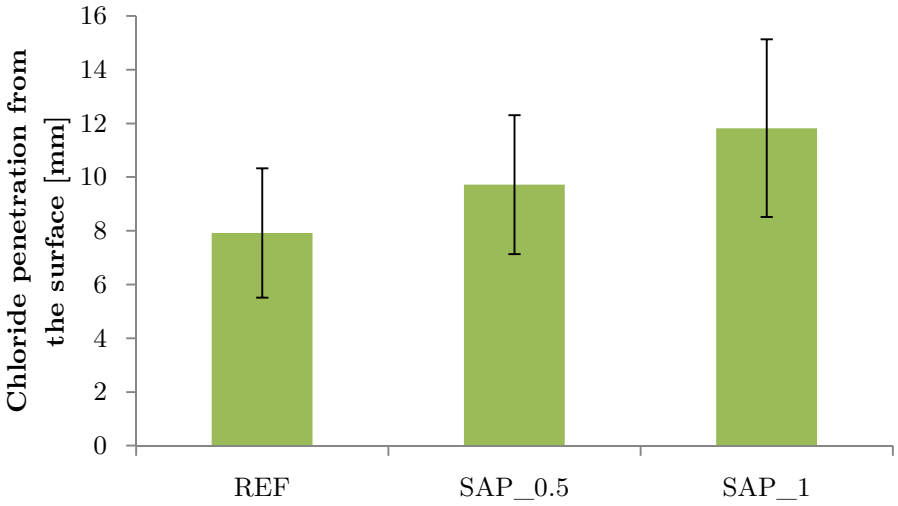

Figure 57: Average chloride penetration from the exposed surface

The average chloride penetration depths from the exposed surface are significantly different from each other (level of significance = 0.05). The average chloride penetration from the surface, together with the standard deviation on the individual measurements as well as the measured minimum and maximum penetration depth for the three different mixtures are summarized in Table 17.

Table 17: Chloride penetration depths from the exposed surface

	Mean [mm]	**St.dev. [mm]**	**Minimum [mm]**	**Maximum [mm]**
REF	7,92	2,41	1,74	18,84
SAP_0.5	9,72	2,58	3,86	18,20
SAP_1	11,82	3,31	3,75	42,75

Increasing the amount of SAPs from 0 m% to 0.5 m% and finally to 1 m% leads in each step to an additional ±2 mm penetration from the surface. The more porous structure due to the presence of SAPs leads to a significant increase in chloride penetration from the surface. From Table 17 it can be seen that there is a large range between the measured minimum and maximum penetration depth. This is due to the fact that the chloride penetration from the surface is not uniform along the sample as concrete is a heterogeneous material. Examples of heterogeneity in concrete are local changes in porosity, variety of aggregate sizes and locations, etc.

The chloride penetration in the direction perpendicular to the crack was measured with intervals of 5 mm and an accuracy of 1 mm, but only at depths larger than the average penetration depth from the exposed surface.
Before all information is brought together in one graph, the observations are first discussed separately for the ease of understanding.

When looking at the crack formation method, the chloride penetration perpendicular to realistic cracks was significantly higher compared to the penetration perpendicular to artificial cracks, see Figure 58.

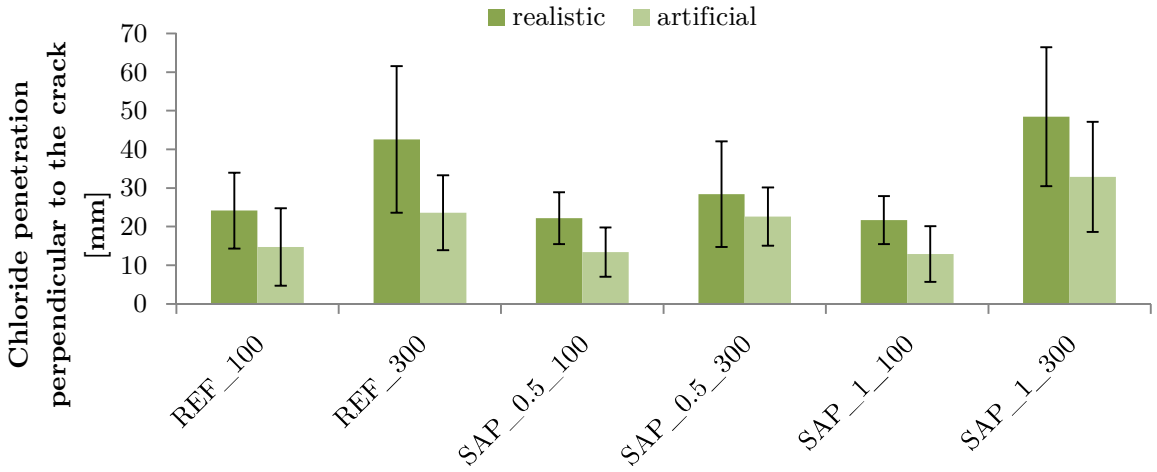

Figure 58: Chloride penetration perpendicular to crack, comparison of crack formation method

Possible explanations can be found when looking at the characteristics of the crack formation method. In case of realistic cracks, micro-cracks along the crack face can occur, creating preferential pathways for the chlorides to penetrate into the concrete. When looking at artificial cracks, the presence of a higher amount of fines at the crack face can impede chloride ingress perpendicular to the crack. However, this last hypothesis should be investigated more into detail to see whether this is indeed the main reason.
When comparing the results for the obtained crack widths, i.e. 100 µm and 300 µm, a similar conclusion as already mentioned earlier can be made: in case of 300 µm cracks, the mean penetration depth perpendicular to the crack is significantly

larger than the ones obtained for 100 µm cracks, see Figure 59. This result is logical as in case of wider cracks, a larger amount of chlorides can more easily penetrate into the crack, resulting in larger penetration depths.

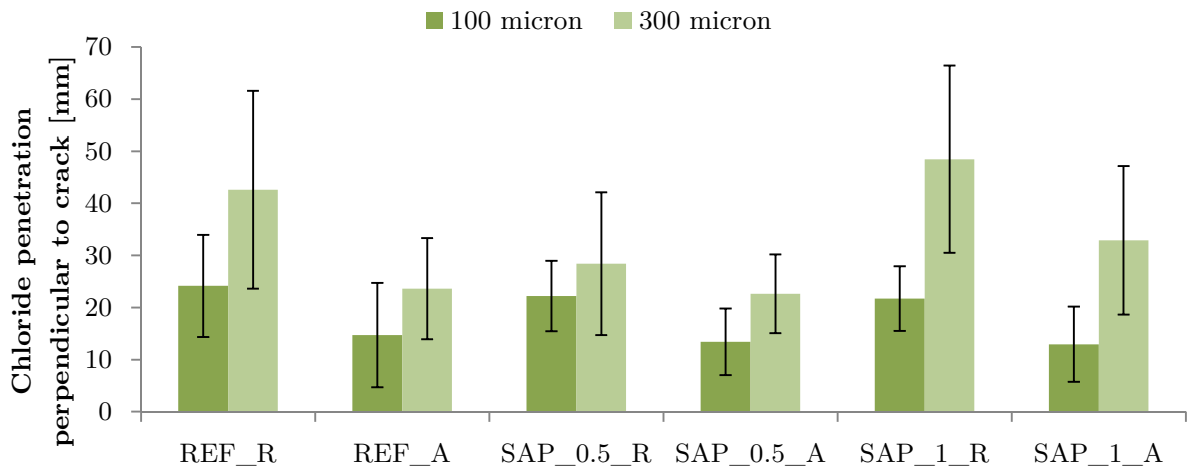

Figure 59: Chloride penetration perpendicular to the crack, comparison of crack widths

When combining the previous information in one graph, it can be seen that all the three mixtures (REF, SAP_0.5 and SAP_1) show similar trends, see Figure 60.

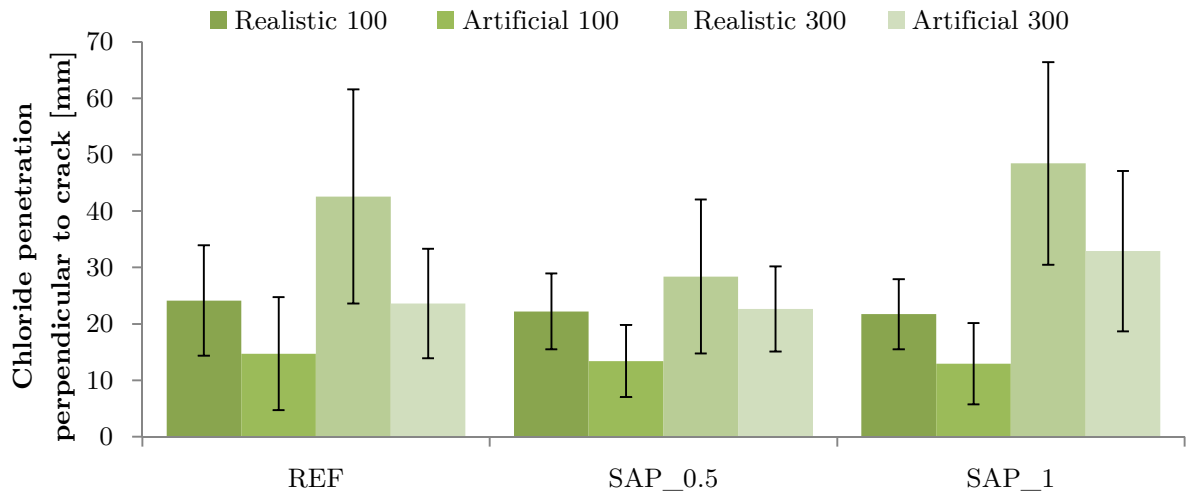

Figure 60: Chloride penetration perpendicular to crack, comparison of mixtures

By means of a one-way ANOVA with Dunnett's T3 test (level of significance 0.05) no significant differences are found between the three mixtures, unless in the case of 300 µm cracks. From the statistical analysis it can be concluded that only in case of large 300 µm cracks the used mixture plays a significant role. However, no clear explanation for this phenomenon is found.
The large standard deviations of the results are again the result of the heterogeneous character of the concrete on one hand, and the variation of the obtained crack widths on the other hand.

The obtained values for both chloride penetration from the surface and perpendicular to the crack are summarized in Table 18.

Table 18: Chloride penetration from the surface and perpendicular to the crack (- = not applicable)

	Surface penetration [mm]	**Penetration perpendicular to crack [mm]**
REF	7.3 ± 1.9	-
REF_100_R	7.2 ± 3.0	24.1 ± 9.8
REF_100_A	7.1 ± 1.6	14.7 ± 10.0
REF_300_R	7.4 ± 2.1	42.6 ± 19.0
REF_300_A	8.6 ± 2.6	23.6 ± 9.7
SAP_0.5	9.9 ± 2.5	-
SAP_0.5_100_R	9.9 ± 2.0	22.2 ± 6.7
SAP_0.5_100_A	10.7 ± 3.1	13.4 ± 6.4
SAP_0.5_300_R	10.9 ± 2.3	28.4 ± 13.7
SAP_0.5_300_A	9.7 ± 2.1	22.6 ± 7.5
SAP_1	12.2 ± 2.4	-
SAP_1_100_R	11.3 ± 2.2	21.7 ± 6.2
SAP_1_100_A	11.4 ± 2.1	12.9 ± 7.2
SAP_1_300_R	12.3 ± 4.1	48.5 ± 18.0
SAP_1_300_A	13.3 ± 4.6	32.9 ± 14.2

In order to compare the chloride penetration from the exposed surface with the penetration perpendicular to the crack, both are plotted on the same graph, see Figure 61.

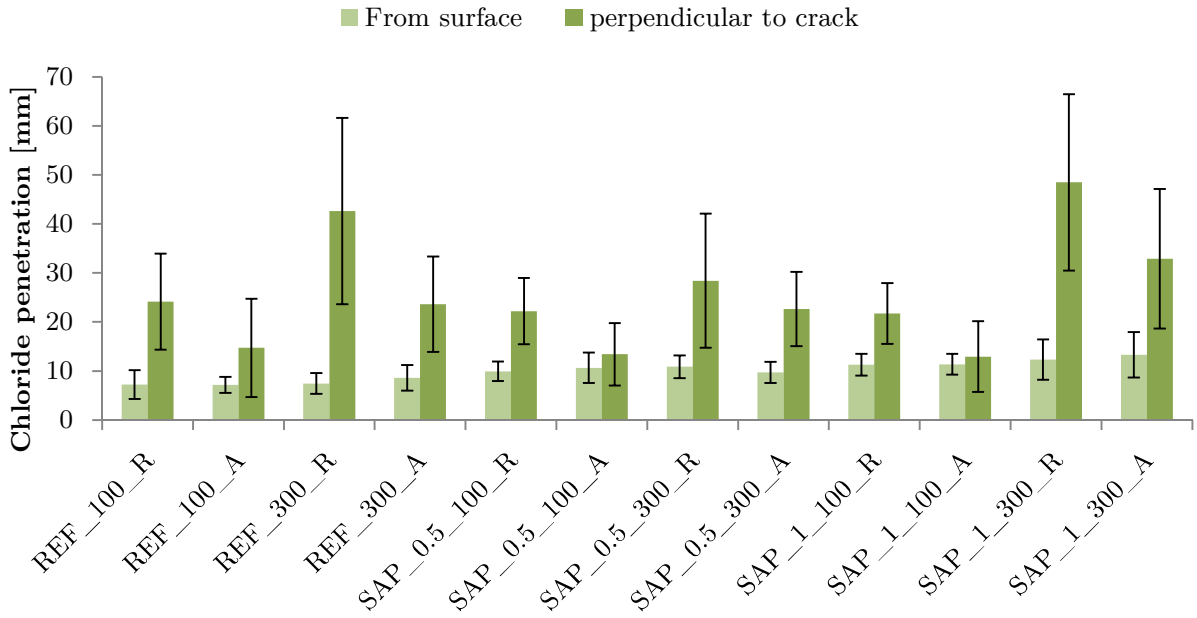

Figure 61: Chloride penetration from the exposed surface and perpendicular to the crack

The penetration depth around the crack (to both sides of the crack) is in most cases approximately twice the penetration depth from the exposed surface. When assuming a symmetrical penetration perpendicular to the crack, this means that the penetration perpendicular to only one side of the crack is similar in nature with the one from the exposed surface. These results are in accordance with the findings of Win et al. [3] and Audenaert et al. [66]. However, in case of 300 µm realistic cracks, the penetration perpendicular to the crack was up to four times higher than the one from the exposed surface. This higher penetration might be due to the presence of micro-cracks along the rough crack surface, which increases the connectivity to interior pores and thus the chloride penetration. This can be the subject of further investigations.
In case of test series SAP_0.5_100_A and SAP_1_100_A, no significant difference was found between penetration from the surface and perpendicular to both sides of the crack. The lower penetration perpendicular to the crack in this case is probably due to the blocking of the fine artificial cracks by impurities.

The more porous structure due to the presence of SAPs leads to a significant increase in chloride penetration from the surface as increasing the amount of SAPs from 0 m% to 0.5 m% and finally to 1 m% leads in each step to an additional ±2 mm penetration from the surface. However, in the case of chloride penetration perpendicular to the crack, no significant influence of the addition of SAPs was found.

When studying the new specimens without extensive cleaning, no surface polishing and occurring autogenous healing, a better behavior could be expected. Due to the healing of the crack, the chloride penetration perpendicular to the crack would be reduced or even reach zero. The healing products will obstruct chloride penetration along the crack and up to the opposite side, so it is supposed that less samples (or ideally none) would be classified in class B, C or D. In this case, the addition of SAPs would have a beneficial influence on the durability of the concrete, as the resistance against chloride penetration in cracked concrete is increased.
This could be a subject for further investigations.

4.5.2 Potentiometric titrations

Before going deeper into the results obtained by means of potentiometric titrations, first some remarks are made. For optimal comparison between the chloride profiles from potentiometric titrations and the CCB by means of spraying $AgNO_3$, the measurements are preferably carried out on the same specimen. However, since this was not possible due to practical reasons, both were determined on different specimens from the same batch.
Another remark is that in fact both methods cannot be compared directly, as in the case of CCB the free chlorides are visualized, whereas in case of titrations, the total chloride content[1] is measured. In literature, a method was found to compare the water-soluble chloride content with the free chloride content [89], but as in this thesis only the acid-soluble chloride content was determined, this method is not applicable. Because of this, no direct comparison of both techniques was performed.

When plotting the measured total chloride concentration (expressed as m% binder) versus the depth below the exposed surface, the total chloride profile is obtained. This is done for three samples per test series. Subsequently, a mathematical profile based on the second law of Fick is fitted to the measured profiles of the three samples. In the following graphs, the individual measurement data are depicted as dots, whereas the fitted profile is a full line.

In Figure 62, Figure 63 and Figure 64 the obtained fitted chloride profiles together with the measured data are plotted for uncracked samples, samples with realistic cracks of 100 µm and samples with artificial cracks of 100 µm respectively.

[1] In this thesis, the total chloride content is equated with the measured acid-soluble chloride content

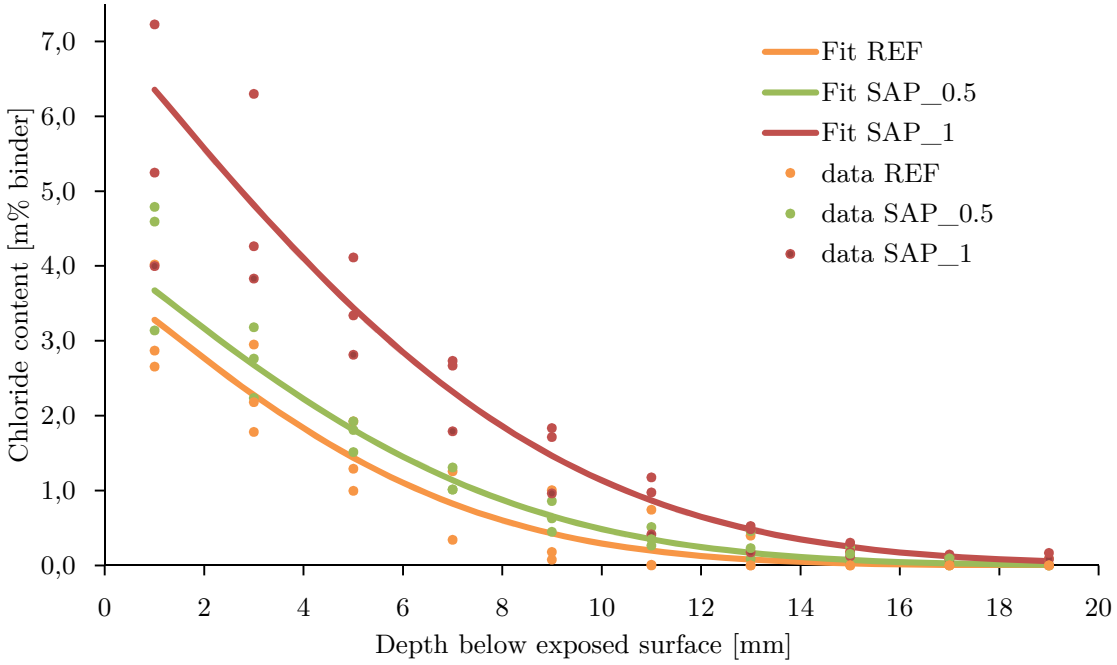

Figure 62: Chloride profiles, test series uncracked

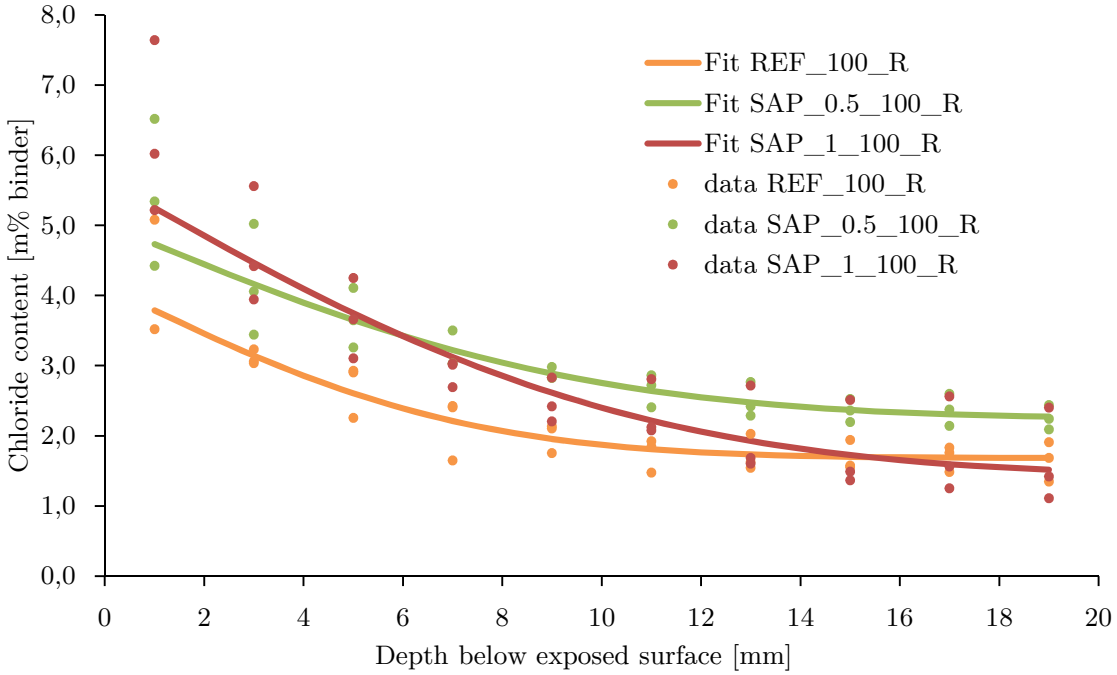

Figure 63: Chloride profiles, test series realistic cracks 100 µm

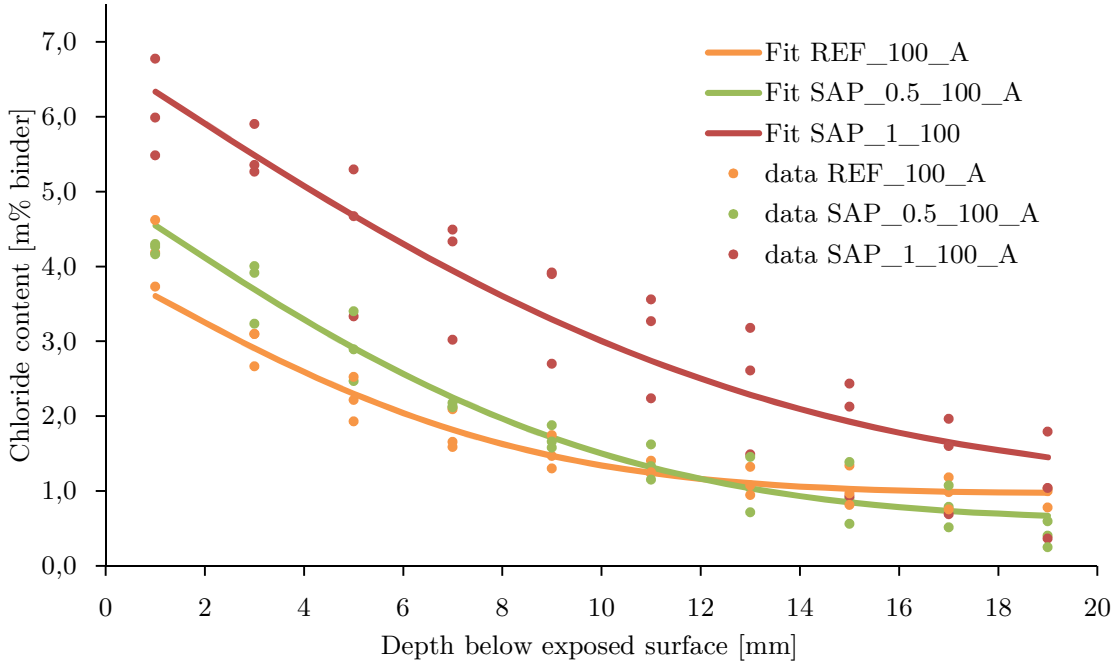

Figure 64: Chloride profiles, test series artificial cracks 100 µm

The chloride concentration in the first layer is much higher than the other concentrations, but decreases exponentially when going to deeper layers.

For uncracked specimens, the chloride content amounts 0% at a depth of 20 mm below the exposed surface. For cracked specimens however, the chloride content does not equal 0% at a depth of 20 mm due to the presence of the crack. In case of realistic cracks, the chloride content at a depth of 20 mm is lying in the range [1.52 – 2.27 m%], whereas in case of artificial cracks the chloride contents at that depth are somewhat lower, namely [0.67 – 1.45 m%]. The latter is probably again due the presence of impurities in the deeper part of the crack.
Comparing the obtained chloride contents with critical chloride contents mentioned in literature is not recommended as in this case the samples are exposed to a solution with unrealisticly high amount of chlorides (165 g NaCl/ℓ). As no conversion formula was found between chloride concentrations obtained in 165 g NaCl/ℓ and in realistic salt solutions, this could be an interesting topic for further research.
The obtained chloride contents in cracked samples are larger than in uncracked samples and will thus initiate corrosion more rapidly. This clearly stresses the importance of finding methods that can heal cracks and as a consequence lower chloride penetration through the cracks. The new batch made near the deadline of this thesis may seem promising.

For all test series, the spread of the chloride content between the different samples decreases when the depth from the exposed surface increases. The chloride content will stagnate to an almost constant value at a certain depth.
For uncracked specimens, a clear trend is visible when comparing the chloride profiles of the different mixtures: the higher the amount of SAPs, the higher the porosity and as a consequence the higher the chloride content. However, the difference between REF and SAP_0.5 is not that pronounced. The latter is promising as in this case the addition of SAPs has no pronounced negative influence on chloride concentrations compared to the reference concrete and could be combined with the beneficial effect of SAPs for crack-healing resulting in crack closing ratios up to 64%, see section 4.4. Further research is needed to verify this hypothesis.
For artificially made cracks, the same trend is observed. However at a depth of 12 mm, the profile of SAP_0.5 dives under the one of REF. As no crack healing was observed at the surface and the chloride profiles obtained from the CCB showed chloride penetration over the entire crack depth, it is unlikely that this is due to healing. More probable explanations for the obtained lower chloride concentrations can lie in the fitting of the profile to the measurements of the three samples, the heterogeneity of the concrete, the variety in obtained crack widths or the blocking of the crack by impurities.
For realistic cracks, the profile of SAP_1 lies almost completely under the profile of SAP_0.5 and at some points even under the profile of REF. It could be that in the lower parts of the crack some healing occurred, resulting in lower chloride concentrations. However, more tests are needed to verify whether this is indeed the result of healing.

From the aforementioned observations, it is difficult to draw conclusions based on average chloride profiles. To interpret the results in a better way, the individual profiles should be taken into account instead of the average profiles. However, due to the large variations between the results obtained from different samples, the heterogeneity of the concrete, the possible blocking of the crack by impurities, the variation in obtained crack widths and the limited amount of tested specimens per test series, it is still difficult to draw general conclusions.

Non-steady-state diffusion coefficients D_{nssd} and chloride surface concentrations C_s are obtained by fitting the second law of Fick to the measured chloride contents, see section 3.2.8.3.

For the three test series uncracked, realistic 100 µm cracks and artificial 100 µm cracks the average surface concentrations together with the standard deviations for the different mixtures are depicted in Figure 65 and summarized in Table 19.

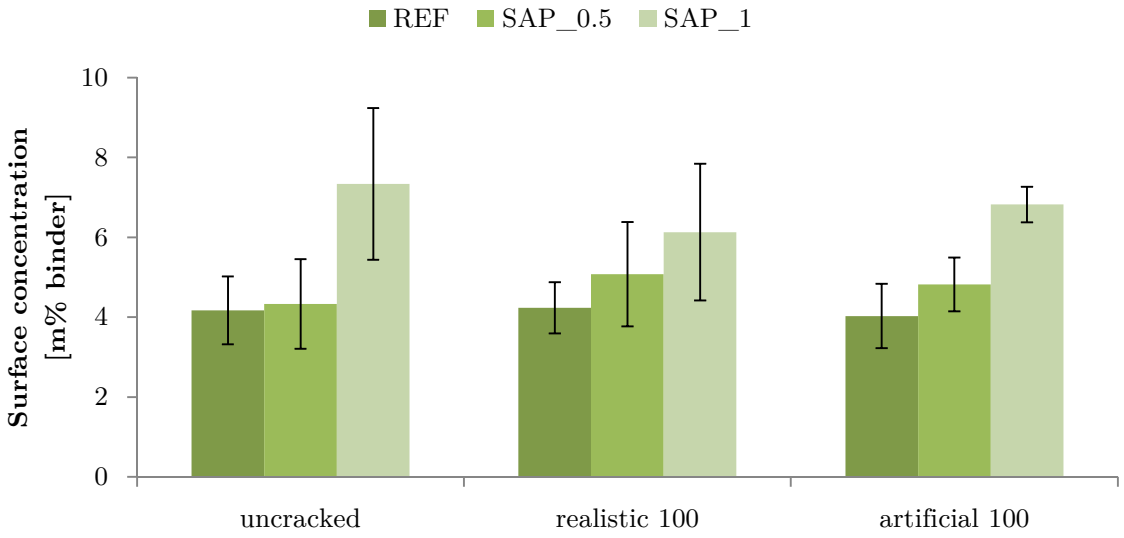

Figure 65: Calculated chloride surface concentrations expressed as m% binder

Table 19: Chloride surface concentrations C_s [m% binder]

		REF	**SAP_0.5**	**SAP_1**
Uncracked	m% binder	4.17 ± 0.85	4.33 ± 1.12	7.34 ± 1.90
Realistic 100 µm	m% binder	4.23 ± 0.64	5.08 ± 1.31	6.13 ± 1.71
Artificial 100 µm	m% binder	4.03 ± 0.81	4.82 ± 0.67	6.82 ± 0.45

The chloride surface concentration increases when the amount of SAPs, and as a consequence also the porosity, is increased. However, this difference was not significant at a significance level of 5%, except for the series SAP_1_100_A which is significantly different from the other artificial crack series.
When the average surface concentrations for uncracked, realistic 100 and artificial 100 are compared, they are not significantly different for none of the studied mixtures. The presence of a crack has thus no significant influence in this case, as the studied parameter is the surface concentration.

For the three test series uncracked, realistic 100 µm cracks and artificial 100 µm cracks the non-steady-state diffusion coefficients together with the standard deviations for the different mixtures are depicted in Figure 66 and summarized in Table 20.

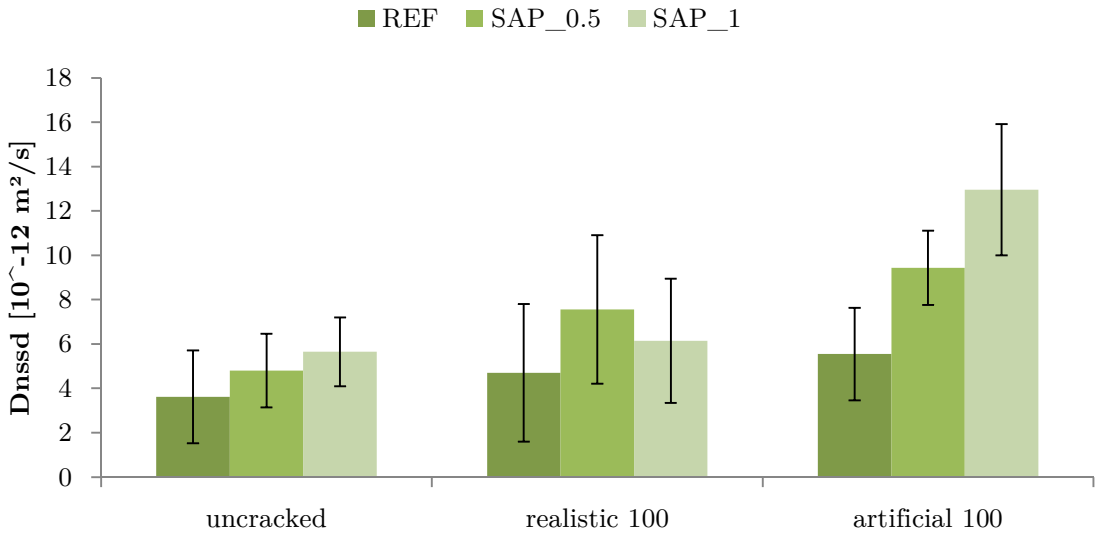

Figure 66: Calculated non-steady-state diffusion coefficients, [10^{-12} m²/s]

Table 20: Non-steady-state diffusion coefficients [10^{-12} m²/s]

		REF	**SAP_0.5**	**SAP_1**
Uncracked	10^{-12} m²/s	3.61 ± 2.10	4.80 ± 1.66	5.65 ± 1.55
Realistic 100 µm	10^{-12} m²/s	4.70 ± 3.11	7.56 ± 3.35	6.15 ± 2.80
Artificial 100 µm	10^{-12} m²/s	5.55 ± 2.09	9.43 ± 1.67	12.95 ± 2.96

In general, the diffusion coefficient increases when the amount of SAPs is increased. The only test series that does not follow this trend is SAP_0.5_100_R. No explanation was found for this phenomenon.
According to a statistical analysis, the increase of diffusion coefficient was found not to be significant at a 5% significance level, except for the series SAP_1_100_A which is significantly different from the other artificial crack series.

Addition of SAPs to the concrete without healing of the cracks thus has no beneficial effect on the resistance against chlorides as both the chloride surface concentration and the chloride diffusion coefficient increase with the higher porosity as a result of the embedded SAPs. Although these results are found not to be significant in this thesis at a 5% significance level, further research should be executed to see whether this is due the observed large standard deviations.

The second batch showed autogenous healing and it could be expected that this has beneficial effects on the resistance against chloride penetration. As chlorides can no longer penetrate into the healed crack, the chloride concentration of cracked specimens would decrease to values similar to uncracked specimens. However, this second batch still needs to be investigated further.

When the average diffusion coefficients for uncracked, realistic 100 and artificial 100 are compared, cracked samples show higher values, especially in the case of artificial cracks. However, this observation was not significant for none of the studied mixtures.
According to Jin et al. [7], diffusion coefficients in concrete with cracks >30 µm are significantly different from the ones in sound concrete and should therefore not be calculated with the second law of Fick. Also Gu [21] suggests that in case of cracked concrete, other experiments and test setups than in case of sound concrete should be used.
Several authors ([7],[21],[23],[27],[65]) state that for crack widths smaller than a critical value, the chloride transport process in the crack is very slow. In this case, the crack has almost no influence on the chloride transport process which thus could be assumed similar to uncracked concrete. Yet, no consensus is found on this critical value: 30 µm ([7],[21]), 50 µm [23], 80 µm ([21],[30]) and 200 µm [65].

Although there is no agreement on this critical value, a reduction of the crack width due to stimulated self-healing upon the addition of SAPs, could have beneficial effects on the resistance against chloride penetration and should be further investigated.

4.6 CO_2 diffusion tests

Even after 12 weeks of exposure to 1 vol% CO_2, the penetration perpendicular to the artificial crack of 500 µm was not visible by spraying phenolphthalein or was very limited in case of cement paste (< 1 mm), see Figure 67. Surprisingly, around very fine shrinkage cracks in the cement paste some carbonation was detected by the phenolphthalein spray, see Figure 68.
The absence of carbonation around the artificial crack of 500 µm is not in correspondence with the (limited) literature about carbonation in cracked concrete. Alahmad et al. [82] found that for crack widths of 60 µm or more, the perpendicular-to-crack carbonation depths are similar to the surface carbonation depth, for both artificial and realistic cracks. The carbon dioxide diffusion through the crack only appeared to be stopped for crack widths smaller than 10 µm. The latter can explain the limited carbonation around the very fine shrinkage cracks.

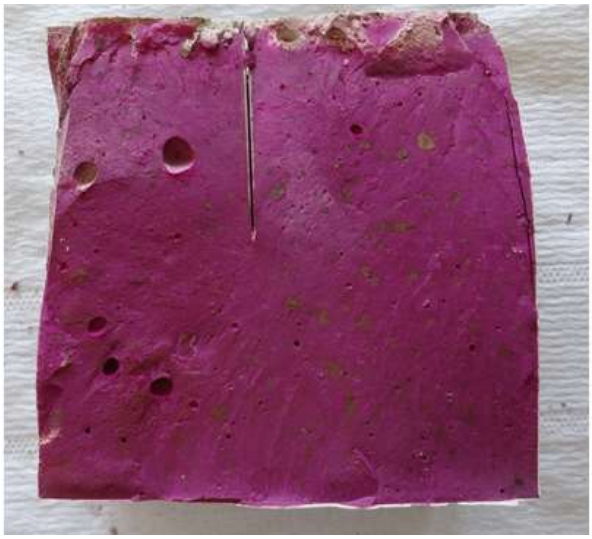

Figure 67: Limited carbonation around artificial crack in cement paste; 12 weeks of exposure

Figure 68: Carbonation around very fine shrinkage cracks in cement paste; 12 weeks of exposure

However, a remark must be made concerning the artificial crack formation. In the paper of Alahmad, the artificial cracks were made by saw cutting, whereas in this thesis, the artificial cracks were made by putting thin brass plates in the fresh concrete. The lack of carbonation around the artificial cracks made by brass plates, suggests that something happened at the plate-mixture interface, resulting in an impermeable layer for CO_2. Further research should verify this hypothesis. This research could focus on the influence of different types of steel plates, the exact composition of the material at the plate-mixture interface or the comparison of these results with artificially made cracks by other methods like for example saw-cutting.

Another explanation could be found in a different relative humidity at the surface of the sample and at the inside of the crack. This is possibly combined with less air circulation inside the crack compared to the air circulation at the surface.
The relative humidity (RH) inside the carbonation chamber is 60 ± 5%, which is favorable for carbonation according to Thiery et al. [81] who stated that for optimum carbonation, the environmental RH should be varying between 50% and 70%. In case the RH inside the crack is lower or higher than this range, the carbonation perpendicular to the crack is slowed down. Relative humidity measurements at the inside of the crack together with carbonation tests should be executed in the future to see the relation between both.

For each mixture studied, the average carbonation depths from the exposed surface together with the standard deviations of the individual measurements are depicted in Figure 69, Figure 70 and Figure 71 for uncracked samples, cracked samples and cracked samples that were stored every 4 weeks in water for 24 hours respectively.

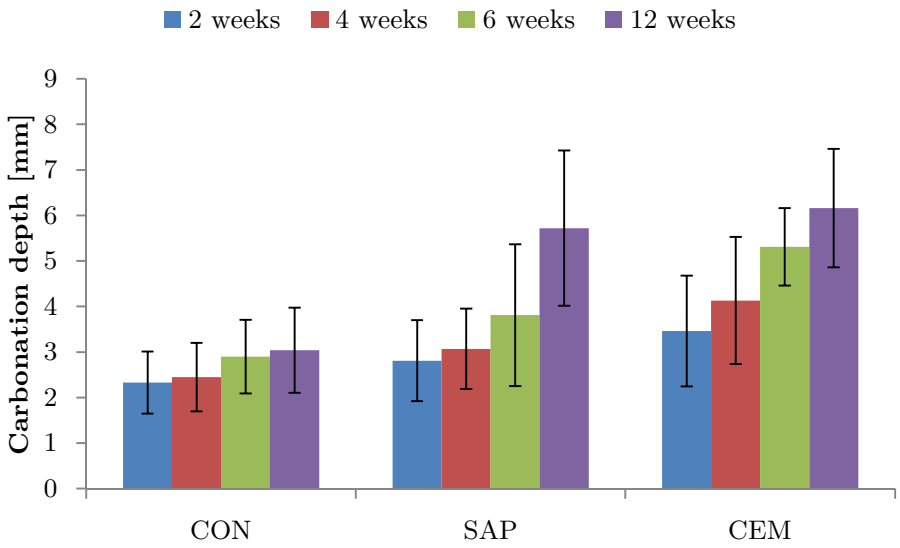

Figure 69: Carbonation depths, uncracked samples

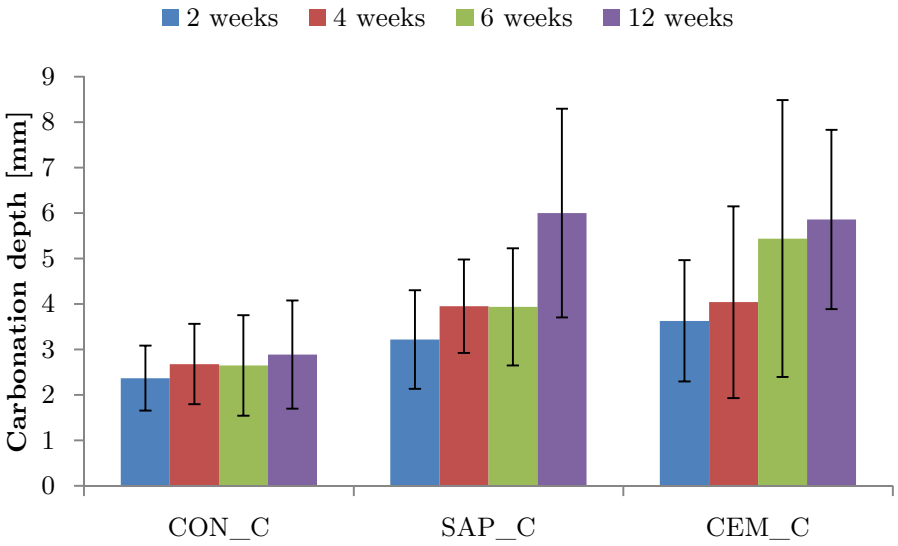

Figure 70: Carbonation depths, cracked samples

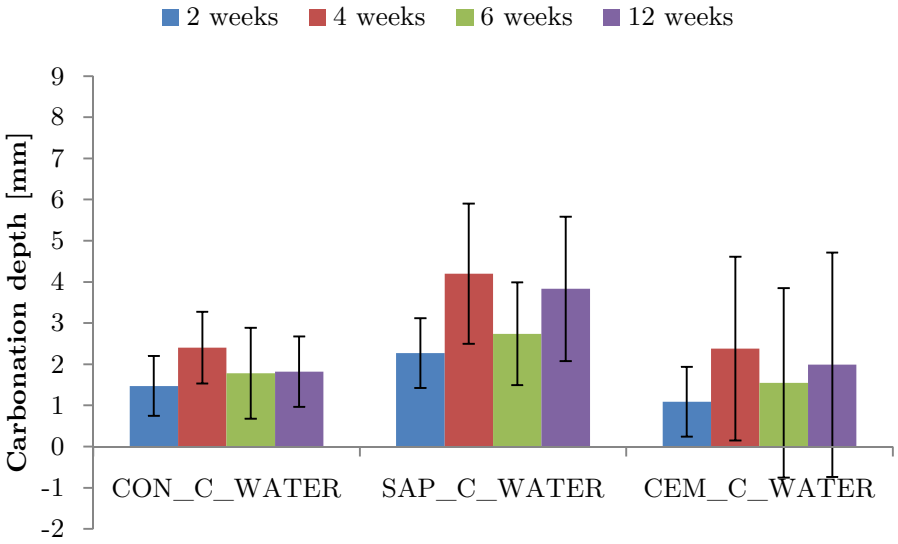

Figure 71: Carbonation depths, cracked samples, stored every 4 weeks in water for 24 hours

Before going into detail on the results, a remark must be made about the measurements after four weeks for cracked samples periodically stored in water (see Figure 71). The average carbonation depth after four weeks of CO_2 exposure is found to be significantly larger than after 6 weeks of exposure. This result seems counterintuitive, as it is assumed that the carbonation front moves deeper into the sample with time.

Different reasons can be found for this observation. A first reason could be errors during execution of the tests at four weeks. However, this is unlikely as the samples of this test series were treated the same way as the uncracked test series

and the cracked test series without immersion in water. As the results of the latter two test series do not show illogical trends, see Figure 69 and Figure 70, it is assumed that no errors were made.
Another explanation could lie in the fact that the measurements were executed each two weeks on different samples. The heterogeneity of the material and the possible different compaction of the samples could indeed be the cause for these results. However, this is unlikely as this is not observed for none of the other measurements and for none of the other test series.
The most likely reason for the observed phenomenon is the periodically immersion in water. The samples tested after four weeks of CO_2 exposure were only immersed once in demineralized water for 24 hours, namely at the beginning of the test (i.e. 0 weeks). The specimens tested at 6 weeks however, were immersed in demineralized water twice, namely at the beginning of the test and after 4 weeks. From this it seems that the extra immersion in water reduces the carbonation depth. An explanation for the latter is found in a paper by Visser [90]. Visser states that for a pH lower than 6.36, the unstable $CaCO_3$ that was formed during the accelerated carbonation reaction, will partially dissolve again, see Figure 72. This also explains the larger reduction in carbonation depth after six weeks for mixtures containing SAPs, as the water stored in the SAPs is also available for the dissolution of $CaCO_3$ even when the samples are no longer immersed in water.
It could be remarked that the samples were immersed in demineralized water, which has a pH of ± 6.5. However, as the water was not refreshed during the time of the experiment and also other people have used this water for their experiments, it could be that the water has become more acid and thus has a pH lower than 6.36. According to the author of this thesis, this explanation is the most likely for the decreased penetration depth between four and six weeks of exposure to CO_2, however more research on this topic could prove this statement.

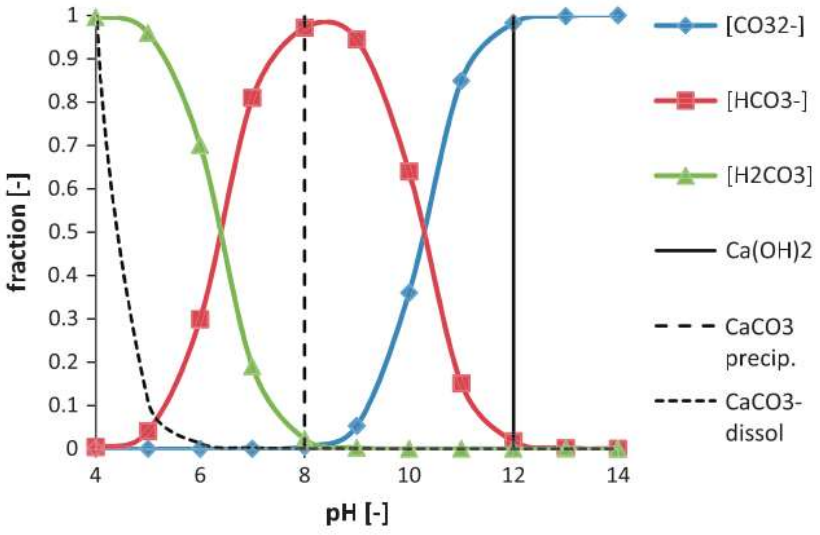

Figure 72: Dissolution boundary for $CaCO_3$ according to Visser [90]

The uncracked and the cracked test series that were not immersed in water show two similar trends: 1) the penetration depth slowly increases in time, due to the low CO_2% in the carbonation chamber and 2) the cement paste has the largest penetration depth, followed by the concrete containing SAPs. The concrete mixture CON has the smallest penetration depth. This phenomenon can be partially explained when examining the obtained values for the initial open porosity, see section 4.2. In section 4.2. CEM showed the largest porosity, followed by SAP and CON. The more open the structure of the concrete, the easier the penetration of CO_2 molecules into the concrete and thus the larger the penetration depth at a certain point in time. The last trend is not valid for the cracked test series that was periodically immersed in water as in this case, the SAP mixture showed larger penetration depths than the CEM mixture, see infra. Another reason can be found when looking at the amount of $Ca(OH)_2$ present in the mixture. $Ca(OH)_2$ will react with CO_2 resulting in the formation of calcium carbonate. The more $Ca(OH)_2$ is present, the more CO_2 can react and the more carbonation will occur. However, after some time, the formed carbonation products will impede the ingress of CO_2 and the carbonation rate is slowed down. As the CEM mixture contains initially the largest amount of $Ca(OH)_2$, this mixture shows larger penetration depths, however it is assumed that the carbonation rate will slow down in time, resulting in smaller penetration depths compared to the concrete mixtures. Prolonged tests are needed to verify this explanation.

Figure 69 shows the average penetration depth in time for the three studied mixtures CON, SAP and CEM in the case no crack is present. For the concrete mixture, the observed increase in penetration depth was only significant between four and six weeks. For the concrete containing SAPs, a similar conclusion can be made, but this time also the increase between 6 and 12 weeks was significant. For the cement paste, all the measurements at different points in time were found to be significantly different.
The penetration of the carbonation front after 12 weeks of exposure is 3.0 mm for CON, 5.7 mm for SAP and 6.2 for CEM.
After 12 weeks, no significant difference between the penetration depth for the SAP and the CEM mixture was found.

Figure 70 shows the penetration depth for cracked samples. For the CON mixture, the increase in penetration depth was only significant between two and four weeks. In between four and six weeks, no significant increase in penetration depth was observed for the SAP mixture. Also for the cement paste, no significant increase in penetration depth was found between two and four weeks on the one hand, and six and twelve weeks on the other hand. The penetration of the carbonation front after 12 weeks of exposure is 2.9 mm for CON, 6.0 mm for SAP and 5.9 mm for CEM. The difference in penetration depths after 12 weeks for SAP and CEM was again found not to be significant.

When comparing the results of this cracked test series after n weeks of exposure with the results of the uncracked series after the same time in the CO_2 chamber, no significant differences are found between the obtained penetration depths. This could be expected because the crack has no influence on the carbonation from the exposed surface.

Figure 71 shows the penetration depth for cracked samples that were stored in demineralized water every 4 weeks for 24 hours. The results after four weeks were not taken into account in the statistical analysis, see supra. For CON and CEM, the increase in penetration depth was not significant between six and twelve weeks of exposure, whereas this increase was significant for the SAP mixture. The penetration of the carbonation front after 12 weeks is 1.8 mm for CON, for 3.8 mm for SAP and 2.0 mm for CEM.
When the samples are periodically immersed in water, the obtained penetration depths are significantly lower than in case the samples are not immersed in water, see Figure 73. In case of CON and SAP, the penetration depth is on average 36% and 32% lower respectively. For CEM, the penetration depth is even 69% lower. The strong reduction in case of the latter is due the large open porosity for cement paste (42%) and the large amount of unhydrated cement particles present that will hydrate upon water immersion, resulting in a more dense structure. When the samples are immersed in water, the open pores are filled with water instead of air. As the carbonation diffusion is much slower in water than in air ([81],[90]), the carbonation rate is low in this case, resulting in smaller penetration depths. The water first needs to dry out before the CO_2 molecules could steadily penetrate into the concrete again.
Furthermore, the remark on the dissolution of $CaCO_3$, see supra, will probably have an effect on the lowered penetration depths when immersed in water.

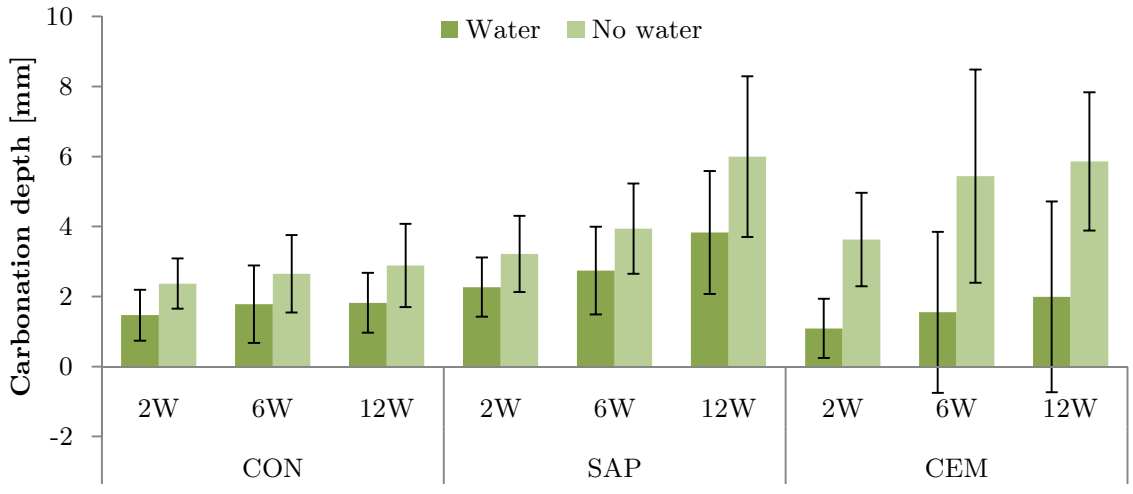

Figure 73: Comparison of penetration depth in case the samples were periodically immersed in water or not

In the case of periodical immersion in water, the SAP mixture shows significantly larger penetration depths than the more porous cement mixture. The SAPs will absorb the water when being immersed in water. After 24 hours of immersion, the samples are placed back in the carbonation chamber. The SAPs will now gradually release the stored water. As a result, the samples containing SAPs will take longer to dry out, what should result in smaller penetration depths as the carbonation rate is slowed down. Also the further hydration of unhydrated cement particles will result in a less porous structure, which is beneficial for the resistance against carbonation. However, instead of the expected smaller carbonation depths in SAP mixtures, larger carbonation depths were observed. A possible explanation can be that carbonation requires a certain amount of water as CO_2 must dissolve first before reacting with Ca^{2+} present in the concrete to form calcium carbonate. The small amounts of water provided by the SAPs seem to be ideal for this purpose, resulting in larger concentrations of dissolved CO_2 and as a consequence a higher production of calcium carbonate. Another explanation could lie in the swelling behavior of the SAPs. Upon immersion in water, the SAPs will swell, possibly blocking part of the open porosity. Due to this blocking, the pores will not be filled with water but remain filled with air, resulting in higher carbonation rates and thus larger carbonation depths.
One of the two aforementioned mechanisms is apparently more dominant than the prolonged drying of the samples and the further hydration. In the end, this results in higher carbonation depths compared to the reference mixture without SAPs.

From this it seems like the addition of SAPs to the concrete has no beneficial effect on the resistance against carbonation. This is contradictory to the findings of Mönnig [84], who found that the addition of SAPs caused a significant retardation of the carbonation rate in 60% RH, in case the amount of added SAPs is smaller than 0.40 m% by cement weight. As the amount used by Mönnig is much lower than the 1 m% SAPs used in this thesis and the samples were not periodically immersed in water but stored at 60% RH, this could be an explanation for the contradictory results. This clearly illustrates the need for further research on this topic in order to provide more insight in the ideal amount of SAPs that should be added to improve the durability of the concrete.

The increase in carbonation depth between six and twelve weeks was found not to be significant, except for the mixtures containing SAP (and the uncracked cement paste). In general this phenomenon can be explained by formula (14) [91]. According to Audenaert, the penetration depth x (mm) can be written as a function of the square root of the exposure time t (weeks):

$$x = A\sqrt{t} \tag{14}$$

With A the carbonation coefficient [$mm/\sqrt{week}$].

This formula indicates that the deeper the carbonation front has progressed into the concrete, the more it will be slowed down as the path that CO_2 needs to travel to encounter non-carbonated material is longer and the open porosity is decreased by the formed carbonation products which will impede the CO_2 ingress.
In this thesis, the open porosity is only determined before the start of the accelerated carbonation test. It would be interesting to also determine the open porosity at certain points in time during the test. By doing this, it could be studied if the open porosity indeed decreases due to the formed carbonation products. Especially in the case of the addition of SAPs this could lead to interesting insights, as no research on this topic has been executed yet.

For each studied mixture, the measured carbonation depths x (in mm) obtained with the phenolphthalein spray are plotted as function of the square root of the exposure time t (in weeks). The samples were already 12 days old when placed in the carbonation chamber and as a consequence some carbonation will already have occurred. Nonetheless, this will be very limited as the CO_2 concentration in air is very low and the samples were stored at 90% RH which is not favorable for carbonation. Therefore, the initial carbonation depth is assumed to be 0 mm. From this fairly linear relationship, the experimental (accelerated) carbonation coefficient $A_{accelerated}$ (in mm/$\sqrt{week}$) can easily be determined. The results are depicted in Figure 74, Figure 75 and Figure 76 for uncracked, cracked and cracked samples periodically stored in water. The found equation of the best fit line through the data points, as well as the R^2 value are plotted on the graph. An R^2 value close to unity means that the data points indeed follow a linear relationship.

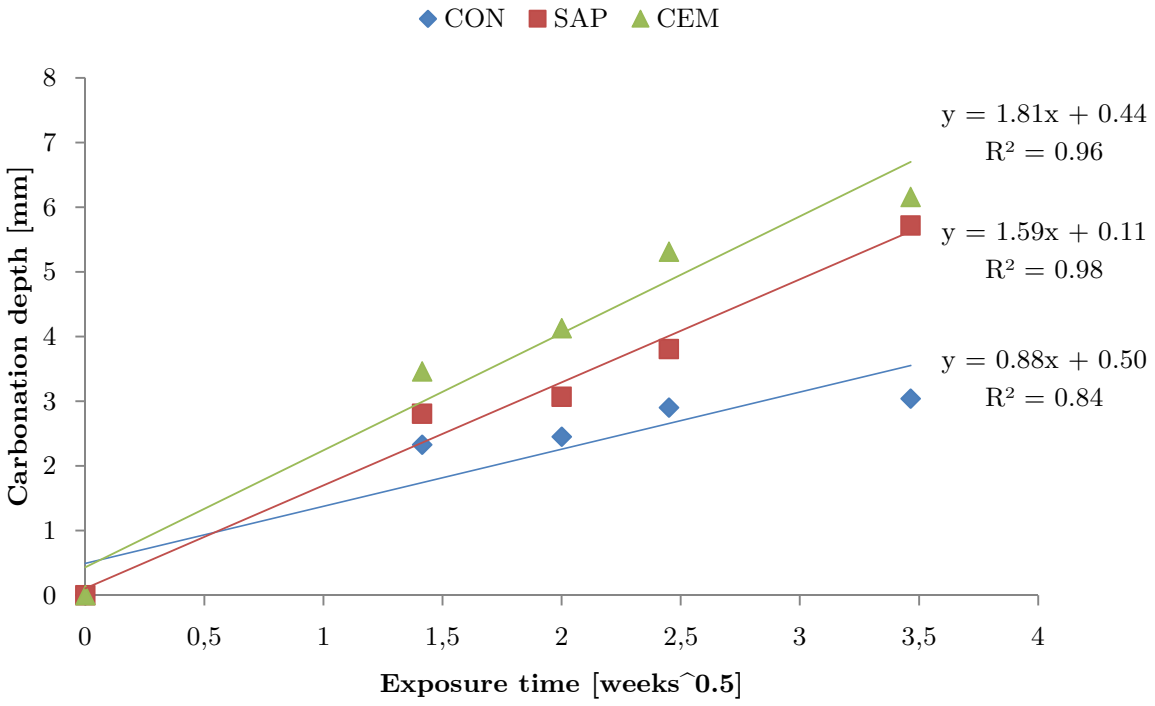

Figure 74: Determination of $A_{accelerated}$, uncracked

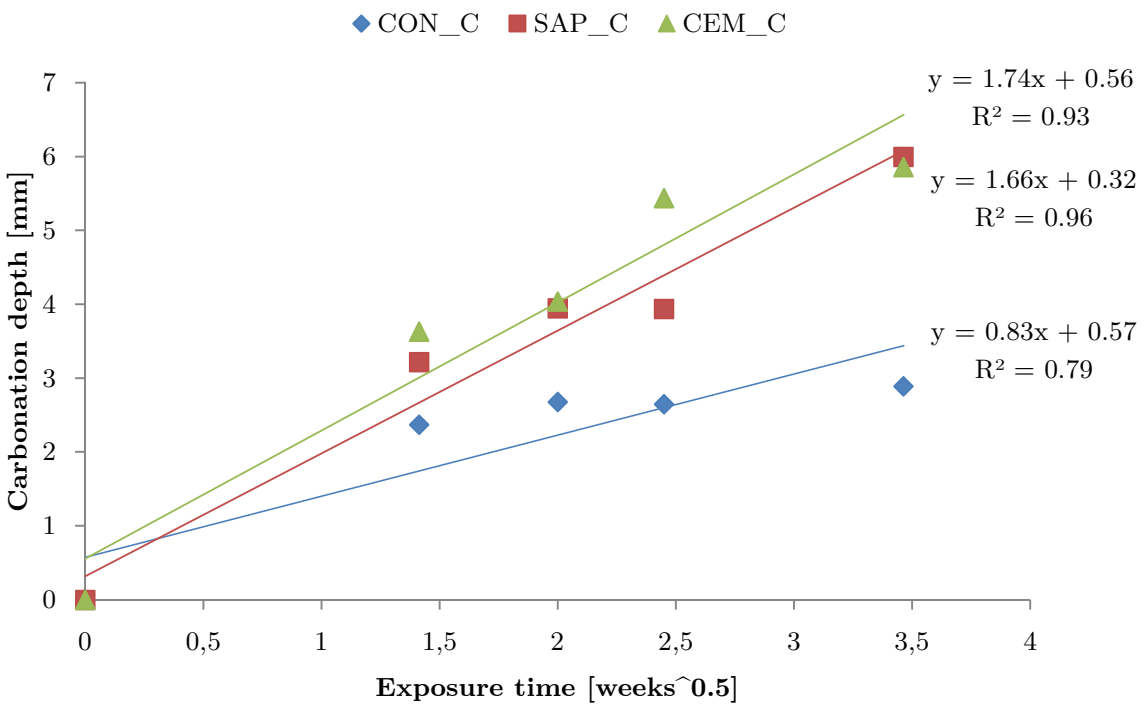

Figure 75: Determination of $A_{accelerated}$, cracked

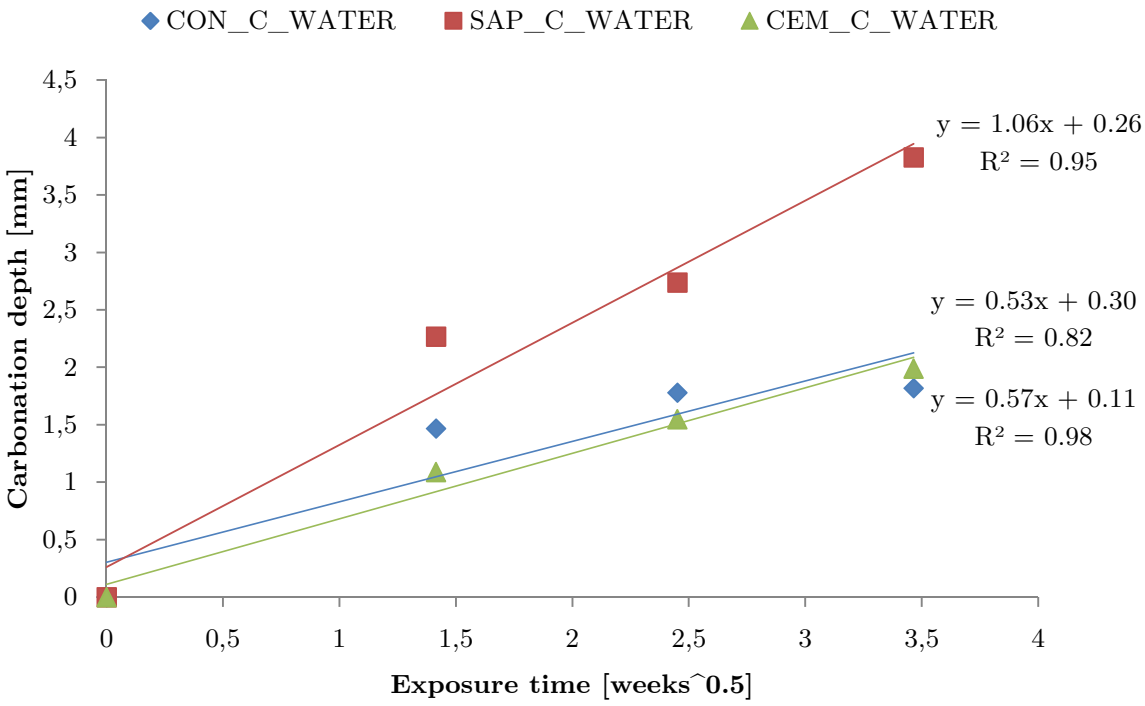

Figure 76: Determination of $A_{accelerated}$, cracked periodically stored in water

From these figures, it can be seen that the equation of the best fit line has the following format:

$$y = A\ x + b \tag{15}$$

The b in equation (15) shows that there is already some initial carbonation at the moment the samples are placed in the carbonation chamber. However it can be seen that this value is very limited (<0.6 mm). Because this value for b is the result of fitting a line through the data points, it could be interesting in future research to determine the real carbonation depth before the start of the carbonation tests.
In general, the obtained R^2 values are quite close to unity, meaning that the data points indeed follow a linear relation. However, the R^2 values of the concrete without SAPs are found to be somewhat lower. This result suggests that in case of concrete mixtures, the linear relationship between the penetration depth and the square root of the time is less pronounced. No explanation was found for the latter.

The carbonation rate $A_{accelerated}$ obtained in this manner cannot be considered a realistic one, because the used CO_2 concentration of 1% exceeds the natural CO_2 concentration in air (0.03%). To obtain a first estimation of the corresponding carbonation rate under real field conditions, Audenaert [91] uses a conversion formula that expresses the ratio of the accelerated and field carbonation coefficients ($A_{accelerated}$ and A_{field}) in terms of their corresponding CO_2 concentrations ($c_{accelerated}$ and c_{field}):

$$\frac{A_{accelerated}}{A_{field}} = \frac{\sqrt{c_{accelerated}}}{\sqrt{c_{field}}} = \frac{\sqrt{1\ \%}}{\sqrt{0.03\ \%}} = 5.77 \tag{16}$$

The obtained values for the carbonation coefficient in both accelerated and field conditions are summarized in Table 21.

Table 21: Accelerated and field carbonation coefficients

		$\mathbf{A_{accelerated}}$ $[\mathbf{mm/\sqrt{week}}]$	$\mathbf{A_{field}}$ $[\mathbf{mm/\sqrt{week}}]$
uncracked	CON	0.88	0.15
	SAP	1.59	0.28
	CEM	1.81	0.31
cracked	CON	0.83	0.14
	SAP	1.66	0.29
	CEM	1.74	0.30
cracked + water	CON	0.53	0.09
	SAP	1.06	0.18
	CEM	0.57	0.10

As these results are in fact only another way of analyzing the data, the same conclusions as earlier can be made again: the carbonation coefficients of uncracked and cracked samples are the largest for CEM mixtures, followed by SAP and CON mixtures. No significant difference is found between the coefficients of cracked and uncracked samples. However, when immersed in water, the addition of SAPs leads to significantly higher carbonation coefficients compared to the CEM and CON mixture. The carbonation coefficients for cracked samples immersed in water are in generally lower than the ones without water immersion.
Carbonation coefficients are frequently used in calculations and predictions models for the life cycle assessment of concrete structures.

According to Glasser et al. [60] and Thiery et al. [81], the abovementioned colorimetric test does not indicate the depth of maximum ingress of CO_2 and the actual carbonation depth could be underestimated. The determination of the carbonation depth by means of a simple ruler is found not to be very accurate and is also dependent on human interpretation. To evaluate the magnitude of this underestimation, the penetration depth is preferably also studied by means of other, more accurate methods like for example thin section analysis, gammadensitometry and thermogravimetric analysis (TGA).

The addition of SAPs to concrete has no apparent beneficial effect on the resistance against carbonation. The combination of the higher open porosity together with the seemingly more easy dissolution of CO_2 in the small amounts of water stored by the SAPs, lead to higher penetration depths compared to the reference concrete.

However, as these findings are not in accordance with findings in literature and some of the results seem contradictory, further research on this topic is needed in order to provide more insight.

5 Conclusions & Further Research

When SAPs are added to the fresh concrete, they will absorb part of the mixing water, resulting in a negative effect on the workability. Therefore, additional water needs to be added to compensate for this loss in workability. The amount of additional water was determined by comparing the flow values of mixtures with and without SAPs on one hand and the results obtained with the filtration method on the other hand. An additional amount of 27 g/g SAP was added and resulted in similar workability. Later on, the SAPs gradually release their water and shrink, leaving empty macro pores in the concrete increasing the porosity of the matrix. This increase in open porosity has a significant influence on both chloride penetration and carbonation and thus on the durability of concrete structures.

The addition of SAPs has a beneficial influence on the self-healing of 100 µm cracks subjected to wet-dry cycles, due to the combined effect of further hydration and the stimulated precipitation of calcium carbonate. Although none of the samples showed 100% healing at the surface after 28 cycles, the mixtures containing SAPs showed higher crack closing ratios (up to 64% and 60% in case of SAP 0.5 m% and SAP 1 m% respectively), compared to the 24% in the reference mixture, even when cracks are too wide to close autogenously (i.e. > 30 µm).
As the studied crack widths of 100 µm are still limited in size and in reality larger crack widths occur frequently, it would be interesting to examine the efficiency of SAPs for self-healing in the case of larger crack widths. This research could also focus on finding the ideal amount of SAPs for the purpose of self-healing and the influence of more wet-dry cycles on self-healing.
Crack healing in this thesis is only based on measurements and observations at the surface of the samples. Possible healing at the inside of the crack is not studied, but as this could have a beneficial effect on the resistance against both chloride penetration and carbonation, this would be an interesting topic for future research. Possible tests for this research are for example thin section analysis, SEM or TGA.

The more porous structure due to the presence of SAPs leads to a significant increase in chloride penetration from the surface. Increasing the amount of SAPs from 0 m% to 0.5 m% and finally to 1 m% leads in each step to an additional ± 2 mm penetration from the surface.
The potentiometric titrations showed that the chloride surface concentration as well as the chloride diffusion coefficient increase with the higher porosity as a result of the embedded SAPs. Although these results are found not to be significant in this thesis at a 5% level of significance, further research should be executed to examine whether this is due to the observed large standard deviations.
The measured chloride contents in cracked concrete are higher than the chloride contents in uncracked concrete. Due to these larger chloride contents corrosion will be initiated more rapidly, and as a result jeopardize the durability of the concrete.

This clearly stresses the importance of finding methods that can heal cracks and as a consequence lower chloride penetration through the cracks.
Several authors ([7],[21],[23],[27],[65]) state that for crack widths smaller than a critical value, the chloride transport process in the crack is very slow. In this case, the crack has almost no influence on the chloride transport process which could be assumed similar to uncracked concrete. Yet, no consensus is found on this critical value: 30 µm ([7],[21]), 50 µm [23], 80 µm ([21],[30]) and 200 µm [65].
Although there is no agreement on this critical value, it is clear that a reduction of the crack width due to the stimulated self-healing upon the addition of SAPs, could have beneficial effects on the resistance against chloride penetration and should be further investigated.

When SAPs are added to the concrete, no beneficial effect on the resistance against carbonation was observed. The combination of the higher open porosity together with the seemingly more easy dissolution of CO_2 in the small amounts of water stored by the SAPs, leads to higher carbonation depths compared to the reference concrete. Nonetheless, the second mechanism can be questioned, as it was expected that due to the available water stored in the SAPs, the carbonation rate would be lowered as the water first needs to dry out before the CO_2 molecules could steadily penetrate into the concrete again. However, in case the swelling of the SAPs leads to partially blocking the open porosity, the pores will not be filled with water but remain filled with air, resulting in even higher carbonation rates and thus larger carbonation depths. One of the two aforementioned mechanisms is apparently more dominant than the prolonged drying of the samples and the further hydration. In the end, this results in higher carbonation depths compared to the reference mixture without SAPs.

As these conclusions are not in accordance with findings in literature and some of the results seem contradictory, further research on this topic is needed. Especially prolonged tests in combination with open porosity tests during the experiment could provide more insight. As carbonation is strongly influenced by the relative humidity, it could also be interesting to measure the RH inside the crack, in order to investigate the possible effect of SAPs on both the RH and the carbonation inside the crack.
The lack of carbonation around the artificial cracks made by brass plates, suggests that a reaction took place at the plate-mixture interface, resulting in an almost impermeable layer for CO_2. Although this topic was not treated in this thesis, it could be interesting to investigate what happens exactly at the mixture-steel plate interface and which components are found at the crack walls as this can have an influence on carbonation depths, chloride penetration and self-healing of the artificial cracks. The focus in this research could be on the bonding between plates and mixture, the amount of fines present at the crack face, the presence of a lubricating layer around the plates etc.

The measured results showed a lot of scatter and as a consequence large standard deviations, which influence the outcome of the statistical analysis. Several reasons contribute to these large standard deviations: heterogeneity of the material (for example local changes in porosity, variety of aggregate sizes and locations etc.), possible different compaction of the samples, variation of the obtained crack widths, blocking of cracks by impurities, the limited amount of samples tested per test series, etc. As most of these things are intrinsic to the material or method and cannot be changed easily, it would be worthwhile to test more samples per test series. By doing this, it would be easier to detect outliers and subsequently omit them in the analysis, possibly resulting in more straightforward conclusions.

The higher porosity due to the addition of SAPs has negative effects on both the chloride penetration and carbonation. Ongoing research on pH-responsive superabsorbent polymers [92] looks promising to counter this problem as depending on the pH of the concrete, the swelling capacity of the SAPs and the release of water inside concrete can be controlled. As pH-responsive SAPs have lower swelling capacity in high pH (around 12.8) the SAPs will swell less during mixing and hardening of the concrete, resulting in a less porous mixture. When a crack occurs however, the pH is lowered, for example due to carbonation or the ingress of seawater. The modified SAPs show a high swelling degree at lower pH (range of 9 – 10) which is ideal for healing and sealing of the crack.

In this thesis, chloride penetration and carbonation are treated and studied separately. However, as carbonation can result in a reduction of the material porosity, this can have a positive influence on the resistance against chloride penetration. Chloride tests on fully carbonated specimens could be executed to examine this hypothesized positive effect.

The second batch made in this thesis showed autogenous healing and this could have beneficial effects on the resistance against both chloride penetration and carbonation. As chlorides and CO_2 can no longer penetrate in fully healed cracks, both the chloride penetration and carbonation of the cracked specimens would decrease to values similar to uncracked concrete. Even in the case the cracks are not completely filled by healing products, it is found in literature that the reduced crack widths can impede chloride and CO_2 ingress, especially in the case they are below a critical crack width.

Still a lot of research is needed on the influence of SAPs on carbonation and chloride penetration, especially in cracked concrete. However, the stimulated self-healing of cracks due to the addition of SAPs could reduce and/or slow down the ingress of harmful substances through cracks significantly and thus increase the service life and durability of concrete structures.

Appendix A

Table 22: Overview of primary studies; the 14 papers from the basic set are marked in blue.

Study			Research question 1a					Research question 1b			Research question 1c		
Author		Year	SAP	Cracks	Self-healing of concrete	Testing self-healing	Concrete healed by SAPs	Influence of crack	Chloride penetration	Testing chloride penetration	Influence of crack	Carbonation	Testing Carbonation
Alahmad	[82]	2009									x	x	x
Aldea	[65]	1999						x	x	x			
Alonso	[61]	2009							x	x			
Andrade	[73]	1999							x	x			
Angst	[62]	2009							x	x			
Audenaert	[20]	2009		x				x	x	x			
Audenaert	[25]	2009		x				x	x	x			
Audenaert	[66]	2009		x				x	x	x			
Baroghel	[71]	2007							x	x			x
Boddy	[59]	1999							x	x			
Castellote	[68]	2001							x	x			
Copuroglu	[29]	2013		x	x	x							
De Belie	[33]	2015		x	x	x	x						
Djerbi	[27]	2008						x	x	x			
Ferreira	[64]	2013						x	x	x		x	
Glasser	[60]	2008							x			x	x
Granger	[32]	2007		x	x	x							
Gruyaert	[93]	2013							x	x		x	x
Gruyaert	[83]	2010							x	x		x	x
Gruyaert	[94]	2011							x	x		x	x
Gruyaert	[4]	2013										x	x
Gu	[21]	2015		x	x			x	x	x			
Ismail	[5]	2008		x				x	x	x			
Jacobsen	[6]	1996		x	x			x	x	x			
Jang	[30]	2011		x				x	x	x			
Jensen	[16]	2008	x										
Jensen	[17]	2011	x										
Jensen	[18]	2002	x										
Jin	[7]	2010						x	x	x			
Lee	[44]	2010	x		x	x	x						
Lee	[47]	2014			x	x							
Li	[41]	2013	x		x	x	x						
Li	[37]	2008			x	x							
Lu	[58]	2013							x	x			
Maes	[24]	2013		x				x	x	x			
Maes	[8]	2012							x	x			
Maes	[9]	2014						x	x	x			
Marsavina	[25]	2009		x				x	x	x			
Mechtcherine	[52]	2012	x				x		x	x			
Meck	[72]	2003							x	x			
Mignon	[43]	2015	x		x	x	x						
Mönnig	[84]	2009	x				x		x	x		x	x
Mori	[77]	2006							x	x			
Mu	[26]	2012		x				x	x	x			
NT build 443	[76]	1995							x	x			
NT Build 492	[75]	1999							x	x			
Rilem TC 178	[74]	2002							x	x			
Rodriguez	[22]	2003						x	x	x			
Sangadji	[42]	2015			x	x							
Savija	[57]	2013						x	x	x			
Savija	[10]	2012						x	x	x			
Savija	[79]	2014						x	x	x			
Schlangen	[28]	2011		x									
Sherir	[51]	2015	x		x	x	x						
Snoeck	[11]	2015	x				x						
Snoeck	[12]	2014	x										
Snoeck	[2]	2012	x		x	x	x						

Snoeck	[13]	2012	x	x	x	x	x										
Snoeck	[53]	2015	x		x	x	x								x		x
Snoeck	[95]	2013	x														
Snoeck	[38]	2015	x		x	x	x										
Snoeck	[14]	2014	x		x	x	x										
Snoeck	[15]	2012	x			x	x										
Spiesz	[67]	2013								x	x						
Stanish	[69]	1997								x	x						
Tang	[96]	2015								x	x						
Ter Heide	[36]	2005			x	x											
Thiery	[81]	2007													x		x
Van den Heede	[80]	2014						x	x	x					x		x
Van den Heede	[55]	2014													x		x
Van den Heede	[23]	2013		x				x	x	x							
Van Tittelboom	[34]	2013	x		x												
Van Tittelboom	[48]	2013	x		x	x	x										
Van Tittelboom	[45]	2012			x	x											
Van Tittelboom	[40]	2012			x	x											
Vantyghem	[46]	2014		x				x	x	x				x	x		x
Wang	[31]	1997		x													
Win	[3]	2004						x	x	x							
Yang	[39]	2009			x	x											
Ye	[78]	2013						x	x	x							
Zhang	[50]	2010				x											
Zhou	[56]	2015								x	x				x		x
Zohuriaan	[19]	2008	x														

References

[1] Kitchenham, B. and Charters, S., "Guidelines for performing Systematic Literature Reviews in Software Engineering," *Engineering*, vol. 2, 2007, p. 1051.

[2] Snoeck, D., Steuperaert, S., Van Tittelboom, K., Dubruel, P., and De Belie, N., "Visualization of water penetration in cementitious materials with superabsorbent polymers by means of neutron radiography," *Cement and Concrete Research*, vol. 42, no. 8, Aug. 2012, pp. 1113–1121.

[3] Win, P. P., Watanabe, M., and Machida, A., "Penetration profile of chloride ion in cracked reinforced concrete," *Cement and Concrete Research*, vol. 34, no. 7, Jul. 2004, pp. 1073–1079.

[4] Gruyaert, E., Van den Heede, P., and De Belie, N., "Carbonation of slag concrete: Effect of the cement replacement level and curing on the carbonation coefficient – Effect of carbonation on the pore structure," *Cement and Concrete Composites*, vol. 35, no. 1, Jan. 2013, pp. 39–48.

[5] Ismail, M., Toumi, a., François, R., and Gagné, R., "Effect of crack opening on the local diffusion of chloride in cracked mortar samples," *Cement and Concrete Research*, vol. 38, no. 8–9, Aug. 2008, pp. 1106–1111.

[6] Jacobsen, S., Marchand, J., and Boisvert, L., "Effect of cracking and healing on chloride transport in OPC concrete," *Cement and Concrete Research*, vol. 26, no. 6, 1996, pp. 869–881.

[7] Jin, W. L., Yan, Y. D., and Wang, H. L., "Chloride diffusion in the cracked concrete," in *Proceedings of FraMCoS-7, May 23-28, 2010*, 2010.

[8] Maes, M., Gruyaert, E., and De Belie, N., "Resistance of concrete with blast-furnace slag against chlorides, investigated by comparing chloride profiles after migration and diffusion," *Materials and Structures*, vol. 46, no. 1–2, Jul. 2012, pp. 89–103.

[9] Maes, M., Van Tittelboom, K., and De Belie, N., "The efficiency of self-healing cementitious materials by means of encapsulated polyurethane in chloride containing environments," *Construction and Building Materials*, vol. 71, Nov. 2014, pp. 528–537.

[10] Šavija, B. and Schlangen, E., "Chloride ingress in cracked concrete - a literature review," in *Advances in Modeling Concrete Service Life: Proceedings of 4th International RILEM PhD Workshop held in Madrid, Spain, November 19, 2010*, 2012, pp. 133–142.

[11] Snoeck, D., Jensen, O. M., and De Belie, N., "The influence of superabsorbent polymers on the autogenous shrinkage properties of cement pastes with supplementary cementitious materials," *Cement and Concrete Research*, vol. 74, no. September, Aug. 2015, pp. 59–67.

[12] Snoeck, D., Schaubroeck, D., Dubruel, P., and De Belie, N., "Effect of high amounts of superabsorbent polymers and additional water on the workability, microstructure and strength of mortars with a water-to-cement ratio of 0.50," *Construction and Building Materials*, vol. 72, no. September 2015, Dec. 2014, pp. 148–157.

[13] Snoeck, D., Van Tittelboom, K., Steuperaert, S., Dubruel, P., and De Belie, N., "Self-healing cementitious materials by the combination of microfibres and superabsorbent polymers," *Journal of Intelligent Material Systems and Structures*, vol. 25, no. 1, Mar. 2012, pp. 13–24.

[14] Snoeck, D., Dubruel, P., and De Belie, N., "How to seal and heal cracks in cementitious materials by using superabsorbent polymers," in *Application of Superabsorbent Polymers and Other New Admixtures in Concrete Construction*, 2014, pp. 375–384.

[15] Snoeck, D., Dubruel, P., and De Belie, N., "Superabsorbent polymers to prevent water movement in cementitious materials," *International Journal of 3R's*, 2012.

[16] Jensen, O. M., "Use of superabsorbent polymers in construction materials," *1st International Conference on Microstructure Related Durability of Cementitious Composites 13-15 October*, no. October, 2008, pp. 757–764.

[17] Jensen, O. M., "Water absorption of superabsorbent polymers in a cementitious environment," *International RILEM Conference on Advances in Construction Materials Through Science and Engineering*, no. September, 2011, pp. 22–35.

[18] Jensen, O. M. and Hansen, P. F., "Water-entrained cement-based materials," *Cement and Concrete Research*, vol. 32, no. 6, 2002, pp. 973–978.

[19] Zohuriaan-Mehr, M. J. and Kabiri, K., "Superabsorbent Polymer Materials: A Review," *Iranian Polymer Journal*, vol. 17, no. 6, 2008, pp. 451–477.

[20] Audenaert, K., Marsavina, L., and De Schutter, G., "Influence of Cracks on the Service Life of Concrete Structures in a Marine Environment," *Key Engineering Materials*, vol. 399, no. August, 2009, pp. 153–160.

[21] Gu, C., "A review of the chloride transport properties of cracked concrete: experiments and simulations," *Journal of Zhejiang University Science A*, vol. 16, no. 2, 2015, pp. 81–92.

[22] Rodriguez, O. G. and Hooton, R. D., "Influence of cracks on chloride ingress into concrete," *ACI Materials Journal*, vol. 100, no. 2, 2003, pp. 120–126.

[23] Van den Heede, P., Maes, M., and De Belie, N., "Influence of active crack width control on the chloride penetration resistance and global warming potential of slabs made with fly ash + silica fume concrete," *Construction and Building Materials*, vol. 67, 2013, pp. 74–80.

[24] Maes, M. and Belie, N. De, "Resistance of cracked concrete to chloride attack," in *Third International Conference on Sustainable Construction Materials and Technologies*, 2013, pp. 1–10.

[25] Marsavina, L., Audenaert, K., De Schutter, G., Faur, N., and Marsavina, D., "Experimental and numerical determination of the chloride penetration in cracked concrete," *Construction and Building Materials*, vol. 23, no. 1, 2009, pp. 264–274.

[26] Mu, S., De Schutter, G., and Ma, B., "Non-steady state chloride diffusion in concrete with different crack densities," *Materials and Structures*, no. September, 2012, pp. 123–133.

[27] Djerbi, a., Bonnet, S., Khelidj, a., and Baroghel-bouny, V., "Influence of traversing crack on chloride diffusion into concrete," *Cement and Concrete Research*, vol. 38, no. 6, 2008, pp. 877–883.

[28] Schlangen, E., Savija, B., Pacheco, J., and Polder, R. B., "Modified Wedge Splitting Test (MWST)— a simple tool for durability investigations of reinforcement corrosion in cracked concrete," in *Concrete Repair, Rehabiliation and Retrofitting III*, 2011, pp. 386–391.

[29] Copuroglu, O., Schlangen, E., Nishiwaki, T., Van Tittelboom, K., Snoeck, D., De Belie, N., and de Rooij, M. R., "Experimental Techniques used to Verify Healing." pp. 19–63, 2013.

[30] Jang, S. Y., Kim, B. S., and Oh, B. H., "Effect of crack width on chloride diffusion coefficients of concrete by steady-state migration tests," *Cement and Concrete Research*, vol. 41, no. 1, 2011, pp. 9–19.

[31] Wang, K., Jansen, D. C., Shah, S. P., and Karr, A. F., "Permeability study of cracked concrete," *Cement and Concrete Research*, vol. 27, no. 3, 1997, pp. 381–393.

[32] Granger, S., Loukili, a., Pijaudier-Cabot, G., and Chanvillard, G., "Experimental characterization of the self-healing of cracks in an ultra high performance cementitious material: Mechanical tests and acoustic emission analysis," *Cement and Concrete Research*, vol. 37, no. 4, 2007, pp. 519–527.

[33] De Belie, N., Van Tittelboom, K., Tsangouri, E., Karaiskos, G., Snoeck, D., Wang, J., Araújo, M., and Van Hemelrijck, D., "Autonomous regeneration of concrete structures by incorporation of self-healing mechanisms," in *International Conference on the Regeneration and Conservation of Concrete Structures, Proceedings*, 2015, pp. 1–10.

[34] Van Tittelboom, K., Snoeck, D., Wang, J., and Belie, N. De, "Most recent advances in the field of self-healing cementitious materials," in *ICSHM 2013 : 4th international conference on self-healing materials*, 2013, pp. 406–413.

[35] Snoeck, D. and De Belie, N., "From straw in bricks to modern use of microfibers in cementitious composites for improved autogenous healing – A review," *Construction and Building Materials*, vol. 95, 2015, pp. 774–787.

[36] Ter Heide, N., "Crack healing in hydrating concrete," 2005.

[37] Li, V. and Yang, E.-H., *Self Healing in Concrete Materials*, vol. 100. 2008.

[38] Snoeck, D., Debaecke, S., and De Be, "Repeated autogenous healing in cementitious composites with microfibres and syperabsorbent polymers," in *XIII International Congerence on Durability of Building Materials and Components*, 2015, no. SEPTEMBER 2014, pp. 73–80.

[39] Yang, Y., Lepech, M. D., Yang, E. H., and Li, V. C., "Autogenous healing of engineered cementitious composites under wet-dry cycles," *Cement and Concrete Research*, vol. 39, no. 5, 2009, pp. 382–390.

[40] Van Tittelboom, K., Gruyaert, E., Rahier, H., and De Belie, N., "Influence of mix composition on the extent of autogenous crack healing by continued hydration or calcium carbonate formation," *Construction and Building Materials*, vol. 37, 2012, pp. 349–359.

[41] Li, V. C., Sakulich, A. R., Reinhardt, H. W., Schlangen, E., Van Tittelboom, K., Snoeck, D., De Belie, N., Joseph, C., Gardner, D. R., Lark, R. J., Mihashi, H., and Nishiwaki, T., "Recovery against Mechanical Actions." pp. 119–215, 2013.

[42] Sangadji, S., "Porous Network Concrete: a bio-inspired building component ot make concrete structures self-healing," 2015.

[43] Mignon, A., Snoeck, D., Schaubroeck, D., Luickx, N., Dubruel, P., Van Vlierberghe, S., and De Belie, N., "pH-responsive superabsorbent polymers: A pathway to self-healing of mortar," *Reactive and Functional Polymers*, vol. 93, no. JUNE, 2015, pp. 68–76.

[44] Lee, H., "Potential of superabsorbent polymer for self-sealing cracks in concrete," *Advances in Applied Ceramics*, vol. 109, no. 5, 2010, pp. 296–302.

[45] Van Tittelboom, K., Snoeck, D., Vontobel, P., Wittmann, F. H., and Belie, N., "Use of neutron radiography and tomography to visualize the autonomous crack sealing efficiency in cementitious materials," *Materials and Structures*, no. August 2015, 2012.

[46] Vantyghem, S., "Tegengaan van wapeningscorrosie door zelfherstel van scheuren in beton," 2014.

[47] Lee, Y.-S. and Ryou, J.-S., "Self healing behavior for crack closing of expansive agent via granulation/film coating method," *Construction and Building Materials*, vol. 71, 2014, pp. 188–193.

[48] Van Tittelboom, K. and De Belie, N., "Self-healing in cementitious materials- A review," *Materials*, vol. 6, no. 6, 2013, pp. 2182–2217.

[49] Snoeck, D. and De Belie, N., "Repeated Autogenous Healing in Strain-Hardening Cementitious Composits by Using Superabsorbent Polymers," *Journal of Materials in Civil Engineering*, vol. 25, no. 7, 2013, pp. 864–870.

[50] Zhang, P., Wittmann, F. H., Zhao, T., and Lehmann, E. H., "Neutron imaging of water penetration into cracked steel reinforced concrete," *Physica B: Condensed Matter*, vol. 405, no. 7, 2010, pp. 1866–1871.

[51] Sherir, M. A. A., Hossain, K. M. A., and Lachemi, M., "Interaction of Superabsorbent Polymers and Admixtures on THe Properties of Engineered Cementitious Composites," in *Building on Our Growth Opportunities*, 2015, pp. 1–10.

[52] Mechtcherine, V. and Reinhardt, H.-W., "STAR 225-SAP Application of Superabsorbent Polymers (SAP) in Concrete Construction," 2012.

[53] Snoeck, D., Velasco, L. F., Mignon, a., Van Vlierberghe, S., Dubruel, P., Lodewyckx, P., and De Belie, N., "The effects of superabsorbent polymers on the microstructure of cementitious materials studied by means of sorption experiments," *Cement and Concrete Research*, vol. 77, no. September, 2015, pp. 26–35.

[54] Mönnig, S., "Water saturated super-absorbent polymers used in high strength concrete," *Otto-Graf-Journal*, vol. 16, 2005, pp. 193–202.

[55] Van Den Heede, P., "Durability and Sustainability of Concrete with High Volumes of Fly Ash," 2014.

[56] Zhou, Y., Gencturk, B., Asce, a M., Willam, K., Asce, F., and Attar, A., "Carbonation-Induced and Chloride-Induced Corrosion in Reinforced Concrete Structures," *Journal of Materials in Civil Engineering*, vol. 27, no. 9, 2015.

[57] Šavija, B., Pacheco, J., and Schlangen, E., "Lattice modeling of chloride diffusion in sound and cracked concrete," *Cement and Concrete Composites*, vol. 42, 2013, pp. 30–40.

[58] Lu, C., Gao, Y., Cui, Z., and Liu, R., "Experimental Analysis of Chloride Penetration into Concrete Subjected to Drying – Wetting Cycles," *Journal of Materials in Civil Engineering*, 2013, pp. 1–10.

[59] Boddy, A., Bentz, E., Thomas, M. D. a, and Hooton, R. D., "Overview and sensitivity study of a multimechanistic chloride transport model," *Cement and Concrete Research*, vol. 29, no. 6, 1999, pp. 827–837.

[60] Glasser, F. P., Marchand, J., and Samson, E., "Durability of concrete - Degradation phenomena involving detrimental chemical reactions," *Cement and Concrete Research*, vol. 38, no. 2, 2008, pp. 226–246.

[61] Alonso, M. C. and Sanchez, M., "Analysis of the variability of chloride threshold values in the literature," *Materials and Corrosion*, vol. 60, no. 8, 2009, pp. 631–637.

[62] Angst, U., Elsener, B., Larsen, C. K., and Vennesland, Ø., "Critical chloride content in reinforced concrete - A review," *Cement and Concrete Research*, vol. 39, no. 12, 2009, pp. 1122–1138.

[63] Gruyaert, E., "Effect of Blast-Furnace Slag as a Cement Replacement on Hydration, Microstructure, Strength and Durability of Concrete," 2011.

[64] Ferreira, M. and Makkonen, L., "Performance and durability of concrete in extreme cold environment - Literature Review," 2013.

[65] Aldea, C.-M., Shah, S. P., and Karr, A. F., "Effect of Cracking on Water and Chloride Permeability of Concrete," *Journal of Materials in Civil Engineering*, no. August, 1999, pp. 181–187.

[66] Audenaert, K., De Schutter, G., and Marsavina, L., "Influence of cracks and crack width on penetration depth of chlorides in concrete," *European Journal of Environmental and Civil Engineering*, vol. 13, no. 5, 2009, pp. 561–572.

[67] Spiesz, P. and Brouwers, H. J. H., "The apparent and effective chloride migration coefficients obtained in migration tests," *Cement and Concrete Research*, vol. 48, 2013, pp. 116–127.

[68] Castellote, M. and Andrade, C., "Round-Robin test on chloride analysis in concrete—Part II: Analysis of water soluble chloride content," *Materials and Structures*, vol. 34, no. 9, 2001, pp. 532–549.

[69] Stanish, K. D., Hooton, R. D., and Thomas, M. D. ., "Testing the Chloride Penetration Resistance of Concrete : A Literature Review," 1997.

[70] Tang, L., "Discussion of 'AFREM test procedures concerning chlorides in concrete: Extraction and titration methods,'" *Materials and Structures*, vol. 34, no. 236, 2005, pp. 128–129.

[71] Baroghel-Bouny, V., Belin, P., Maultzsch, M., and Henry, D., "AgNO3 spray tests: advantages, weaknesses, and various applications to quantify chloride ingress into concrete.," *Materials and Structures*, vol. 40, no. 8, 2007, pp. 783–799.

[72] Meck, E. and Sirivivatnanon, V., "Field indicator of chloride penetration depth," *Cement and Concrete Research*, vol. 33, no. 8, 2003, pp. 1113–1117.

[73] Andrade, C., Castellote, M., Alonso, C., and González, C., "Relation between colourimetric chloride penetration depth and charge passed in migration tests of the type of standard ASTM C1202-91," *Cement and Concrete Research*, vol. 29, no. 3, 1999, pp. 417–421.

[74] Rilem TC 178, "Rilem Technical Committees Rilem Tc 178-Tmc : ' Testing and Modelling Chloride Penetration in concrete,'" *Materials and Structures*, vol. 35, 2002, pp. 586–588.

[75] NT Build 492, "Concrete , Mortar and Cement-Based Repair Materials : chloride migration coefficient from non-steady-state migration experiments," *Measurement*, 1999, pp. 1–8.

[76] NT Build 443, "Concrete, Hardened: Accelerated Chloride Penetration." 1995.

[77] Mori, D., Yamada, K., Hosokawa, Y., and Yamamoto, M., "Applications of Electron Probe Microanalyzer for Measurement of Cl Concentration Profile in Concrete," *Journal of Advanced Concrete Technology*, vol. 4, no. 3, 2006, pp. 369–383.

[78] Ye, H., Tian, Y., Jin, N., Jin, X., and Fu, C., "Influence of cracking on chloride diffusivity and moisture influential depth in concrete subjected to simulated environmental conditions," *Construction and Building Materials*, vol. 47, no. August, 2013, pp. 66–79.

[79] Šavija, B., Schlangen, E., Pacheco, J., Millar, S., Eichler, T., and Wilsch, G., "Chloride ingress in cracked concrete: a laser induced breakdown spectroscopy

(LIBS) study," *Journal of Advanced Concrete Technology*, vol. 12, no. 10, 2014, pp. 425–442.

[80] Van Den Heede, P. and De Belie, N., "A service life based global warming potential for high-volume fly ash concrete exposed to carbonation," *Construction and Building Materials*, vol. 55, 2014, pp. 183–193.

[81] Thiery, M., Villain, G., Dangla, P., and Platret, G., "Investigation of the carbonation front shape on cementitious materials: Effects of the chemical kinetics," *Cement and Concrete Research*, vol. 37, no. 7, 2007, pp. 1047–1058.

[82] Alahmad, S., Toumi, a., Verdier, J., and François, R., "Effect of crack opening on carbon dioxide penetration in cracked mortar samples," *Materials and Structures*, vol. 42, no. 5, 2009, pp. 559–566.

[83] Gruyaert, E., Maes, M., and Belie, N. De, "A comparative study of the durability of ordinary portland cement concrete and concrete containing (high) percentages of blast-furnace slag," in *International RILEM Conference on Material Science*, 2010, vol. III, pp. 241–251.

[84] Mönnig, S., "Superabsorbing additions in concrete : applications, modelling and comparison of different internal water sources," 2009.

[85] Xiang, H., Lee, D., Wong, H. S., and Buenfeld, N., "Self-Sealing Cement-Based Materials Using Superabsorbent Polymers," in *International RILEM Conference on Use of Superabsorbent Polymers and Other New Additives in Concrete 15-18 August*, 2010, no. August.

[86] Schröfl, C., Mechtcherine, V., and Gorges, M., "Relation between the molecular structure and the efficiency of superabsorbent polymers (SAP) as concrete admixture to mitigate autogenous shrinkage," *Cement and Concrete Research*, vol. 42, no. 6, 2012, pp. 865–873.

[87] Brüdern, a.-E. and Mechtcherine, V., "Multifunctional use of SAP in strain-hardening cement-based composites," *International RILEM Conference on Use of Superabsorbent Polymers and Other New Additives in Concrete 15-18 August*, no. August, 2010, pp. 11–22.

[88] Tittelboom, K. Van, Wang, J., Araújo, M., Snoeck, D., Gruyaert, E., Debbaut, B., Derluyn, H., Cnudde, V., Tsangouri, E., Hemelrijck, D. Van, and Belie, N. De, "Comparison of different approaches for self-healing concrete in a large-scale lab test," *CONSTRUCTION & BUILDING MATERIALS*, vol. 107, 2016, pp. 125–137.

[89] Yuan, Q., "Fundamental studies on test methods for the transport of chloride ions in cementitious materials," 2008.

[90] Visser, J. H. M., "Influence of the carbon dioxide concentration on the resistance to carbonation of concrete," *Construction and Building Materials*, vol. 67, 2014, pp. 8–13.

[91] Audenaert, K., "Transportmechanismen in zelfverdichtend beton in relatie met carbonatatie en chloridepenetratie," Ghent University, 2006.

[92] Mignon, A., Graulus, G.-J., Snoeck, D., Martins, J., De Belie, N., Dubruel, P., and Van Vlierberghe, S., "pH-sensitive superabsorbent polymers: a potential candidate material for self-healing concrete," *Journal of Materials Science*, vol. 50, no. 2, 2014, pp. 970–979.

[93] Gruyaert, E., Maes, M., and De Belie, N., "Performance of BFS concrete: K-Value concept versus equivalent performance concept," *Construction and Building Materials*, vol. 47, 2013, pp. 441–455.

[94] Gruyaert, E., Van Den Heede, P., Maes, M., and De Belie, N., "Investigation of the influence of blast-furnace slag on the resistance of concrete against organic acid or sulphate attack by means of accelerated degradation tests," *Cement and Concrete Research*, vol. 42, no. 1, 2012, pp. 173–185.

[95] Snoeck, D. and Belie, N. De, "The influence of superabsorbent polymers on the microstructure and permeability of cementitious materials," in *International Conference on Concrete under Severe Conditions - Environment and Loading, At Nanjing*, 2013, no. SEPTEMBER 2013, pp. 1–11.

[96] Tang, W., Kardani, O., and Cui, H., "Robust evaluation of self-healing efficiency in cementitious materials – A review," *Construction and Building Materials*, vol. 81, no. APRIL, 2015, pp. 233–247.

List of Figures

List of Tables